UNIWERSYTET GDAŃSKI

WYDZIAŁ OCEANOGRAFII I GEOGRAFII

KAROLINA TRZCIŃSKA

CHARAKTERYSTYCZNE CECHY ROZPRASZANIA WSTECZNEGO SYGNAŁÓW AKUSTYCZNYCH OD SIEDLISK DENNYCH W POŁUDNIOWYM BAŁTYKU

CHARACTERISTIC FEATURES OF ACOUSTIC SIGNALS BACKSCATTERING FROM BENTHIC HABITATS IN THE SOUTHERN BALTIC SEA

Promotor: **Prof. dr hab. Jarosław Tęgowski**

Promotor pomocniczy: **Dr Jens Schneider von Deimling**

Praca doktorska zrealizowana w Zakładzie Geofizyki, Instytutu Oceanografii, Uniwersytetu Gdańskiego

GDYNIA, 2022

PODZIĘKOWANIA

Serdecznie dziękuję promotorom Profesorowi Jarosławowi Tęgowskiemu oraz Doktorowi Jensowi Schneiderowi von Deimling za cenne nauki, poświęcony czas i cierpliwość.

I sincerely thank the supervisors Professor Jarosław Tęgowski and Doctor Jens Schneider von Deimling for their valuable teachings, time and patience.

Dziękuję osobom, które służyły pomocą i wiedzą podczas moich studiów doktorskich: Aleksandrze Kruss, Pawłowi Poćwiardowskiemu, Marii Rucińskiej, Dominikowi Pałganowi, Jakubowi Zdroikowi, Łukaszowi Janowskiemu i Grzegorzowi Kolatowi.

Dziękuję Mężowi, Rodzinie, całemu Zakładowi Geofizyki oraz Przyjaciołom za wsparcie podczas realizacji pracy doktorskiej.

Dziękuję Radmiłowi Kozie, Bartłomiejowi Arciszewskiemu oraz załodze statku Oceanograf za pomoc w realizacji pomiarów, czasami w trudnych warunkach atmosferycznych.

Dziękuję wszystkim Państwu – Profesorom, Doktorom oraz Pracownikom, którzy na przestrzeni wielu lat uczyliście mnie, na zajęciach dydaktycznych lub poza nimi, jak zdobywać wiedzę i rozwijać pasje.

FINANSOWANIE BADAŃ

Praca powstała w trakcie realizacji projektu BONUS ECOMAP (Baltic Sea environmental assessments by innovative opto-acoustic remote sensing, mapping, and monitoring), wspieranego przez program BONUS (art. 185), finansowanego wspólnie przez UE i Federalne Ministerstwo Edukacji i Badań Naukowych Niemiec (BMBF), Narodowe Centrum Badań i Rozwoju Polski (NCBR; numer grantu BONUSBB/ECOMAP/07/2017) oraz Fundusz Innowacji Danii (Innovationsfonden).

PUBLIKACJE WCHODZĄCE W SKŁAD DYSERTACJI

1. Janowski L., **Trzcinska K.**, Tegowski J., Kruss A., Rucinska-Zjadacz M., Pocwiardowski P. Nearshore benthic habitat mapping based on multi-frequency, multibeam echosounder data using a combined object-based approach: A case study from the Rowy Site in the Southern Baltic Sea. *Remote Sens*. 2018, 10, 1983. https://doi.org/10.3390/rs10121983

   Wkład własny: 35%
   IF: 4.848, 5-letni IF: 5.353

2. **Trzcinska K.**, Janowski L., Nowak J., Rucinska-Zjadacz M., Kruss A., Schneider von Deimling J., Pocwiardowski P., Tegowski J. Spectral features of dual-frequency multibeam echosounder data for benthic habitat mapping. *Mar. Geol*. 2020, 427, 106239. https://doi.org/10.1016/j.margeo.2020.106239

   Wkład własny: 80%
   IF: 3.548, 5-letni IF: 3.585

3. **Trzcinska K.**, Tegowski J., Pocwiardowski P., Janowski L., Zdroik J., Kruss A., Rucinska M., Lubniewski Z., Schneider von Deimling J. Measurement of Seafloor Acoustic Backscatter Angular Dependence at 150 kHz Using a Multibeam Echosounder. *Remote Sens*. 2021, 13, 4771. https://doi.org/10.3390/rs13234771

   Wkład własny: 75%
   IF: 4.848, 5-letni IF: 5.353

Łączny IF: 13.244, Łączny 5-letni IF: 14,291

INNE PUBLIKACJE NIE WCHODZĄCE W SKŁAD DYSERTACJI

1. Matciak M., Bieleninik S., Botur A., Podgórski M., **Trzcińska K.**, Dragańska K., Jaśniewicz D., Kurszewska A., Wenta M. Observations of presumable groundwater seepage occurrence in Puck Bay (the Baltic Sea). *Oceanological and Hydrobiological Studies*, Volume 44, Issue 2, June 2015 pp. 267-272. DOI: https://doi.org/10.1515/ohs-2015-0025

   IF: 0.821, 5-letni IF: 0.809

2. Tegowski J., **Trzcinska K.**, Kasprzak M., Nowak J. Statistical and spectral features of the corrugated seafloor shaped by the Hans glacier in Svalbard. *Remote Sensing* 8:744 September 2016 DOI: 10.3390/rs8090744

   IF: 4.848, 5-letni IF: 5.353

3. Janowski L., Tylmann K., **Trzcinska K.**, Rudowski S., Tegowski J., Exploration of glacial landforms by object-based image analysis and spectral parameters of digital elevation model. *IEEE Transactions on Geoscience and Remote Sensing*, 2022 vol. 60, pp. 1-17, Art no. 4502817, doi: 10.1109/TGRS.2021.3091771.

   IF: 5.6, 5-letni IF: 7.107

4. Tęgowski J., Koza R., Pawliczka Vel Pawlik I., Skóra K., **Trzcińska K.**, Zdroik J. Statistical, spectral and wavelet features of the ambient noise detected in the southern Baltic sea. Recenzowany artykuł pokonferencyjny w: 23rd International Congress on Sound and Vibration, 2016, Publisher: International Institute of Acoustics and Vibration (IIAV) (na liście Web of Science)

5. Tęgowski J., **Trzcińska K.**, Janowski Ł., Kruss A., Kusek K., Nowak J. Comparison of Backscatter and Seabed Topographic Characteristics Recorded by Multibeam Echosounder at Rewal Area - Southern Baltic Sea. Recenzowany artykuł pokonferencyjny w: Proc. of 2018 Joint Conference on Acoustics, p. 303-306, 11-14.09.2018, Ustka, doi:10.1109/ACOUSTICS.2018.8502330. (na liście Web of Science)

6. Tegowski J., Janowski L., **Trzcinska K.**, Rucinska-Zjadacz M., Pocwiardowski P., Kusek K. Multibeam and singlebeam multifrequency classification of bottom habitats – the complementation of two approaches. Recenzowany artykuł pokonferencyjny w: 5th Underwater Acoustics Conference and Exhibition, 2019, UACE2019, Kreta, Grecja, 791-798. (na liście MNiSW)

Łączny IF: 11.269, Łączny 5-letni IF: 13.269

SPIS TREŚCI

STRESZCZENIE

Badania oceanograficzne często wiążą się z potrzebą rozpoznania dna morskiego – jego kształtu, typu osadu, pokrycia przez kolonie fito- lub zoobentosu, a więc występowania siedlisk dennych. Do wydzielania obszarów występowania odmiennych siedlisk z powodzeniem stosowane są różne cechy batymetrii i informacje o natężeniu sygnału akustycznego rozproszonego wstecz, rejestrowanego przez echosondy wielowiązkowe (Diesing i Thorsnes 2018; Lecours i in. 2015; Held i Schneider von Deimling 2019). Zastosowanie miernika przechyłów oraz pomiar pozycji podczas badań umożliwiają uzyskanie dokładnie zlokalizowanych map o rozdzielczości przestrzennej rzędu kilku centymetrów (Montereale Gavazzi i in. 2016). Rejestracje wykonywane za pomocą echosond wielowiązkowych w ostatnich latach z dużym powodzeniem są stosowane w celu kartowania dna. Umożliwiają one jednoczesną rejestrację danych batymetrycznych w kilkuset punktach i podczas przemieszczania się jednostki badawczej tworzą precyzyjny model dna morskiego oraz mapę natężenia sygnału akustycznego rozproszonego wstecz. Wyniki tych prac są bardzo przydatne dla organów administrujących żeglugą oraz inwestorów planujących konstrukcje posadowione na dnie morskim. Badania dna morskiego są również niezwykle istotne w czasach gwałtownych zmian klimatycznych i środowiskowych, umożliwiając monitorowanie środowiska dna morskiego i występujących tam siedlisk bentosowych. Kartowanie i klasyfikacja siedlisk dennych dostarcza informacji niezbędnych do utworzenia Morskich Obszarów Chronionych. Działania takie mieszczą się w Ramowej Dyrektywie w Sprawie Strategii Morskiej 2008/56/WE, Ramowej Dyrektywie Wodnej 2000/60/WE oraz Dyrektywie Siedliskowej 92/43/EWG. Zakładają one potrzebę opracowania metod mapowania i monitoringu dna morskiego.

Obok informacji o batymetrii najczęściej rejestrowaną informacją o dnie za pomocą echosondy wielowiązkowej jest względne natężenie sygnału akustycznego rozproszonego wstecz. Jest ono zależne od czynników związanych z urządzeniem pomiarowym, takich jak: częstotliwość sygnału, czułość odbiornika, charakterystyka kierunkowa przetwornika; czynników związanych ze środowiskiem, przez które transmitowana jest fala akustyczna i powracający sygnał jak temperatura i zasolenie; czynników związanych z geofizycznymi cechami dna morskiego, jak nierówność powierzchni dna, czy gęstość osadu. Dodatkowo względne natężenie sygnału akustycznego rozproszonego wstecz od dna morskiego rejestrowanego przez echosondę wielowiązkową wykazuje silną zależność od kąta padania na dno. Na rysunku 1 przedstawiłam przykład takiej zależności zarejestrowanej podczas moich badań.

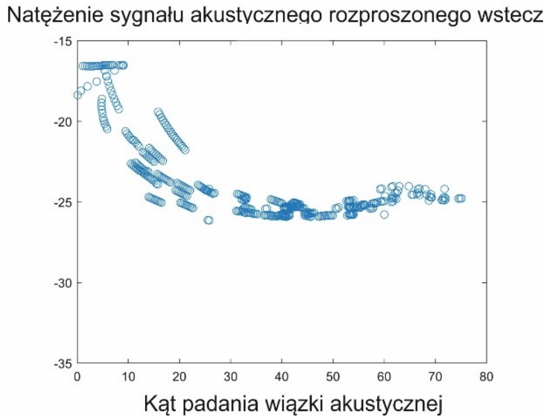

Rys. 1. Przykład zależności kątowej natężenia sygnału akustycznego rozproszonego wstecz od dna morskiego.

Informacje zawarte w sygnałach rozproszonych wstecz są wykorzystywane w algorytmach bezinwazyjnej klasyfikacji dna morskiego, jednakże zależność kątowa natężenia takiego sygnału znacznie utrudnia poprawną klasyfikację. Problemem do rozwiązania jest ujednolicenie mapy natężeń sygnałów akustycznych rozproszonych wstecz poprzez sprowadzenie natężenia sygnałów w całym badanym akwenie do wartości odpowiadających jednemu kątowi padania wiązki akustycznej na dno. Próbę takiej korekcji zrealizowano w komercyjnym oprogramowaniu FMGT QPS z narzędziem o nazwie Geocoder (Fonseca i Calder 2005). Przygotowałam mapy względnego natężenia sygnałów rozproszonych wstecz badanego obszaru, wykorzystując narzędzie Geocoder, jednak w opracowanych tak mapach zaobserwowałam duże błędy dla kątów padania bliskich 0°. Dlatego zdecydowałam się opracować własną metodę zmiennego wzmocnienia kątowego (publikacja 3), co było niełatwym zadaniem.

Akustyczna klasyfikacja i mapowanie dna morskiego przy użyciu powtarzalnych, zautomatyzowanych metod wciąż wymaga ulepszenia, pomimo postępu dokonanego w ostatnich latach. Parametry dna obliczone dla batymetrii i natężenia sygnału akustycznego rozproszonego wstecz są bezpośrednio związane z przestrzennym zasięgiem siedlisk i często wykorzystywane w klasyfikacji dna morskiego. Niektóre z ostatnich publikacji podkreślają potrzebę wprowadzenia nowych parametrów opisujących dno morskie do kartowania siedlisk bentosowych (Diesing i in. 2016), dlatego zastosowałam parametry widmowe obliczone z cyfrowego modelu terenu, które są zupełnie nowe w nadzorowanej klasyfikacji siedlisk bentosowych.

Wyniki pomiarów natężenia sygnału akustycznego rozproszonego wstecz wykonane z użyciem różnej częstotliwości emitowanego sygnału lub podczas oddzielnych rejsów pomiarowych, prezentowane przez badaczy, zazwyczaj znacznie różnią się zakresami wartości. Utrudnia to wykonanie automatycznej lub półautomatycznej klasyfikacji siedlisk bentosowych. Na obserwowane różnice wpływa wiele czynników, takich jak: częstotliwość emitowanego sygnału akustycznego, zmieniająca się podczas różnych pomiarów absorpcja fal akustycznych w wodzie, czy kierunek płynięcia jednostki podczas wykonywania pomiarów oraz zmieniające się parametry fizyczne opisujące powierzchnię dna i osad na nim występujący.

Pomimo częstego stosowania w pracach badawczych względnego natężenia sygnałów rozproszonych wstecz od dna nie informują one o rzeczywistych własnościach rozpraszających, ponieważ ich wartość zależy nie tylko od typu osadu na dnie, ale również od urządzenia pomiarowego i czynników związanych z parametrami wysyłanego impulsu. To rzeczywiste wartości siły rozpraszania wstecznego (ang. bottom backscattering strength - BBS) są immanentną cechą siedlisk bentosowych. By je zarejestrować, niezbędne jest zastosowanie echosondy skalibrowanej akustycznie, skorygowanie wyniku o absorbcję dźwięku w wodzie oraz o straty związane z geometrycznym rozchodzeniem się dźwięku i uwzględnienie wielkości powierzchni, od której zarejestrowany sygnał został rozproszony. Akustyczna kalibracja echosondy wielowiązkowej nie jest prostą sprawą. Od niedawna na rynku dostępne są echosondy wielowiązkowe firm Kongsberg i NORBIT skalibrowane akustycznie. Nadal informacje o rzeczywistych wartościach siły rozpraszania wstecznego różnych siedlisk bentosowych dla częstotliwości sygnałów powyżej 100 kHz są w literaturze niezwykle rzadkie. Modele teoretyczne rozpraszania sygnałów akustycznych na dnie morskim działają dla zakresu częstotliwości od 10 kHz do 100 kHz (model APL-UW 1994). Wiele echosond jednowiązkowych używa sygnałów o częstotliwościach mieszczących się w tym przedziale, natomiast echosondy wielowiązkowe i sonary boczne używają znacznie wyższych częstotliwości. Badaczom nadal brak szczegółowych informacji o rozpraszaniu dźwięku wstecz od dna morskiego dla częstotliwości sygnału sondującego większej niż 100 kHz. Charakterystyki kątowe rzeczywistej siły rozpraszania wstecznego są fizyczną cechą siedlisk bentosowych i stanowią ich ważną akustyczną właściwość. Poznanie tych cech siedlisk bentosowych umożliwi stworzenie katalogu natężeń sygnałów akustycznych rozproszonych wstecz zależnych od częstotliwości sygnału, kąta padania oraz parametrów środowiska. Umożliwi to lepsze niż dotychczas zrozumienie procesów środowiskowych zachodzących na dnie morskim lub wpływających na nie. Pomiar bezwzględnych wartości zależności kątowych siły rozpraszania wstecznego jest również niezbędny do oceny zmienności w czasie i przestrzeni charakterystyk siedlisk bentosowych. Względne natężenie sygnałów rozpraszanych wstecz było najskuteczniejszym parametrem w klasyfikacji siedlisk dennych w licznych pracach (publikacja 1; Gaida i in. 2020; Buscombe i in. 201; Preston 2009). Podkreśla to znaczenie tego parametru i zwraca uwagę na konieczność jak najdokładniejszego pomiaru, aby móc go wykorzystać do badań w jak najbardziej efektywny sposób (Lurton i Lamarche 2015).

Cele pracy

Głównym celem pracy doktorskiej jest zbudowanie wiarygodnego systemu akustycznej charakterystyki siedlisk dennych, na który składa się:

- wykonanie cyfrowego modelu dna badanych rejonów wraz z jego parametryzacją,
- wykonanie mapy natężenia sygnału akustycznego rozproszonego wstecz sprowadzonego do jednego kąta padania,
- poznanie charakterystyk kątowych bezwzględnej siły sygnału akustycznego rozproszonego wstecz od dna dla sygnałów o wybranej częstotliwości.
- bezinwazyjna klasyfikacja siedlisk bentosowych.

Ponadto celem pracy jest znalezienie parametrów opisujących powierzchnię dna, które zwiększają siłę predykcji w klasyfikacji nadzorowanej i nie są zależne od częstotliwości sygnału wykorzystywanego podczas rejestracji dna echosondą wielowiązkową i nie są także zależne od innych zmian względnych wartości natężenia sygnału akustycznego podczas różnych kampanii pomiarowych. Dodatkowym celem jest stworzenie własnego, empirycznego algorytmu do korekcji zależności kątowej natężenia sygnału rozproszonego wstecz, który umożliwia dalsze wykorzystanie tego parametru w procesie klasyfikacji.

Obszar badań

Do testowania nowych metod badawczych wybrano obszar dna morskiego, który na niewielkim obszarze skupia rożne typy siedlisk bentosowych. W akwenie pomiarowym o powierzchni ~1,4 km^2 położonym w odległości ok 1,5 km na północ od portu Rowy w południowym Bałtyku zarejestrowano dane batymetryczne oraz natężenia sygnałów rozproszonych wstecz za pomocą echosondy wielowiązkowej (publikacja 1, publikacja 2, publikacja 3). Z zarejestrowanych danych przygotowano cyfrowy model batymetrii oraz mapę względnych wartości natężenia sygnału akustycznego rozproszonego wstecz od dna. W badanym obszarze występują: obszary pokryte bardzo drobnym piaskiem (VFS), piaskiem lub piaskiem ze żwirem miejscami tworzącym ripplemarki (S), żwir piaszczysty lub piasek żwirowy (SG-GS), głazy i otoczaki pokryte małżami *Mytilus trossulus* (B), głazy i otoczaki pokryte małżami *Mytilus trossulus,* porośnięte krasnorostami (R) oraz sztuczna struktura jaką jest wrak statku (A). Podczas pomiarów pobrano próbki osadów czerpaczem Van Veen'a oraz wykonano rejestracje video kamerą umieszczoną na zdalnie kierowanym pojeździe podwodnym. Łącznie zinwentaryzowano 57 miejsc dna morskiego. Pobrane próbki osadów zostały przeanalizowane laboratoryjnie w celu określenia ich składu granulometrycznego, natomiast miejsca występowania dużych głazów, w których nie udało się pozyskać próbek osadów, oceniono wizualnie na podstawie zarejestrowanego nagrania wideo. Następnie punkty inwentaryzacji przyporządkowano do sześciu wymienionych wcześniej grup (Folk i Ward 1957; Wentworth 1922).

Opis wykonanych prac wchodzących w skład dysertacji

Klasyfikacja siedlisk dennych

W ostatnich latach w badaniach hydroakustycznych intensywnie poszukuje się jak najlepszych metod geomorfologicznej analizy dna morskiego (Goff i Jordan 1988; Wilson i in. 2007; Micallef i in. 2012; Diesing i Thorsnes 2018; Gafeira i in. 2018; Lucieer i in. 2018). Do klasyfikacji siedlisk bentosowych stosowane są różne metody (Diesing i in. 2020), które ogólnie możemy podzielić na klasyfikację nadzorowaną i nienadzorowaną, w której nie rozróżnia się na początku ilości i cech wynikowych klas. Często do określenia klas oraz miejsca ich występowania in situ wykorzystywane są próbki osadów dennych. Podczas grupowania na podstawie analizy map parametrów przypisywane do poszczególnych klas mogą być pojedyncze piksele lub piksele zgrupowane w obiekty o podobnych cechach. Wreszcie sposób przypisania danych do poszczególnych grup może być realizowany za pomocą różnych metod jak maszyna wektorów nośnych, las losowy, algorytm grupowania k-średnich, k-najbliższych sąsiadów, drzewa klasyfikacji i regresji, sieci neuronowe (Diesing i in. 2020; publikacja 1; publikacja 2). Punkty zinwentaryzowane na dnie morza mogą być podzielone na dwie grupy – grupę treningową, która bierze udział w „uczeniu” algorytmu prawidłowego przypisania klas oraz grupę walidacyjną służącą sprawdzeniu poprawności predykcji. Metoda klasyfikacji polegająca na wykorzystaniu nadzorowanej analizy obiektowej realizowanej w oprogramowaniu eCognition z wykorzystaniem wieloskalowej segmentacji, algorytmu doboru cech Boruta i porównania wyników kilku algorytmów klasyfikujących osiąga bardzo dobre rezultaty opisane między innymi ogólną dokładnością na poziomie powyżej 80% (publikacja 1; Janowski i in. 2020) dlatego została wybrana do klasyfikacji siedlisk w moim badaniu.

W przypadku nadzorowanej analizy obiektowej (publikacja 1; publikacja 2), czynnikami wejściowymi do klasyfikacji są próbki osadów dennych, mapy batymetryczne, mapy względnego natężenia sygnału akustycznego rozproszonego wstecz od dna morskiego oraz mapy obliczonych z nich parametrów. Parametry statystyczne obliczane w wielu pracach dla batymetrii to nachylenie (slope), kierunek ekspozycji (aspect), krzywizna (curvature), odchylenie standardowe (standard deviation). Przykłady parametrów obliczanych dla mapy względnego natężenia sygnału rozproszonego wstecz to odchylenie standardowe oraz parametry teksturalne (macierze współwystępowania poziomów szarości - GLCM) (Haralick i in. 1973; Montereale Gavazzi i in. 2017; Prampolini i in. 2018; Samsudin i Hasan 2017), w tym homogeniczność i kontrast. W badaniach metod klasyfikacji siedlisk bentosowych na szczególną uwagę zasługują analizy w wielu skalach przestrzennych (Lecours i in. 2015; Misiuk i in. 2018). Istnieje wiele możliwych do przygotowania map parametrów, dlatego ważne jest określenie, które z nich w sposób istotny opisują badany obszar. Realizuje się to poprzez algorytm doboru cech Boruta (Kursa i Rudnicki 2010) określający wskaźnik ważności (important score) lub poprzez analizę składowych głównych (Jolliffe 2002), która określa stopień korelacji wzajemnej poszczególnych zmiennych. Do grupowania siedlisk należy wybrać mapy parametrów, które w sposób istotny opisują zmienność badanego obszaru i nie są ze sobą silnie skorelowane (publikacja 2).

Jedną z najnowszych tendencji w mapowaniu siedlisk bentosowych jest wykorzystanie wieloczęstotliwościowych danych rejestrowanych przez echosondy wielowiązkowe. Zależność natężenia sygnału akustycznego rozproszonego wstecz od częstotliwości zaobserwowano w badaniach laboratoryjnych i terenowych, sprawdzając wartość tego parametru dla różnych typów osadów (publikacja 1; Jackson i in. 1986; Urick 1983; Feldens i in. 2018; Gaida i in. 2018). Rejestracje akustyczne osadów dna morskiego przeprowadzone na kilku częstotliwościach często dostarczają więcej informacji na temat fizycznych i biologicznych właściwości siedlisk dna morskiego w porównaniu z badaniami wykorzystującymi jedną częstotliwość. Zaobserwowano, że drobne osady, takie jak piaski i muły inaczej rozpraszają sygnały akustyczne o danej częstotliwości, niż osady grubsze, takie jak żwir, muszle lub głazy (Jackson i in. 1986; Gaida i in. 2018).

Lyons i inni (2002) opisali jedno z pierwszych zastosowań Dwuwymiarowej Transformacji Fouriera (2D FFT) do charakterystyki dna morskiego o wysokiej rozdzielczości. Zastosowanie 2D FFT umożliwiło uzyskanie przestrzennego rozkładu widmowej gęstości mocy cyfrowego modelu terenu. Ta sama technika została zastosowana w kilku innych badaniach (np.: Briggs i in. 2005). Metoda została udoskonalona i zastosowana do analizy batymetrii o wysokiej rozdzielczości uzyskanej z nowoczesnych pomiarów hydroakustycznych, w tym z wykorzystaniem echosond wielowiązkowych (Cazenave i in. 2008; Lefebvre i in. 2009). Schönke i inni (2017) zastosowali transformację Fouriera do opisu mikro nierówności dna morskiego, stosując podwodne skanowanie laserem w południowo-wschodniej części Morza Północnego.

Zaproponowałam, aby w klasyfikacji siedlisk bentosowych zastosować parametry opisujące badany obszar obliczone z cyfrowego modelu dna morskiego. Wprowadziłam do analizy obiektowej nową grupę parametrów widmowych obliczonych z cyfrowego modelu dna (publikacja 2). Są nimi: moment widmowy m0, moment widmowy m2, średnia częstotliwość, szerokość widmowa, skośność widmowa, współczynnik dobroci (Q-factor), skośność widmowa zdefiniowana dla momentów centralnych, wymiar fraktalny. Cyfrowy model dna podzieliłam na małe kwadraty, przy czym każdy kolejny kwadrat zachodził w 90% na położenie poprzedniego a w każdym z nich obliczyłam gęstość widmową mocy korzystając z algorytmu 2D FFT (Rys. 2).

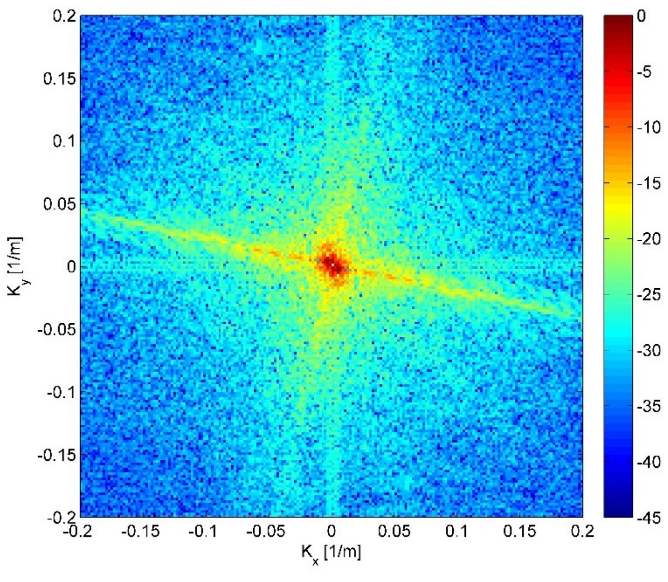

Rys. 2. Przykład gęstości widmowej mocy obliczonej w oknie obejmującym fragment cyfrowego modelu terenu.

W każdym z okien (Rys. 2) robiłam przekroje gęstości widmowej mocy co 5 stopni i z tak otrzymanych dwuwymiarowych przekrojów obliczyłam parametry widmowe. Uśrednione wyniki parametru z poszczególnych okien złożyłam w mapę przestrzennego rozkładu parametru w badanym obszarze. Na Rys. 3 przedstawiłam przykładowy parametr - moment widmowy 2, który został obliczony w oknie o wielkości 20x20 m.

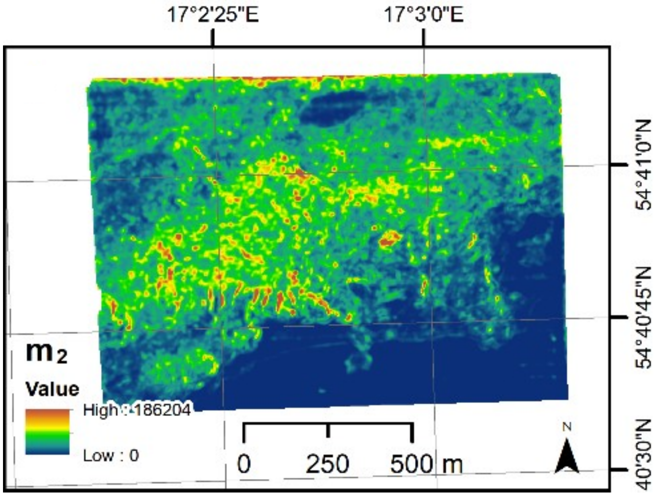

Rys. 3. Mapa rozkładu wartości parametru moment widmowy (m2), obliczonego w ruchomym oknie 20x20 m.

W publikacji 2 przygotowano zestawienie map przykładowych parametrów mogących brać udział w procesie klasyfikacji dna, w tym parametry statystyczne, widmowe oraz macierze współwystępowania poziomów szarości. Następnie sprawdzono, które spośród 62 map parametrów są najistotniejsze w klasyfikacji nadzorowanej wykorzystując algorytm doboru cech Boruta (Kursa i Rudnicki 2010). Ten algorytm doboru cech wykorzystuje uczenie maszynowe typu random forest (RF) (Breiman 2001). Klasyfikację obiektową OBIA zrealizowano stosując oprogramowanie eCognition (publikacja 1; publikacja 2; Blaschke 2010; Janowski i in. 2020). W algorytmie segmentacji wielorozdzielczej (MS) piksele o podobnych cechach zostały połączone w grupy o określonych kształtach i rozmiarach (Benz i in. 2004). Najlepszy wynik klasyfikacji osiągnięto metodą - maszyna wektorów nośnych (Support Vector Machine - SVM). Otrzymano 86% ogólnej dokładności predykcji, porównując wynik klasyfikacji ze zbiorem próbek osadów walidacyjnych.

Rzeczywista wartość siły rozpraszania wstecznego od dna

Standardy hydrograficzne IHO (2008) w sposób szczegółowy opisują jakość pomiarów batymetrycznych echosondą wielowiązkową, jednak standardy związane z pomiarami echosondą wielowiązkową rozpraszania wstecznego niezmiernie rzadko są opisywane w literaturze. Kompendium dobrych praktyk w zakresie rejestracji i przetwarzania natężenia sygnałów rozpraszanych wstecz opracowane przez grupę BSWG GeoHab, jest pierwszym tego typu dokumentem skupiającym się na jakości danych o natężeniu sygnału akustycznego rozproszonego wstecz rejestrowanego przez echosondę wielowiązkową (Lurton i Lamarche 2015). Natężenie sygnałów akustycznych rozproszonych wstecz powinno być rejestrowane urządzeniami skalibrowanymi akustycznie, dając dostęp do rzeczywistej siły rozpraszania wstecznego (Lurton i Lamarche 2015; Eleftherakis i in. 2018).

Dostarczenie rzeczywistych wartości siły rozpraszania wstecznego dna morskiego wymaga użycia sonaru, którego charakterystyka i czułość podczas nadawania i odbioru sygnału są dobrze znane przy określonej częstotliwości i kącie padania na dno morskie. Ponadto wymaga to zastosowania dokładnych kompensacji strat transmisji oraz powierzchni rewerberacji (Lurton i Lamarche 2015; Eleftherakis i in. 2018). W ostatnich latach opublikowano wyniki zaledwie kilku badań siedlisk bentosowych z wykorzystaniem skalibrowanej akustycznie echosondy wielowiązkowej (Wendelboe 1018; Eleftherakis i in. 2014; Weber i in. 2018; Roche i in. 2018). Prace te przedstawiają wybrane charakterystyki rzeczywistej siły rozpraszania wstecznego dla kilku typów siedlisk przy zastosowaniu sygnałów o różnych częstotliwościach przy znanych parametrach środowiska. Gdy takie pomiary staną się częste, możliwe będzie stworzenie kompleksowego katalogu przedstawiającego charakterystyki kątowe rzeczywistej siły rozpraszania wstecznego dla różnych siedlisk bentosowych.

Do pomiarów prezentowanych w publikacji 3 wykorzystałam echosondę wielowiązkową iWBMSh (model STX) skalibrowaną akustycznie przez jej producenta - firmę NORBIT. Dodatkowo zarejestrowane wartości natężenia rozpraszania wstecznego zostały przeze mnie skorygowane o wielkość powierzchni rewerberacji oraz przyporządkowane do kątów padania wiązki akustycznej na dno. W publikacji zaprezentowałam krzywe przedstawiające kątowe zależności rzeczywistej siły rozpraszania wstecznego dla siedlisk dennych występujących w badanym obszarze dla sygnału akustycznego o częstotliwości 150 kHz. Jest to niezwykle ważny wynik w kontekście poznania akustycznej charakterystyki siedlisk bentosowych.

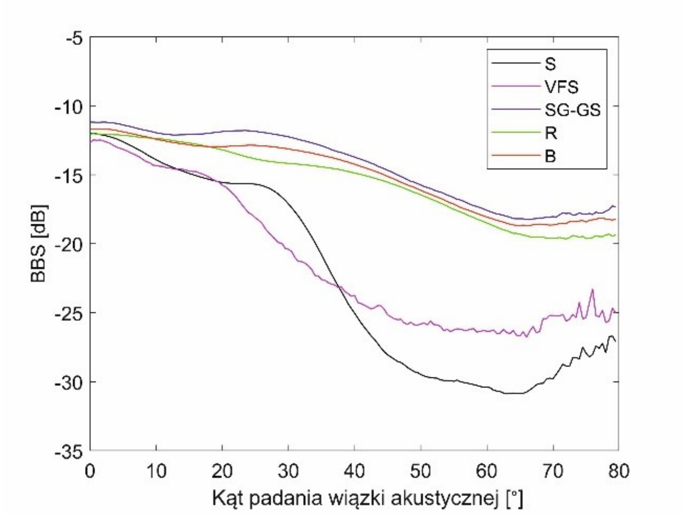

Rys. 4. Wyniki wartości rzeczywistej siły rozpraszania wstecznego w funkcji kąta padania dla obszarów pokrytych bardzo drobnym piaskiem (VFS), piaskiem lub piaskiem ze żwirem miejscami tworzącym ripplemarki (S), żwiru piaszczystego lub piasku żwirowego (SG-GS), głazów i otoczaków pokrytych małżami *Mytilus trossulus* (B), głazów i otoczaków pokrytych małżami *Mytilus trossulus,* porośniętych krasnorostami (R) dla sygnałów akustycznych o częstotliwości 150 kHz.

Uzyskane wartości rzeczywistej siły rozpraszania wstecznego wyniosły: od -12 do -31 dB dla obszarów pokrytych piaskiem lub piaskiem ze żwirem miejscami tworzącym ripplemarki (S); od -12,5 do -27 dB dla obszarów pokrytych bardzo drobnym piaskiem (VFS); od -10,5 do -18 dB dla żwiru piaszczystego lub piasku żwirowego (SG-GS); od -12 do -20 dB dla głazów i otoczaków pokrytych małżami *Mytilus trossulus* i porośniętych krasnorostami (R) oraz -11,5 do -18 dB dla głazów i otoczaków pokrytych małżami *Mytilus trossulus* (B).

W przypadku płaskich w makroskali typów dna (obszary pokryte bardzo drobnym piaskiem, obszary pokryte piaskiem lub piaskiem ze żwirem miejscami tworzącym ripplemarki) zaobserwowałam duży spadek rzeczywistej siły rozpraszania wstecznego wraz ze wzrostem odchylenia kierunku padania fali od pionu a w przypadku dna o bardziej nieregularnym kształcie (żwir piaszczysty lub piasek żwirowy, głazy i otoczaki pokryte małżami *Mytilus trossulus*, głazy i otoczaki pokryte małżami *Mytilus trossulus* i porośnięte krasnorostami) spadek wartości rzeczywistej siły rozpraszania wstecznego dla bardziej odchylonych wiązek ten jest mniejszy. Wartości rzeczywistej siły rozpraszania wstecznego uzyskane dla żwiru piaszczystego lub piasku żwirowego, głazów i otoczaków pokrytych małżami *Mytilus trossulus* i porośniętych krasnorostami oraz głazów i otoczaków pokrytych małżami *Mytilus trossulus* były wyższe niż dla obszarów pokrytych piaskiem lub piaskiem ze żwirem miejscami tworzącym ripplemarki i obszary pokryte bardzo drobnym piaskiem. Krzywe wartości rzeczywistej siły rozpraszania wstecznego dla obszarów pokrytych piaskiem lub piaskiem ze żwirem miejscami tworzącym ripplemarki i obszarów pokrytych bardzo drobnym piaskiem w przedstawionych przeze mnie badaniach miały charakterystyczne kształty typowe dla krzywej osadów drobnoziarnistych w modelu APL-UW (1994).

Korekcja względnego natężenia sygnału rozproszonego wstecz od dna polegająca na zmiennym wzmocnieniu kątowym

Względne natężenie sygnału akustycznego rozproszonego wstecz wykazuje silną zależność od kąta padania. Na Rys. 5 przedstawiono przykładową mapę wartości względnego natężenia sygnałów rozproszonych wstecz w funkcji kąta padania zarejestrowanych przeze mnie w akwenie pomiarowym.

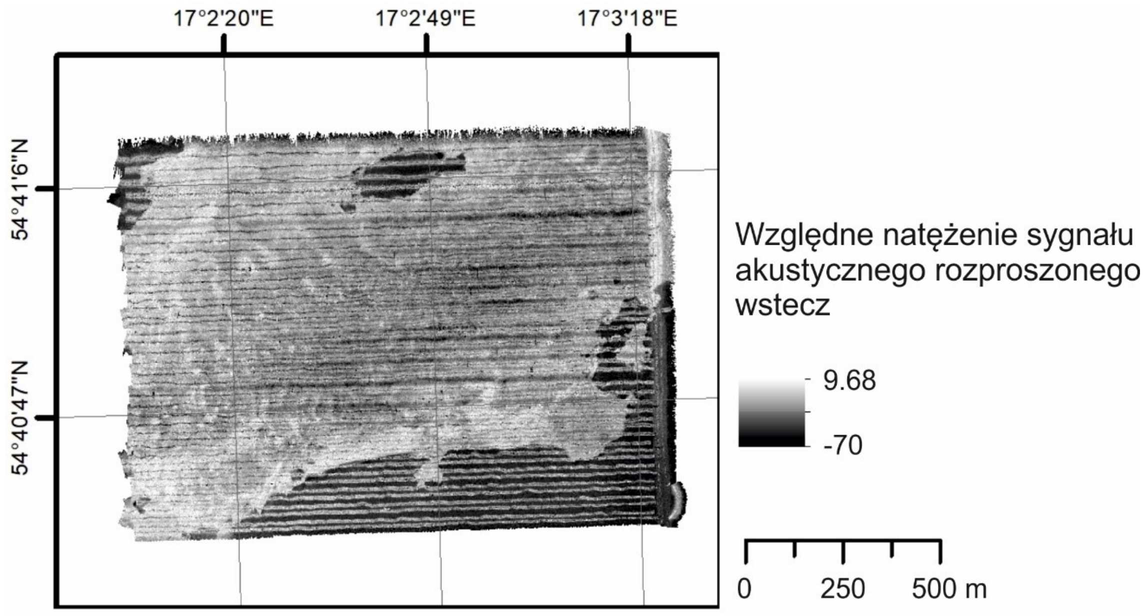

Rys. 5. Mapa względnych wartości natężenia sygnałów akustycznych rozproszonych wstecz zarejestrowana w akwenie Rowy w południowym Bałtyku.

Opracowałam empiryczną metodę korekcji polegającą na zmiennym wzmocnieniu kątowym (publikacja 3). Wykorzystuje ona uśrednione wartości zmierzonego natężenia sygnału akustycznego rozproszonego wstecz, a nie założenia modelowe, tak jak to uczyniono w standardowym oprogramowaniu Geocoder. Wysokiej jakości mapy rozpraszania wstecznego sprowadzone do jednego kąta padania są niezbędne do przeprowadzenia dokładnej klasyfikacji siedlisk bentosowych. Wszystkie pomiary natężenia sygnału akustycznego rozproszonego wstecz w badanym obszarze sprowadziłam do wartości odpowiadających rozpraszaniu wstecznemu dla kąta padania 40° w celu sporządzenia jednorodnej mapy łatwej do interpretacji oraz dalszego wykorzystania w programach realizujących klasyfikację. Zaproponowany przeze mnie algorytm umożliwia sprowadzenie siły rozpraszania wstecznego do dowolnego kąta padania wiązki akustycznej na dno.

Nowatorska procedura korekcji polega na podziale danych zarejestrowanych przez echosondę wielowiązkową na grupy, z których każda zawiera sekwencję 50 impulsów, a każdy impuls kilkaset zarejestrowanych odebranych sygnałów (wykorzystywana echosonda operowała na 512 wiązkach odbiorczych). Dla uproszczenia przyjęłam założenie, że właściwości rozpraszania wstecz sygnału akustycznego od dna morskiego są stałe w każdej sekwencji zarejestrowanych impulsów. Każdy zarejestrowany sygnał przypisałam do odpowiedniego przedziału kąta padania. Ze wszystkich danych zarejestrowanych w danej sekwencji obliczyłam średnie wartości natężenia sygnału akustycznego rozproszonego wstecz dla różnych kątów padania. Następnie sprawdziłam, jaka wartość odpowiada kątowi padania 40 stopni i obliczyłam współczynnik korekcji dla poszczególnych kątów padania. Każdą zarejestrowaną wartość natężenia sygnału akustycznego rozproszonego wstecz przemnożyłam ze współczynnikiem korekcji odpowiednim dla danego kąta padania. Współczynniki korekcji były obliczane oddzielnie dla każdej sekwencji 50 impulsów.

Na Rys. 6 przedstawiłam mapę względnych wartości natężenia sygnałów akustycznych rozproszonych wstecz o wartościach przeliczonych do kąta padania 40°. Wynik procedury korekcyjnej jest przedstawiony w postaci mapy obliczonych wartości względnego natężenia sygnału akustycznego rozproszonego wstecz po korekcji nazwanej BBS-Coder.

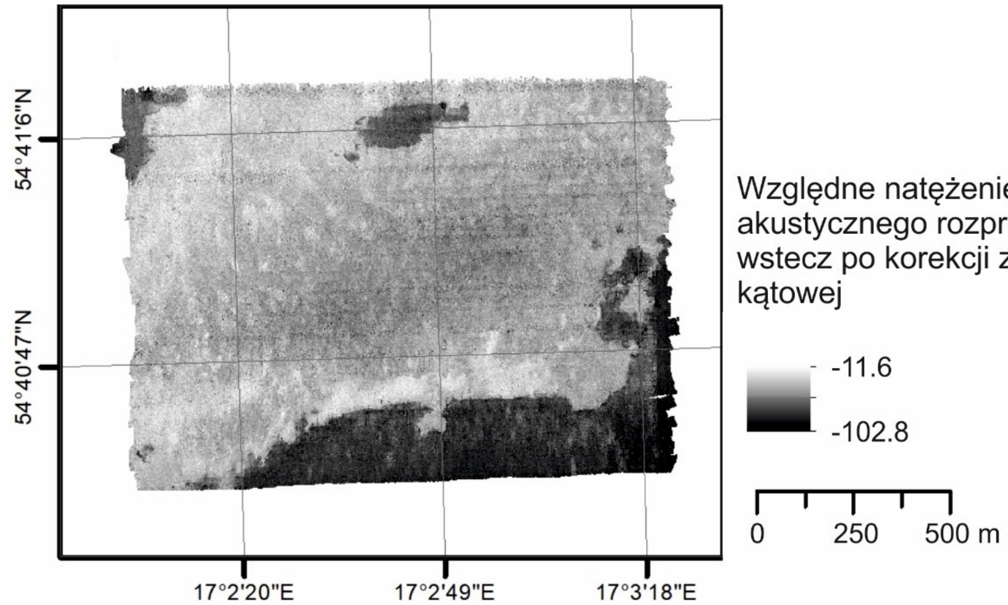

Rys. 6. Rezultat działania algorytmu BBS-Coder - mapa względnych wartości natężenia sygnałów akustycznych rozproszonych wstecz o wartościach przeliczonych do kąta padania 40° zarejestrowana w akwenie Rowy w południowym Bałtyku.

Narzędzie Geocoder (Fonseca i Calder 2005) umożliwiło przygotowanie map względnego natężenia sygnału akustycznego rozproszonego wstecz badanego obszaru bez zależności kątowych. Jednak dla kątów padania bliskich 0° otrzymano wysokie odchylenie standardowe wartości parametru prezentowanego na mapie. Geocoder przypisuje informację o ważności do próbek rozpraszania wstecznego. Dane dla kątów padania bliskich 0° i blisko 90° mają niską ważność, natomiast próbki w środkowym zakresie mają wyższe wartości i większy wpływ na końcową mapę mozaikową rozpraszania wstecznego (Fonseca i Calder 2005). W przypadku przedstawionej przeze mnie korekcji polegającej na zmiennym wzmocnieniu kątowym (publikacja 3), gdy w jednym oknie mapy rastrowej występowały dane o rozpraszaniu zarejestrowane z różnym kątem padania, wszystkie wartości zostały uśrednione zgodnie z przyporządkowaniem przestrzennym do siatki rastrowej. Przedstawiona przeze mnie metoda polegającej na zmiennym wzmocnieniu kątowym jest prostym i efektywnym narzędziem do przygotowania mapy mozaikowej rozpraszania wstecznego, przydatnej do klasyfikacji siedlisk dna morskiego.

Podsumowanie i wnioski

Przygotowując dysertację, wykonałam cyfrowy model dna badanego obszaru na północ od miejscowości Rowy w południowym Bałtyku oraz przygotowałam mapy parametrów widmowych modelu cyfrowego powierzchni dna. W celu zbadania akustycznej charakterystyki siedlisk dennych w badanym obszarze zmierzyłam i obliczyłam rzeczywiste wartości siły rozpraszania wstecznego sygnałów akustycznych. W dysertacji wykorzystałam bardzo efektywną metodę klasyfikacji wykorzystującą analizę obiektową, którą ulepszyłam o wykorzystanie parametrów widmowych cyfrowego modelu terenu. Ponadto opracowałam metodę ujednolicenia mapy natężeń sygnałów akustycznych rozproszonych wstecz nazwaną w publikacji 3 BBS-Coder, poprzez sprowadzenie natężenia sygnałów w całym badanym akwenie do wartości odpowiadających jednemu kątowi padania wiązki akustycznej na dno. Za jej pomocą przygotowałam mapę natężenia sygnału akustycznego rozproszonego wstecz sprowadzonego do kąta padania 40°.

Podsumowanie i wnioski dotyczące akustycznej klasyfikacji siedlisk bentosowych

Parametry widmowe opisujące dno morskie obliczone dla cyfrowego modelu terenu (publikacja 2) nie są zależne od zmiennych parametrów środowiska, takich jak natężenie sygnału rozproszonego wstecz od dna, dlatego dobrze realizują cel postawiony w dysertacji. Są ważne w opracowaniu powtarzalnych i jednorodnych metod klasyfikacji siedlisk dna morskiego. To zupełnie nowatorskie podejście umożliwia w sposób półautomatyczny i powtarzalny klasyfikować siedliska bentosowe południowego Bałtyku (publikacja 2) jak również znalazło zastosowanie w predykcji lądowych form postglacjalnych, co potwierdza skuteczność i uniwersalność metody (Janowski i in. 2021 - praca mojego współautorstwa nie wchodząca do dysertacji, opublikowana w IEEE Transactions on Geoscience and Remote Sensing, IF=5,6). Otrzymane wyniki badań potwierdzają wysoką efektywność parametrów widmowych w rozpoznawaniu siedlisk bentosowych, co potwierdza wysoka zgodność (86%) wyników klasyfikacji z próbkami osadów dennych w procesie walidacji (publikacja 2).

W pracy przedstawiłam osiem parametrów widmowych opisujących powierzchnię dna. Znaczenie parametrów widmowych zostało wyrażone za pomocą tak zwanego wskaźnika ważności (importance score) jako rezultatu algorytmu selekcji cech Boruta. Siedem z ośmiu zaproponowanych parametrów widmowych znacznie poprawiło moc predykcyjną klasyfikatorów nadzorowanych (publikacja 2). Najistotniejszymi parametrem w tym badaniu była mapa natężenia sygnału akustycznego rozproszonego wstecz od dna morskiego dla emitowanych sygnałów o częstotliwościach 400 kHz i 150 kHz. Natomiast kolejnym, istotnym parametrem był wymiar fraktalny obliczony z nachylenia widma. Co ciekawe, wyniki analizy algorytmu Boruta wskazują, że niektóre parametry widmowe mają większe znaczenie dla prawidłowej klasyfikacji niż batymetria, z której zostały obliczone. Na uwagę zasługuje fakt, że wszystkie inne wyekstrahowane cechy, w tym parametry geomorfologiczne, statystyczne i teksturalne batymetrii i natężenia sygnału akustycznego rozproszonego wstecz, nie zostały uznane za istotne. Wynik ten podkreśla, że zastosowanie parametrów widmowych może znacznie poprawić klasyfikację nadzorowaną i mapowanie siedlisk bentosowych. Przedstawiona przeze mnie metoda dowiodła swojej skuteczności na obszarze o złożonej geomorfologii. Odpowiednie zastosowanie nowych parametrów zwiększyło dokładność klasyfikacji w stosunku do prac przedstawionych w publikacji 1. Dodatkowo potwierdzono, że istnieją umiarkowane różnice w rozpraszaniu wstecznym badanych siedlisk dla częstotliwości 150 kHz i 400 kHz i oba te parametry mają wysoki wskaźnik ważności. Potwierdza to użyteczność podejścia wieloczęstotliwościowego w mapowaniu siedlisk dennych.

Można zauważyć duże podobieństwo między mapami parametrów widmowych a niektórymi cechami mapy względnego natężenia sygnału akustycznego rozproszonego wstecz. Jest ono niezwykle istotne dla mocy predykcji klasyfikatorów nadzorowanych. Parametry widmowe mogą być bardzo przydatne do mapowania siedlisk bentosowych, gdy dostępna jest tylko batymetria. Jednak uwzględnienie parametrów spektralnych wymaga danych batymetrycznych o wysokiej rozdzielczości i jakości. Wszelkie artefakty związane z błędami podczas pomiarów echosondą wielowiązkową mogą zniekształcić obraz batymetryczny i wpływać na obliczone wartości parametrów widmowych. Jednakże nowoczesne systemy kompensacji ruchu podczas pomiarów echosondą wielowiązkową dobrze radzą sobie z korygowaniem tych błędów.

Kolejnym ciekawym zagadnieniem może być wykorzystanie tego typu parametrów widmowych do klasyfikacji cyfrowych modeli terenu o różnym pochodzeniu. Przykładem takiego zastosowania jest klasyfikacja morfologiczna form polodowcowych z wykorzystaniem cyfrowego modelu terenu między innymi z pomiarów lidarowych (Janowski i in. 2021 - praca mojego współautorstwa nie wchodząca do dysertacji, opublikowana w IEEE Transactions on Geoscience and Remote Sensing, IF=5,6).

Przedmiotem dalszych badań powinno być ustalenie optymalnej wielkości okna przesuwnego, w którym obliczane są parametry widmowe, aby mały jak największy wpływ na prawidłową predykcję siedlisk.

Podsumowanie i wnioski o pomiarach rzeczywistej siły rozpraszania wstecznego

Akustyczna kalibracja echosondy wielowiązkowej umożliwia pomiar wartości rzeczywistej siły rozpraszania wstecznego, które są istotną geoakustyczną cechą siedlisk bentosowych i są pomocne w ich dyferencjacji. Niestety wyniki pomiarów bezwzględnych wartości siły rozpraszania wstecznego zarejestrowanych echosondą wielowiązkową przedstawiających całą zależność kątową są niezwykle rzadkie i niewystarczające (Wendelboe 2018; Eleftherakis 2018). Każda fizycznie poprawna metoda kalibracji poprawia jakość danych i dostarcza cennych informacji. Przedstawiona przeze mnie w publikacji 3 metodyka uzyskania bezwzględnych wartości siły rozpraszania wstecznego umożliwia odtworzenie procesu pomiaru i analizy danych poprzez wykorzystanie skalibrowanej przez producenta echosondy i uzupełnienie o korekcję związaną z powierzchnią rewerberacji oraz korekcją kątów padania. Ważność bezwzględnych wartości siły rozpraszania wstecznego sprawia, że należy zawsze, gdy to możliwe stosować skalibrowane akustycznie echosondy.

Względne wartości natężenia sygnału akustycznego rozproszonego wstecz były skutecznie wykorzystywane do klasyfikacji siedlisk bentosowych (publikacja 1; Gaida i in. 2020; Buscombe i in. 2014; Preston 2009), jednak dla bardziej zaawansowanych analiz środowiskowych konieczne jest określenie bezwzględnych wartości siły rozpraszania wstecznego. Przykładem jest badanie zmienności dobowej i sezonowej rozpraszania wstecz przez trawy morskie, ponieważ różnica poziomu siły rozpraszania wstecznego o kilka dB może decydować o zmienności (Feldens i in. 2018). Rejestracje względnych wartości rozpraszania wstecznego od dna morskiego przeprowadzone w innym czasie w innych obszarach a często za pomocą innego modelu echosondy wielowiązkowej dają bardzo odmienne wyniki dla tych samych siedlisk bentosowych. Użycie bezwzględnych wartości siły rozpraszania wstecznego umożliwi porównanie tych wyników. Należy jednak pamiętać, że pozornie podobne siedliska denne mogą znacznie różnić się od siebie właściwościami fizycznymi, takimi jak liczba i wielkość pęcherzyków gazowych w osadzie, gęstość osadu i innych, co wpływa na powstanie różnic w bezwzględnych wartościach siły rozpraszania wstecznego. Konieczne są intensywne badania, aby poznać rzeczywiste wartości rozpraszania wstecz różnych siedlisk bentosowych. Przykłady pomiarów przedstawionych w różnych badaniach wskazują na dużą zmienność rzeczywistej siły rozpraszania wstecznego, dlatego ważne jest znalezienie empirycznych wartości granicznych rzeczywistej siły rozpraszania wstecznego dla konkretnych siedlisk w różnych basenach. Przedstawione dotychczas badania opisujące charakterystyki kątowe rzeczywistej siły rozpraszania wstecznego są bardzo rzadkie i niewystarczające do poznania cech siedlisk bentosowych, dlatego w publikacji 3 opisałam ten problem, przedstawiłam sposób korekcji danych oraz charakterystyki siedlisk dennych badanego obszaru w południowym Bałtyku. To jedna z pierwszych tego typu prac na świecie.

W publikacji 3 przedstawiłam kątową zależność rzeczywistej siły rozpraszania wstecznego dla pięciu siedlisk bentosowych w Morzu Bałtyckim przy częstotliwości sygnału akustycznego 150 kHz. Korekcje zarejestrowanych danych o rozpraszaniu obejmowały wykorzystanie skalibrowanej akustycznie echosondy wielowiązkowej, korekcję nachylenia dna w obszarze rewerberacji sygnału oraz zastosowanie powierzchni rewerberacji.

Wyniki pomiarów rzeczywistej siły rozpraszania wstecznego w funkcji kąta padania przedstawione w publikacji 3 są zbieżne z przewidywaniami teoretycznymi jak również z wynikami uzyskanymi przez innych autorów, którzy przeprowadzili pomiary echosondą wielowiązkową (Eleftherakis 2018; Fonseca i in 2009). W przedstawionych przeze mnie badaniach dla kątów padania od 25 do 65 krzywa bezwzględnych wartości siły rozpraszania wstecznego wykazała znaczny spadek wartości większy niż w modelu APL (APL-UW 1994) przy 100 kHz. Może to być związane z wyższą częstotliwością stosowanego sygnału - 150 kHz.

W niektórych badaniach zauważono trend rosnącej wartości rzeczywistej siły rozpraszania wstecznego wraz ze wzrostem częstotliwości [Williams i in. 2002; Williams i in. 2009]. Wyższe wartości rzeczywistej siły rozpraszania wstecznego dla wyższych częstotliwości mogą być związane z silnym rozpraszaniem sygnałów na chropowatej powierzchni dna, natomiast stopień nierówności dna jest opisany parametrem Rayleigha i zależy od długości fali akustycznej, skali nierówności obecnych na powierzchni rozpraszającej i kąta padania (Ogilvy 1991).

Rzeczywiste wartości siły rozpraszania wstecznego są bardzo potrzebne do charakterystyki siedlisk bentosowych i stanowią ich ważną akustyczną właściwość. Zróżnicowane charakterystyki kątowe o znanym nachyleniu krzywej i znanym zakresie wartości dla odpowiednich siedlisk dennych mogą w przyszłości posłużyć do klasyfikacji z właściwym przypisaniem obszarów do klas siedlisk pomimo małej liczby próbek osadów dennych lub ich braku. Rzeczywiste wartości siły rozpraszania wstecznego umożliwią lepsze niż dotychczas zrozumienie procesów środowiskowych zachodzących na dnie morskim a ich poznanie jest częścią badań podstawowych.

Podsumowanie i wnioski o BBS-Coder

Do analizy obiektowej (OBIA), analizy teksturalnej (GLCM) czy automatycznej klasyfikacji niezbędne są skartowane wartości siły rozpraszania wstecznego bez widocznej zależności kątowej. Najczęściej stosowanym narzędziem pozwalającym na sprowadzenie wartości sygnałów rozproszonych wstecz do jednego kąta padania jest Geocoder (Fonseca i Calder 2005).

W mapach mozaikowych względnego natężenia sygnału akustycznego rozproszonego wstecz badanego obszaru przygotowanych za pomocą narzędzia Geocoder występują duże błędy dla kątów padania bliskich 0°, dlatego opracowałam własną metodę korekcji. Sprowadza ona siłę rozpraszania wstecznego do wybranego kąta padania równego 40 stopni i w efekcie redukuje wpływ kąta padania.

Przedstawiony algorytm do korekcji polegającej na zmiennym wzmocnieniu kątowym BBS-Coder (publikacja 3) jest prosty i efektywny. Zostanie udostępniony do szerokiego użytku na stronie projektu ECOMAP (https://www.bonus-ecomap.eu/). Bardzo dobra jakość map rozpraszania wstecznego utworzonych za pomocą BBS-Coder wskazuje na ich przydatność do kartowania siedlisk bentosowych i zrównoważonego zarządzania zasobami dna morskiego.

ABSTRACT

Oceanographic studies often involve identification of the seabed – its shape, sediment type, coverage by phyto- or zoobenthic colonies, and thus the presence of benthic habitats. Various bathymetry features and backscattered acoustic signal intensity information recorded by multibeam echosounders have been successfully used to separate areas of distinct habitats (Diesing and Thorsnes 2018; Lecours et al. 2015; Held and Schneider von Deimling 2019). The use of a gyrocompass and measurement of position during surveys enable the production of accurately located maps with spatial resolution of several centimeters (Montereale Gavazzi et al. 2016). Recordings made with multibeam echosounders have been used with great success in recent years for seafloor mapping. They allow simultaneous recording of bathymetric data at several hundred points and, during the movement of the survey vessel, produce an accurate model of the seabed and a map of the intensity of the backscattered acoustic signal. The results of these works are very useful for navigation authorities and for investors planning structures located on the seabed. Seabed surveys are also extremely important in times of rapid climatic and environmental change, allowing the monitoring of the seabed environment and the benthic habitats present. Mapping and classification of benthic habitats provides the information necessary to establish Marine Protected Areas. Such activities are included in Marine Strategy Framework Directive 2008/56/EC, Water Framework Directive 2000/60/EC and Habitats Directive 92/43/EEC. These include the need to develop methods for mapping and monitoring the seabed.

In addition to bathymetric information, the most commonly recorded information about the seabed with a multibeam echosounder is the relative intensity of the backscattered acoustic signal. It depends on factors related to the measuring device, such as signal frequency, receiver sensitivity, directional characteristics of the transducer; factors related to the environment through which the acoustic wave and the returning signal are transmitted, such as temperature and salinity; factors related to geophysical features of the seabed, such as seafloor surface roughness or sediment density. In addition, the relative intensity of the acoustic signal backscattered from the seabed, recorded by a multibeam echosounder, shows a strong dependence on the angle of incidence on the seabed. Figure 1 shows an example of this relationship recorded during my research.

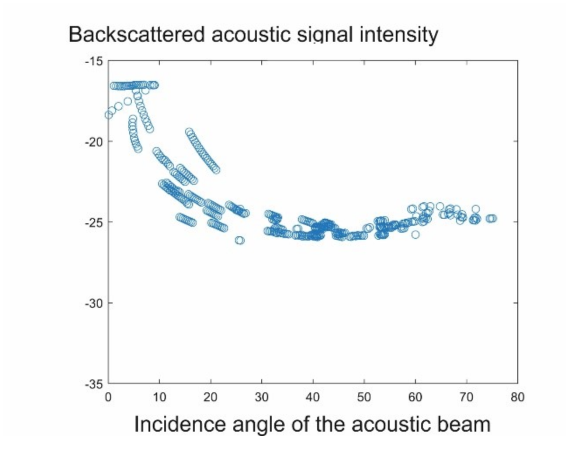

Fig. 1. Example of the angular dependence of the intensity of an acoustic signal backscattered from the seafloor.

The information contained in backscattered signals is used in non-invasive seafloor classification algorithms; however, the angular dependence of the intensity of such a signal makes correct classification very difficult. The problem to be solved is to unify the intensity map of backscattered acoustic signals by bringing the intensity of the signals throughout the study area to values corresponding to a single angle of incidence of the acoustic beam on the bottom. An example of such a correction was implemented in the commercial FMGT QPS software with a tool called Geocoder (Fonseca and Calder 2005). I prepared maps of the relative intensity of backscattered signals over the study area using the Geocoder tool, but I observed large errors in such maps for incidence angles close to 0°. Therefore, I decided to develop my own angle varying gain method (publication 3), which was a challenging task.

Acoustic seafloor classification and mapping using repeatable, automated methods still needs improvement, despite the progress made in recent years. Seabed parameters calculated for bathymetry and intensity of backscattered acoustic signals are directly related to the spatial extent of habitats and often used in seabed classification. Some recent publications highlight the need for new parameters describing the seafloor for benthic habitat mapping (Diesing et al. 2016), so I used spectral parameters calculated from a digital terrain model that are completely new to supervised benthic habitat classification.

The results of backscattered acoustic signal intensity measurements presented by researchers, made using different frequencies of the emitted signal or during separate measurement cruises, usually differ significantly in the ranges of values. This makes it difficult to conduct an automatic or semi-automatic classification of benthic habitats. The observed differences are influenced by a number of factors such as the frequency of the emitted acoustic signal, changing absorption of acoustic waves in the water during different measurements, or the direction of the vessel during the measurements as well as changing physical parameters describing the bottom surface and the sediment present on it.

Although relative intensities of bottom backscattered signals are often used in research work, they do not inform about the actual scattering properties, because their value depends not only on the type of sediment on the bottom, but also on the measuring device and factors related to the parameters of the pulse sent. It is the real values of bottom backscattering strength (BBS) that are an immanent feature of benthic habitats. To record them, it is necessary to use an acoustically calibrated echosounder, correct the result for sound absorption in the water and for losses associated with geometric sound propagation, and to take into account the size of the surface from which the recorded signal was scattered. Acoustic calibration of a multibeam echosounder is not a simple task. Recently, acoustically calibrated multibeam echosounders from Kongsberg and NORBIT have been available on the market. There is still very little information in the literature on the real values of backscattering strength of different benthic habitats for signal frequencies above 100 kHz. Theoretical models of the scattering of acoustic signals on the seabed work for the frequency range from 10 kHz to 100 kHz (APL-UW model 1994). Many singlebeam echosounders use signals with frequencies within this range, while multibeam echosounders and sidescan sonars use much higher frequencies. Researchers still lack detailed information on the backscattering of sound from the seafloor for sonar signal frequencies greater than 100 kHz. Angular characteristics of the actual backscattering strength are a physical feature of benthic habitats and are an important acoustic property thereof. Knowledge of these characteristics of benthic habitats will enable the creation of a catalog of backscattered acoustic signal intensities dependent on signal frequency, angle of incidence, and environmental parameters. This will enable a better understanding of environmental processes occurring on or affecting the seafloor than has been possible to date.

Measuring the absolute values of the angular dependence of backscattering strength is also necessary to assess spatial and temporal variability in benthic habitat characteristics. The relative strength of backscattered signals has been the most effective parameter for benthic habitat classification in many works (publication 1; Gaida et al. 2020; Buscombe et al. 2014; Preston 2009). This emphasizes the importance of this parameter and draws attention to the need to measure it as accurately as possible so that it can be used for research in the most efficient way (Lurton and Lamarche 2015).

Thesis Objectives

The main objective of the dissertation is to build a reliable system for acoustic characterization of seabed habitats, which consists of:

- building a digital model of the seabed of the studied regions together with its parameterization,
- building a map of the intensity of the backscattered acoustic signal brought to a single angle of incidence,
- determining the angular characteristics of the absolute strength of the acoustic signal backscattered from the seabed for signals of selected frequency.
- non-invasive classification of benthic habitats.

Furthermore, the objective of this dissertation is to find parameters describing the seabed surface that increase the prediction power in supervised classification and are not dependent on the frequency of the signal used when recording the seabed with a multibeam echosounder and are also not dependent on other changes in relative acoustic signal intensity values during different measurement campaigns. An additional objective is to develop an in-house empirical algorithm for correcting the angular dependence of the backscattered signal intensity, which enables further use of this parameter in the classification process.

Study area

To test the new research methods, an area of the seabed was selected, which comprises different types of benthic habitats within a small area. Bathymetric data and backscattered signal intensities were recorded with a multibeam echosounder in a survey area of ~1.4 km^2 located about 1.5 km north of the port of Rowy in the southern Baltic Sea (publication 1; publication 2; publication 3). A digital bathymetry model and a map of relative intensities of acoustic signal backscattered from the bottom were prepared from the recorded data. In the study area, there are areas covered with very fine sand (VFS), sand or sand with gravel locally forming ripple marks (S), sandy gravel or gravelly sand (SG-GS), boulders and pebbles covered with mussels *Mytilus trossulus* (B), boulders and pebbles covered with mussels *Mytilus trossulus*, overgrown with red algae (R), and an artificial structure, i.e. a shipwreck (A). Sediment samples were collected with a Van Veen grab sampler and video recordings were made with a camera on a remotely operated vehicle (ROV). A total of 57 seabed locations were surveyed and inventoried. The collected sediment samples were analyzed in a laboratory to determine their granulometric composition, while locations of large boulders where sediment samples could not be obtained were visually assessed from recorded video. Inventory points were then assigned to the six groups listed previously (Folk and Ward 1957; Wentworth 1922).

Description of the work carried out as part of the dissertation

Classification of benthic habitats

In recent years, hydroacoustic studies have intensively searched for the best possible methods of geomorphological analysis of the seafloor (Goff and Jordan 1988; Wilson et al. 2007; Micallef et al. 2012; Diesing and Thorsnes 2018; Gafeira et al. 2018; Lucieer et al. 2018). Different methods are used to classify benthic habitats (Diesing et al. 2020), which can generally be divided into supervised and unsupervised classification, where the number and characteristics of the resulting classes are not distinguished at the beginning of the process. Often, bottom sediment samples are used to determine the classes and where they occur in situ. During clustering based on parameter map analysis, classes may be assigned to individual pixels or pixels grouped into objects with similar features. Finally, the way of assigning data to different groups can be done by different methods such as support vector machine, random forest, k-means clustering algorithm, k-nearest neighbors, classification and regression trees, neural networks (Diesing et al. 2020; publication 1; publication 2). The points inventoried on the seafloor can be divided into two groups – a training group that participates in "teaching" the algorithm for correct class assignment and a validation group for checking the correctness of the prediction. The classification method based on supervised object-based analysis implemented in eCognition software using multi-scale segmentation, the Boruta feature selection algorithm and comparison of the results of several classification algorithms produces very good results described, among others, by an overall accuracy of more than 80% (publication 1; Janowski et al. 2020) was therefore selected for habitat classification in my study.

In the case of supervised object-based analysis (publication 1; publication 2), the input factors for classification are bottom sediment samples, bathymetric maps, maps of relative intensity of the acoustic signal backscattered from the seafloor, and maps of parameters calculated from these. Statistical parameters calculated in many works for bathymetry include slope, aspect, curvature and standard deviation. Examples of parameters calculated for relative intensity of backscattered signal maps are standard deviation and textural parameters (gray level co-occurrence matrices – GLCM) (Haralick et al. 1973; Montereale Gavazzi et al. 2017; Prampolini et al. 2018; Samsudin and Hasan 2017), including homogeneity and contrast. In the study of benthic habitat classification methods, analyses at multiple spatial scales deserve special attention (Lecours et al. 2015; Misiuk et al. 2018). There are many possible parameters to prepare maps, so it is important to determine which of them significantly describe the study area. This is accomplished through the Boruta feature selection algorithm (Kursa and Rudnicki 2010), determining the importance score, or by principal component analysis (Jolliffe 2002), which determines the degree of cross-correlation of individual variables. For habitat clustering, parameter maps that significantly describe the variability of the study area and are not highly correlated with each other should be selected (publication 2).

One of the recent trends in benthic habitat mapping is the use of multifrequency data recorded by multibeam echosounders. The frequency dependence of backscattered acoustic signal intensity has been observed in laboratory and field studies, testing the value of this parameter for different sediment types (publication 1; Jackson et al. 1986; Urick 1983; Feldens et al. 2018; Gaida et al. 2018). Acoustic recordings of seafloor sediments conducted at several frequencies often provide more information on physical and biological properties of seafloor habitats compared to studies using a single frequency. It has been observed that fine sediments such as sands and silts scatter acoustic signals at a given frequency differently than coarser sediments such as gravel, shells, or boulders (Jackson et al. 1986; Gaida et al. 2018).

Lyons et al. (2002) described one of the first applications of the Two-Dimensional Fourier Transform (2D FFT) to high-resolution seafloor characterization. The use of 2D FFT made it possible to obtain a spatial distribution of the power spectral density of the digital terrain model. The same technique has been used in several other studies (e.g., Briggs et al. 2005). The method has been improved and applied to analyze high-resolution bathymetry obtained from modern hydroacoustic measurements, including multibeam echosounders (Cazenave et al. 2008; Lefebvre et al. 2009). Schönke et al. (2017) applied the Fourier transform to describe seafloor micro irregularities using underwater laser scanning in the southeastern North Sea.

For the classification of benthic habitats, I proposed to use parameters describing the study area, calculated from the digital seabed model. I introduced a new group of spectral parameters calculated from the digital seabed model into the object analysis (publication 2). These are: spectral moment m0, spectral moment m2, mean frequency, spectral width, spectral skewness, Q-factor, spectral skewness defined for central moments, and fractal dimension. I divided the digital bottom model into small squares, each successive square overlapping 90% of the position of the previous one and in each square I calculated the power spectral density using the 2D FFT algorithm (Fig. 2).

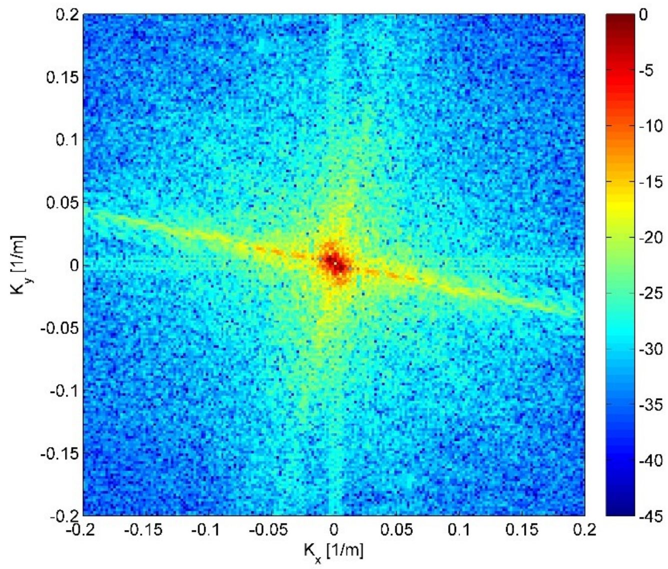

Fig. 2. Example of power spectral density computed in a window covering a section of a digital elevation model.

In each of the windows (Fig. 2), I made cross-sections of the power spectral density every 5 degrees and calculated the spectral parameters from the thus obtained two-dimensional cross-sections. The averaged results of a parameter from each window were combined into a map of the spatial distribution of that parameter in the studied area. In Fig. 3, I have presented an example of the parameter – spectral moment 2, which was calculated in a 20x20 m window.

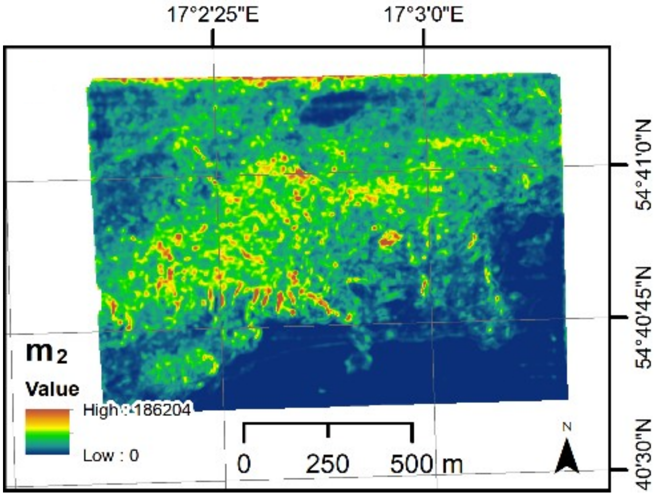

Fig. 3. Distribution map of the spectral moment (m2) values, calculated in a 20x20 m moving window.

In publication 2, a set of sample parameter maps that may be involved in the seafloor classification process was prepared, including statistical parameters, spectral parameters, and gray level co-occurrence matrices. It was then verified which of the 62 parameter maps were most relevant for supervised classification using the Boruta feature selection algorithm (Kursa and Rudnicki 2010). This feature selection algorithm uses random forest (RF) machine learning (Breiman 2001). OBIA object-based classification was implemented using eCognition software (publication 1; publication 2; Blaschke 2010; Janowski et al. 2020). In the multi-resolution segmentation algorithm (MS), pixels with similar features were combined into groups with specific shapes and sizes (Benz et al. 2004). The best classification result was achieved with the method – Support Vector Machine (SVM). An overall prediction accuracy of 86% was obtained when comparing the classification result with a set of validation sediment samples.

The absolute value of the bottom backscattering strength

The IHO Hydrographic Standards (2008) describe in detail the quality of multibeam echosounder bathymetric measurements, but the standards associated with multibeam backscatter echosounder measurements are extremely rare in the literature. The compendium "Backscatter measurements by seafloor-mapping sonars: Guidelines and Recommendations", developed by the BSWG GeoHab group, is the first document of its kind to focus on the quality of backscattered acoustic signal intensity data recorded by a multibeam echosounder (Lurton and Lamarche 2015). The intensity of backscattered acoustic signals should be recorded with acoustically calibrated devices, giving access to the real strength of backscattering (Lurton and Lamarche 2015; Eleftherakis et al. 2018).

Providing real values of seafloor backscattering strength requires the use of a sonar whose characteristics and sensitivity during signal transmission and reception are well determined at a given frequency and angle of incidence on the seafloor. Furthermore, it requires the use of accurate transmission loss compensations and reverberation surfaces (Lurton and Lamarche 2015; Eleftherakis et al. 2018). In recent years, results of only a few studies of benthic habitats using an acoustically calibrated multibeam echosounder have been published (Wendelboe 1018; Eleftherakis et al. 2014; Weber et al. 2018; Roche et al. 2018). These papers present selected characterizations of the real backscattering strength for several habitat types using signals of different frequencies under known environmental parameters. When such measurements become frequent, it will be possible to create a comprehensive catalog showing the angular characteristics of the real backscattering strength for different benthic habitats.

For the measurements presented in publication 3, I used an iWBMSh multibeam echosounder (model STX) acoustically calibrated by its manufacturer, NORBIT. Additionally, the recorded backscattering intensity values were corrected by me for the size of the reverberation area and assigned to the angles of incidence of the acoustic beam on the bottom. In the publication, I presented curves showing the angular dependence of the real backscattering strength for benthic habitats present in the study area for an acoustic signal at 150 kHz. This is an extremely important result in the context of understanding the acoustic characteristics of benthic habitats.

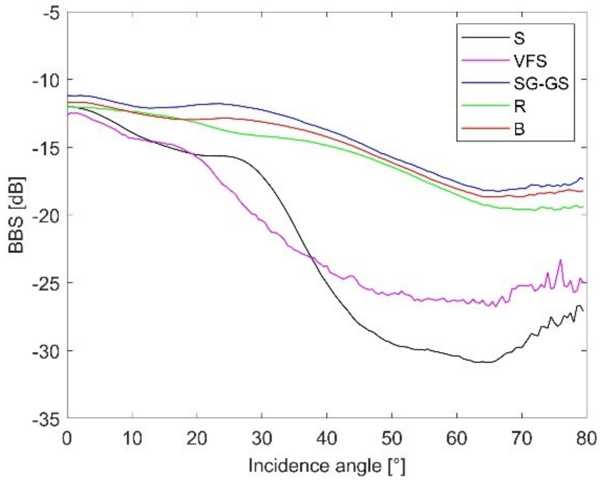

Fig. 4. Results of the real value of the backscattering strength as a function of incidence angle for areas covered with very fine sand (VFS), sand or sand with gravel locally forming ripple marks (S), sandy gravel or gravelly sand (SG-GS), boulders and pebbles covered with mussels *Mytilus trossulus* (B), boulders and pebbles covered with mussels *Mytilus trossulus*, overgrown with red algae (R) for acoustic signals of 150 kHz.

The real values of backscattering strength obtained in the study were as follows: –12 to –31 dB for areas covered with sand or sand with gravel locally forming ripple marks (S); –12.5 to –27 dB for areas covered with very fine sand (VFS); –10.5 to –18 dB for sandy gravel or gravelly sand (SG–GS); –12 to –20 dB for boulders and pebbles covered with *Mytilus trossulus* and overgrown with red algae (R); and –11.5 to –18 dB for boulders and pebbles covered with *Mytilus trossulus* (B).

For macroscale flat seabed types (areas covered with very fine sand, areas covered with sand or sand with gravel locally forming ripple marks), I observed a large reduction in the real backscattering strength with increasing deviation of the wave direction from vertical, and for more irregularly shaped seabed types (sandy gravel or gravelly sand, boulders and pebbles covered with the bivalve *Mytilus trossulus*, boulders and pebbles covered with the bivalve *Mytilus trossulus* and overgrown with red algae), the decrease in the value of the real backscattering strength for more tilted beams was smaller. The real backscattering strength values obtained for sandy gravel or gravelly sand, boulders and pebbles covered with clams *Mytilus trossulus* and overgrown with red algae, and boulders and pebbles covered with *Mytilus trossulus* were higher than for areas covered with sand or sand with gravel locally forming ripple marks and areas covered with very fine sand. The absolute backscattering strength curves for areas covered with sand or sand with gravel locally forming ripple marks and areas covered with very fine sand in the studies I have presented had characteristic shapes typical of the fine-grained sediment curve in the APL-UW model (1994).

Angle varying gain correction of the relative intensity of the signal backscattered from the seabed

The relative intensity of the backscattered acoustic signal shows a strong dependence on the angle of incidence. Fig. 5 shows an example map of the relative intensity values of backscattered signals as a function of incidence angle recorded by me in the measurement area.

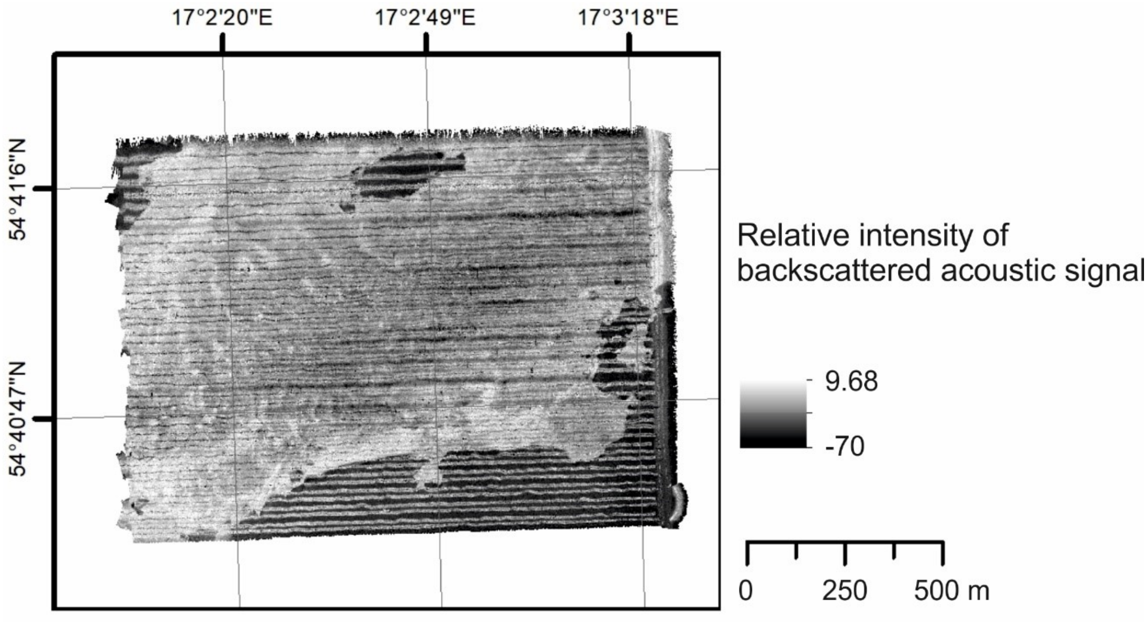

Fig. 5. Map of relative intensity values of backscattered acoustic signals recorded in the Rowy area in the southern Baltic Sea.

I developed an empirical correction method based on angle varying gain (publication 3). It uses averaged values of the measured backscattered acoustic signal intensity rather than model assumptions as is done in the standard Geocoder software. High quality backscattering maps reduced to a single angle of incidence are necessary to perform accurate benthic habitat classification. I reduced all backscattered acoustic signal intensity measurements in the study area to values corresponding to backscattering for an incidence angle of 40° in order to produce a homogeneous map that is easy to interpret and further use in programs that perform classification. The algorithm I propose makes it possible to bring the backscattering strength to any angle of incidence of the acoustic beam on the seabed.

The novel correction procedure involves dividing the data recorded by the multibeam echosounder into groups, each containing a sequence of 50 impulses and each impulse containing several hundred recorded received signals (the echosounder used operated on 512 receiver beams). For simplicity, I assumed that the backscattering properties of the acoustic signal from the seabed were constant in each sequence of recorded pulses. I assigned each recorded signal to an appropriate incidence angle interval. From all the data recorded in a given sequence, I calculated average values of the backscattered acoustic signal intensity for different incidence angles. I then checked what value corresponded to an incidence angle of 40 degrees and calculated the correction factor for each incidence angle. I multiplied each recorded backscattered acoustic signal intensity value with the correction factor appropriate for that incidence angle. The correction factors were calculated separately for each sequence of 50 impulses.

In Fig. 6, I have presented a map of the relative intensity values of backscattered acoustic signals with values converted to an incidence angle of 40°. The result of the correction procedure is shown as a map of the calculated values of the relative intensity of the backscattered acoustic signal after the correction called BBS-Coder.

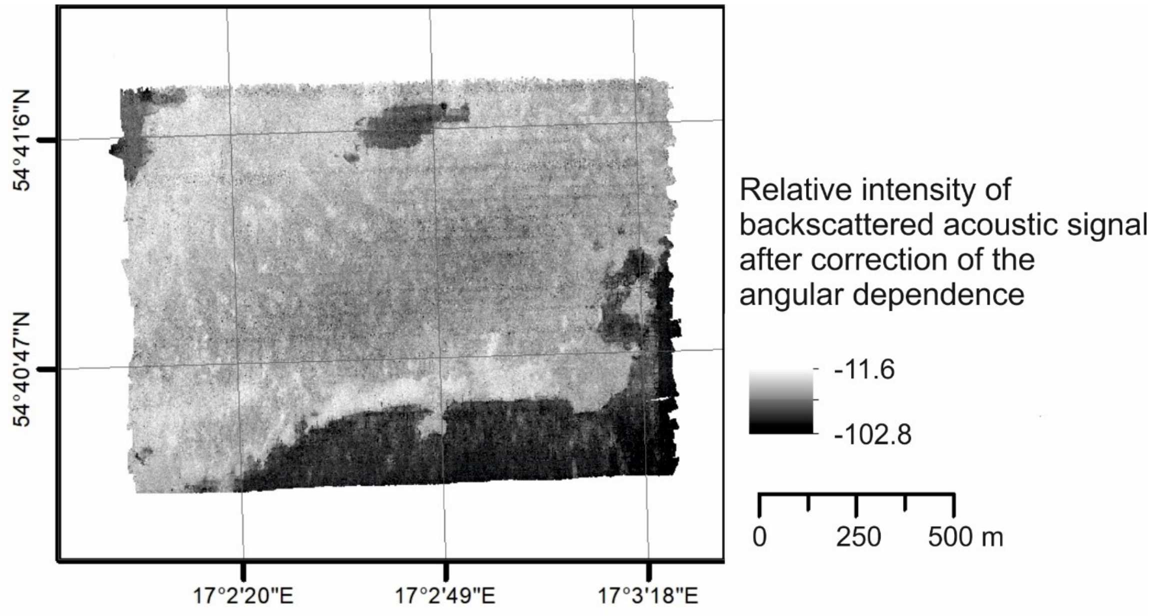

Fig. 6. Result of the BBS-Coder algorithm – a map of relative intensities of backscattered acoustic signals converted to 40° incidence angle, recorded in the Rowy area in the southern Baltic Sea.

The Geocoder tool (Fonseca and Calder 2005) allowed the preparation of maps of the relative intensity of the backscattered acoustic signal of the study area without angular dependence. However, for incidence angles close to 0°, a high standard deviation of the parameter value presented in the map was obtained. The Geocoder assigns validity information to backscattering samples. Data for incidence angles near 0° and near 90° have low validity, while samples in the middle range have higher validity values and greater influence on the final backscattering mosaic map (Fonseca and Calder 2005). In the case of the angle varying gain correction I presented (publication 3), when scattering data recorded with different incidence angles were present in a single raster map window, all values were averaged according to the spatial assignment to the raster grid. The method I have presented, based on angle varying gain, is a simple and effective tool for preparing a backscatter mosaic map useful for seabed habitat classification.

Summary and conclusions

While preparing the dissertation, I created a digital model of the seabed of the study area north of Rowy in the southern Baltic Sea and prepared maps of spectral parameters of the digital model of the seabed surface. To investigate the acoustic characteristics of the benthic habitats in the study area, I measured and calculated the real backscattering strength of acoustic signals. In the dissertation, I used a very effective classification method using object-based analysis, which I improved by using spectral parameters of the digital terrain model. In addition, I developed a method to unify the intensity map of backscattered acoustic signals, referred to in publication 3 as BBS-Coder, by bringing the signal intensities throughout the study area to values corresponding to one angle of incidence of the acoustic beam on the seabed. Using it, I prepared a backscattered acoustic signal intensity map reduced to an incidence angle of 40°.

Summary and conclusions on acoustic classification of benthic habitats

The spectral parameters describing the seafloor calculated for the digital elevation model (publication 2) are not dependent on variable environmental parameters, such as the intensity of the signal backscattered from the seafloor, and therefore fulfill well the objective set in the dissertation. They are important in developing repeatable and homogeneous methods for seafloor habitat classification. This completely novel approach makes it possible to semi-automatically and repeatably classify benthic habitats of the southern Baltic Sea (publication 2) and has also been applied in the prediction of terrestrial postglacial forms, which confirms the effectiveness and universality of the method (Janowski et al. 2021 – my co-authored paper not included in the dissertation, published in IEEE Transactions on Geoscience and Remote Sensing, IF = 5.6). The obtained results confirm the high efficiency of spectral parameters in identifying benthic habitats, which is evidenced by the high agreement (86%) of classification results with bottom sediment samples in the validation process (publication 2).

In this publication 2, I have presented eight spectral parameters describing the seafloor surface. The importance of the spectral parameters was expressed by the so-called importance score as a result of the Boruta feature selection algorithm. Seven of the eight proposed spectral parameters significantly improved the predictive power of the supervised classifiers (publication 2). The most significant parameter in this study was the intensity map of the backscattered acoustic signal from the seabed for the emitted signals at 400 kHz and 150 kHz. The next significant parameter was the fractal dimension calculated from the slope of the spectrum. Interestingly, the results of the Boruta algorithm analysis indicate that some spectral parameters are more important for correct classification than the bathymetry from which they were calculated. It is noteworthy that all other extracted features, including geomorphological, statistical and textural parameters of bathymetry and backscattered acoustic signal intensity, were not identified as significant. This result highlights that the use of spectral parameters can significantly improve supervised classification and mapping of benthic habitats. The method I presented proved its effectiveness in an area with complex geomorphology. The appropriate use of new parameters increased the classification accuracy over the work presented in publication 1. In addition, it was confirmed that there are moderate differences in the backscattering of the studied habitats for 150 kHz and 400 kHz, and both parameters have a high validity index. This confirms the utility of the multi-frequency approach in mapping benthic habitats.

A strong similarity can be observed between the spectral parameter maps and some features of the relative intensity map of the backscattered acoustic signal. It is extremely important for the predictive power of supervised classifiers. Spectral parameters can be very useful for mapping benthic habitats when only bathymetry is available. However, the inclusion of spectral parameters requires high resolution and quality bathymetric data. Any artifacts associated with errors during multibeam echosounder measurements can distort the bathymetric image and affect the calculated spectral parameter values. However, modern motion compensation systems during multibeam echosounder measurements are good at correcting these errors.

Another interesting issue may be the use of such spectral parameters for classification of digital terrain models of different origins. An example of such an application is the morphological classification of glacial forms using a digital terrain model from i.a. lidar measurements (Janowski et al. 2021 – my co-authored paper not included in dissertation, published in IEEE Transactions on Geoscience and Remote Sensing, IF = 5.6).

Further research should focus on determining the optimal size of the sliding window in which spectral parameters are calculated to have as much influence as possible on the correct prediction of habitats.

Summary and conclusions about measurements of the real backscattering strength

Acoustic calibration of the multibeam echosounder allows measurement of real values of the backscattering strength, which are an important geoacoustic feature of benthic habitats and are helpful in their differentiation. Unfortunately, the results of measuring values of the real backscattering strength recorded with a multibeam echosounder representing the entire angular relationship are extremely rare and insufficient (Wendelboe 2018; Eleftherakis 2018). Any physically correct calibration method improves data quality and provides valuable information. The methodology I present in publication 3 for obtaining real absolute values of backscattering strength makes it possible to replicate the measurement and data analysis process by using the manufacturer's calibrated echosounder and supplementing it with corrections related to the reverberation area and incidence angle corrections. The validity of absolute values of backscattering strength makes it necessary to use acoustically calibrated echosounders whenever possible.

Relative values of backscattered acoustic signal strength have been effectively used to classify benthic habitats (publication 1; Gaida et al. 2020; Buscombe et al. 2014; Preston 2009), but for more advanced environmental analyses, real values of backscattering strength are needed. An example is the study of diurnal and seasonal variability of backscattering by seagrasses, as a difference of a few dB in the backscattering strength level can determine the variability (Feldens et al. 2018). Recordings of relative values of backscatter from the seabed made at different times in different areas and often using a different multibeam echosounder model give very different results for the same benthic habitats. Using absolute values of backscattering strength will allow a comparison of these results. However, it is important to keep in mind that apparently similar benthic habitats may differ significantly in physical properties, such as the number and size of gas bubbles in the sediment, sediment density, and others, which contributes to differences in absolute values of backscattering strength. Intensive research is necessary to determine absolute backscattering strength values of different benthic habitats. Examples of measurements presented in various studies indicate a large variation in real backscattering strength, so it is important to find empirical limits of the actual backscattering strength for specific habitats in different basins. The studies presented so far describing the angular characteristics of the real backscattering strength are very rare and insufficient to know the characteristics of benthic habitats, therefore in publication 3 I described this problem, presented the method of data correction and the characteristics of benthic habitats of the study area in the southern Baltic Sea. This is one of the first works of this kind in the world.

In publication 3, I presented the angular dependence of the actual backscattering strength for five benthic habitats in the Baltic Sea at an acoustic signal frequency of 150 kHz. Corrections to the recorded scattering data included the use of an acoustically calibrated multibeam echosounder, correction of the seabed slope in the signal reverberation area, and the use of a reverberation area.

The results of measurements of the real backscattering strength as a function of incidence angle presented in publication 3 are consistent with theoretical predictions as well as with results obtained by other authors who performed measurements with a multibeam echosounder (Eleftherakis 2018; Fonseca et al. 2009). In the study I presented, for incidence angles ranging from 25 to 65, the curve of real values of the backscattering strength showed a significant decrease in values greater than that in the APL model (APL-UW 1994) at 100 kHz. This may be related to the higher frequency of the applied signal – 150 kHz.

In some studies, a trend of increasing values of the real backscattering strength with increasing frequency was observed (Williams et al. 2002; Williams et al. 2009). Higher values of the real backscattering strength for higher frequencies may be related to the strong scattering of signals on the rough bottom surface, while the degree of bottom roughness is described by the Rayleigh parameter and depends on the acoustic wavelength, the magnitude of the roughness present on the scattering surface and the angle of incidence (Ogilvy 1991).

Real values of backscattering strength are essential for characterizing benthic habitats and represent their important acoustic property. Differential angular characteristics with a known slope of the curve and a known range of values for the corresponding benthic habitats can in the future be used for classification with proper assignment of areas to habitat classes despite little or no bottom sediment sampling. Real values of backscattering strength will provide a better understanding of environmental processes on the seafloor than ever before and learning about them is part of basic research.

Summary and conclusions about BBS-Coder

For object-based analysis (OBIA), textural analysis (GLCM) or automatic classification, mapped values of the backscattering intensity without an apparent angular dependence are necessary. The most commonly used tool to reduce backscattered signal values to a single angle of incidence is Geocoder (Fonseca and Calder 2005).

Mosaic maps of the relative intensity of the backscattered acoustic signal of the study area prepared with the Geocoder tool have large errors for incidence angles close to 0°, so I developed my own correction method. It reduces the backscattering intensity to a selected incidence angle of 40° and, as a result, reduces the effect of the incidence angle.

The algorithm presented for correction involving angle varying gain BBS-Coder (publication 3) is simple and effective. It will be made available for wide use on the ECOMAP project website (https://www.bonus-ecomap.eu/). The very good quality of the backscatter maps created with BBS-Coder indicates their suitability for benthic habitat mapping and sustainable seabed resource management.

BIBLIOGRAFIA

APL-UW, 1994. High-Frequency Ocean Environmental Acoustics Models Handbook; Defense Technical Information Center: Seattle, WA, USA, 1994; APL-UW TR 9407

Benz, U.C., Hofmann, P., Willhauck, G., Lingenfelder, I., Heynen, M., 2004. Multi-resolution, object-oriented fuzzy analysis of remote sensing data for GIS-ready information. ISPRS J. Photogramm. Remote Sens. 58, 239–258. https://doi.org/10.1016/j.isprsjprs.2003.10.002

Blaschke, T., 2010. Object based image analysis for remote sensing. ISPRS J. Photogramm. Remote Sens. 65, 2–16. https://doi.org/10.1016/j.isprsjprs.2009.06.004

Breiman, L., 2001. Random Forests. Mach. Learn. 45, 5–32, https://doi.org/10.1023/A:1010933404324

Briggs, K.B., Lyons, A.P., Pouliquen, E., Mayer, L.A., Richardson, M.D., 2005. Seafloor Roughness, Sediment Grain Size and Temporal Variability, in Underwater Acoustic Measurements: Technologies and Results. Heraklion, Crete, Greece, pp. 29–37

Buscombe, D., Grams, P.E., Kaplinski, M.A., 2014. Characterizing riverbed sediment using high-frequency acoustics: Scattering signatures of Colorado River bed sediment in Marble and Grand Canyons. J. Geophys. Res. Earth Surf. 119, 2692–2710. https://doi.org/10.1002/2014JF003191

Cazenave, P.W., Lambkin, D.O., Dix, J.K., 2008. Quantitative bedform analysis using decimetre resolution swath bathymetry. In: CARIS 12th International User Group Conference. United Kingdom, Bath

Diesing, M., Mitchell, P., Stephens, D., 2016. Image-based seabed classification: what can we learn from terrestrial remote sensing? ICES Journal of Marine Science: Journal du Conseil 73, 2425–2441. https://doi.org/10.1093/icesjms/fsw118

Diesing, M., Thorsnes, T., 2018. Mapping of Cold-Water Coral Carbonate Mounds Based on Geomorphometric Features: An Object-Based Approach. Geosciences, 8(2), 34. DOI: 10.3390/geosciences8020034

Diesing, M., Mitchell, P. J., O'Keeffe, E., Montereale Gavazzi G. O. A., Le Bas, T., 2020. Limitations of Predicting Substrate Classes on a Sedimentary Complex but Morphologically Simple Seabed. Remote Sensing, 12, 3398

Eleftherakis, D., Snellen, M., Amiri-Simkooei, A., Simons, D.G., Siemes, K., 2014. Observations regarding coarse sediment classification based on multi-beam echo-sounder's backscatter strength and depth residuals in Dutch rivers. J. Acoust. Soc. Am. 135, 3305–3315. https://doi.org/10.1121/1.4875236

Eleftherakis, D., Berger, L., Le Bouffant, N., Pacault, A., Augustin, J.M., Lurton, X., 2018. Backscatter calibration of high-frequency multibeam echosounder using a reference single-beam system, on natural seafloor. Mar. Geophys. Res. 39, 55–73. https://doi.org/10.1007/s11001-018-9348-5

Feldens, P., Schulze, I., Papenmeier, S., Schönke, M., Schneider von Deimling, J., 2018. Improved Interpretation of Marine Sedimentary Environments Using Multi-Frequency Multibeam Backscatter Data. Geosciences, 8(6), 214. DOI: 10.3390/geosciences8060214

Folk, R.L., Ward, W.C., 1957. A Study in the Significance of Grain-Size Parameters. Journal of Sedimentary Petrology, 27, 3-26. DOI: 10.1306/74D70646-2B21-11D7-8648000102C1865D

Fonseca, L.; Calder, B., 2005. Geocoder: An Efficient Backscatter Map Constructor. In Proceedings of the U.S. Hydro 2005 Conference, San Diego, CA, USA, 22 September 2005; p. 9

Fonseca, L., Brown, C., Calder, B., Mayer, L., Rzhanov, Y., 2009. Angular range analysis of acoustic themes from Stanton Banks Ireland: A link between visual interpretation and multibeam echosounder angular signatures. Appl. Acoust. 70, 1298–1304. https://doi.org/10.1016/j.apacoust.2008.09.008

Gafeira, J., Dolan, M., Monteys, X., 2018. Geomorphometric Characterization of Pockmarks by Using a GIS-Based Semi-Automated Toolbox. Geosciences, 8(5), 154. DOI: 10.3390/geosciences8050154

Gaida, T., Tengku Ali, T., Snellen, M., Amiri-Simkooei, A., van Dijk, T., Simons, D., 2018. A Multispectral Bayesian Classification Method for Increased Acoustic Discrimination of Seabed Sediments Using Multi-Frequency Multibeam Backscatter Data. Geosciences, 8(12), 455. DOI: 10.3390/geosciences8120455

Gaida, T.C., Mohammadloo, T.H., Snellen, M., Simons, D.G., 2020. Mapping the seabed and shallow subsurface with multi-frequency multibeam echosounders. Remote Sens. 12, 52. https://doi.org/10.3390/rs12010052

Goff, J.A., Jordan, T.H., 1988. Stochastic modelling of seafloor morphology: Inversion of Sea Beam data for second-order statistics. Journal of Geophysical Research: Solid Earth, 93, 13589–13608. DOI: 10.1029/JB093iB11p13589

Haralick, R.M., Shanmugam, K., Dinstein, I.H., 1973. Textural Features for Image Classification. IEEE Trans. Syst. Man Cybern. SMC-3, 610–621

Held, P., Schneider von Deimling, J., 2019. New Feature Classes for Acoustic Habitat Mapping - A Multibeam Echosounder Point Cloud Analysis for Mapping Submerged Aquatic Vegetation (SAV). Geosciences, 9(5), 235. DOI: 10.3390/geosciences9050235

IHO, 2008. Standards for Hydrographic Surveys. Monaco. Available online: https://iho.int/uploads/user/pubs/standards/s-44/S-44_5E.pdf (accessed on 24 November 2021).

Jackson, D.R., Baird, A.M., Crisp, J.J., Thomson, P.A.G., 1986. High-frequency bottom backscatter measurements in shallow water. The Journal of the Acoustical Society of America, 80, 1188-1199. DOI: 10.1121/1.393809

Janowski, L., Madricardo, F., Fogarin, S., Kruss, A., Molinaroli, E., Kubowicz-Grajewska, A., Tegowski, J., 2020. Spatial and Temporal Changes of Tidal Inlet Using Object-Based Image Analysis of Multibeam Echosounder Measurements: A Case from the Lagoon of Venice, Italy. Remote Sens. 12, 2117. https://doi.org/10.3390/rs12132117

Janowski, L., Tylmann, K., Trzcinska, K., Rudowski S., Tegowski, J., 2022. Exploration of Glacial Landforms by Object-Based Image Analysis and Spectral Parameters of Digital Elevation Model, in IEEE Transactions on Geoscience and Remote Sensing, vol. 60, pp. 1-17, Art no. 4502817, doi: 10.1109/TGRS.2021.3091771

Jolliffe, I. T., 2002. Principal Component Analysis. Springer Series in Statistics. New York: Springer-Verlag. doi:10.1007/b98835. ISBN 978-0-387-95442-4

Kursa, M.B.; Rudnicki, W.R., 2010. Feature Selection with the Boruta Package. J. Stat. Softw. 36. DOI: 10.18637/jss.v 036.i11

Lecours, V., Devillers, R., Schneider, D.C., Lucieer, V.L., Brown, C.J., & Edinger, E.N., 2015. Spatial scale and geographic context in benthic habitat mapping: review and future directions. Marine Ecology Progress Series, 535, 259-284. DOI: 10.3354/meps11378

Lefebvre, A., Thompson, C.E.L., Collins, K.J., Amos, C.L., 2009. Use of a high-resolution profiling sonar and a towed video camera to map a Zostera marina bed, Solent, UK. Estuar. Coast. Shelf Sci. 82, 323–334. https://doi.org/10.1016/j.ecss.2009.01.027

Lucieer, V., Lecours, V., Dolan, M., 2018. Charting the Course for Future Developments in Marine Geomorphometry: An Introduction to the Special Issue. Geosciences, 8(12), 477. DOI: 10.3390/geosciences8120477

Lurton, X., Lamarche, G. (Eds.), 2015. Backscatter Measurements by Seafloor-Mapping Sonars. Guidelines and Recommendations; GeoHab Backscatter Working Group: 2015. Available online: https://geohab.org/wp-content/uploads/2018/09/BWSG-REPORT-MAY2 015.pdf (accessed on 24 November 2021)

Lyons, A.P., Fox, W.L.J., Hasiotis, T., Pouliquen, E., 2002. Characterization of the two dimensional roughness of wave-rippled sea floors using digital photogrammetry. IEEE J. Ocean. Eng. 27, 515–524. https://doi.org/10.1109/JOE.2002.1040935

Micallef, A., Le Bas, T.P., Huvenne, V.A.I., Blondel, P., Hühnerbach, V., Deidun, A., 2012. A multi-method approach for benthic habitat mapping of shallow coastal areas with high-resolution multibeam data. Continental Shelf Research, 39-40, 14-26. DOI: 10.1016/j.csr.2012.03.008

Misiuk, B., Lecours, V., Bell, T., 2018. A multiscale approach to mapping seabed sediments. PLoS ONE, 13, e0193647. DOI: 10.1371/journal.pone.0193647

Montereale Gavazzi, G., Madricardo, F., Janowski, L., Kruss, A., Blondel, P., Sigovini, M., Foglini, F., 2016. Evaluation of seabed mapping methods for fine-scale classification of extremely shallow benthic habitats – Application to the Venice Lagoon, Italy. Estuarine, Coastal and Shelf Science, 170, 45-60. DOI: 10.1016/j.ecss.2015.12.014

Montereale-Gavazzi, G., Roche, M., Lurton, X., Degrendele, K., Terseleer, N., Van Lancker, V., 2017. Seafloor change detection using multibeam echosounder backscatter: case study on the Belgian part of the North Sea. Marine Geophysical Research, 39, 229-247. DOI: 10.1007/s11001-017-9323-6

Ogilvy, J., 1991. Theory of Wave Scattering from Random Rough Surfaces; Adam Higler: Bristol, UK

Prampolini, M., Blondel, P., Foglini, F., Madricardo, F., 2018. Habitat mapping of the Maltese continental shelf using acoustic textures and bathymetric analyses. Estuarine, Coastal and Shelf Science, 207, 483-498. DOI: 10.1016/j.ecss.2017.06.002

Preston, J., 2009. Automated acoustic seabed classification of multibeam images of Stanton Banks. Appl. Acoust. 70, 1277–1287. https://doi.org/10.1016/j.apacoust.2008.07.011

Roche, M., Degrendele, K., Vrignaud, C., Loyer, S., Le Bas, T., Augustin, J.M., Lurton, X., 2018. Control of the repeatability of high frequency multibeam echosounder backscatter by using natural reference areas. Mar. Geophys. Res. 39, 89–104. https://doi.org/10.1007/s11001-018-9343-x

Samsudin, S.A., Hasan, R.C., 2017. Assessment of Multibeam Backscatter Texture Analysis for Seafloor Sediment Classification. ISPRS - International Archives of the Photogrammetry, Remote Sensing and Spatial Information Sciences, XLII-4/W5, 177-183. DOI: 10.5194/isprs-archives-XLII-4-W5-177-2017

Schönke, M., Feldens, P., Wilken, D., Papenmeier, S., Heinrich, C., Schneider von Deimling, J., Held, P., Krastel, S.J.G.-M.L., 2017. Impact of Lanice conchilega on seafloor microtopography off the island of Sylt (German Bight, SE North Sea). Geo-Mar. Lett. 37, 305–318. https://doi.org/10.1007/s00367-016-0491-1

Urick, R.J., 1983. Principles of Underwater Sound. New York: McGraw-Hill

Weber, T.C., Rice, G., Smith, M., 2018. Toward a standard line for use in multibeam echo sounder calibration. Mar. Geophys. Res. 39, 75–87. https://doi.org/10.1007/s11001-017-9334-3

Wendelboe, G., 2018. Backscattering from a sandy seabed measured by a calibrated multibeam echosounder in the 190–400 kHz frequency range. Mar. Geophys. Res. 39, 105–120. https://doi.org/10.1007/s11001-018-9350-y

Wentworth, C. K., 1922. A Scale of Grade and Class Terms for Clastic Sediments. The Journal of Geology, 30 (5): 377–392. DOI: 10.1086/622910

Williams, K.L., Jackson, D.R., Thorsos, E.I., Tang, D., Briggs, K.B., 2002. Acoustic backscattering experiments in a well characterized sand sediment: Data/model comparisons using sediment fluid and Biot models. IEEE J. Ocean. Eng. 27, 376–387. doi: 10.1109/JOE.2002.1040925

Williams, K.L., Jackson, D.R., Tang, D., Briggs, K.B., Thorsos, E.I., 2009. Acoustic Backscattering from a Sand and a Sand/Mud Environment: Experiments and Data/Model Comparisons. IEEE J. Ocean. Eng. 34, 388–398. doi: 10.1109/JOE.2009.2018335

Wilson, M.F.J., O'Connell, B., Brown, C., Guinan, J.C., Grehan, A.J., 2007. Multiscale Terrain Analysis of Multibeam Bathymetry Data for Habitat Mapping on the Continental Slope. Marine Geodesy, 30, 3-35. doi: 10.1080/01490410701295962

PUBLIKACJA 1

Janowski L., **Trzcinska K.**, Tegowski J., Kruss A., Rucinska-Zjadacz M., Pocwiardowski P. Nearshore benthic habitat mapping based on multi-frequency, multibeam echosounder data using a combined object-based approach: A case study from the Rowy Site in the Southern Baltic Sea. *Remote Sens*. 2018, 10, 1983. https://doi.org/10.3390/rs10121983

remote sensing

MDPI

Article

Nearshore Benthic Habitat Mapping Based on Multi-Frequency, Multibeam Echosounder Data Using a Combined Object-Based Approach: A Case Study from the Rowy Site in the Southern Baltic Sea

Lukasz Janowski [1,*], Karolina Trzcinska [1], Jaroslaw Tegowski [1], Aleksandra Kruss [1], Maria Rucinska-Zjadacz [1] and Pawel Pocwiardowski [2]

1 Institute of Oceanography, University of Gdansk, al. Marszalka Pilsudskiego 46, 81-378 Gdynia, Poland; karolina.trzcinska@phdstud.ug.edu.pl (K.T.); j.tegowski@ug.edu.pl (J.T.); aleksandra.kruss@ve.ismar.cnr.it (A.K.); maria.rucinska-zjadacz@ug.edu.pl (M.R.-Z.)

2 NORBIT-Poland Sp. z o.o., al. Niepodleglosci 813-815/24, 81-810 Sopot, Poland; pawel@norbit.com

* Correspondence: lukasz.janowski@ug.edu.pl or ocelj@ug.edu.pl; Tel.: +48-58-523-6820

Received: 29 October 2018; Accepted: 4 December 2018; Published: 7 December 2018

check for updates

Abstract: Recently, the rapid development of the seabed mapping industry has allowed researchers to collect hydroacoustic data in shallow, nearshore environments. Progress in marine habitat mapping has also helped to distinguish the seafloor areas of varied acoustic properties. As a result of these new developments, we have collected a multi-frequency, multibeam echosounder dataset from the valuable nearshore environment of the southern Baltic Sea using two frequencies: 150 kHz and 400 kHz. Despite its small size, the Rowy area is characterized by diverse habitat conditions and the presence of red algae, unique on the Polish coast of the Baltic Sea. This study focused on the utilization of multibeam bathymetry and multi-frequency backscatter data to create reliable maps of the seafloor. Our approach consisted of the extraction of 70 secondary features of bathymetric and backscatter data, including statistic and textural attributes of different scales. Based on ground-truth samples, we have identified six habitat classes and selected the most relevant features of the bathymetric and backscatter data. Additionally, five types of image processing pixel-based and object-based classifiers were tested. We also evaluated the performance of algorithms using an accuracy assessment based on the validation subset of the ground-truth samples. Our best results reached 93% overall accuracy and a kappa coefficient of 0.90, confirming that nearshore seabed habitats can be accurately distinguished based on multi-frequency, multibeam echosounder measurements. Our predictive habitat mapping of shallow euphotic zones creates a new scientific perspective and provides relevant data for the management of natural resources. Object-based approaches previously used in various environments and areas suggest that methodology presented in this study may be scalable.

Keywords: habitat mapping; multibeam echosounder; multi-frequency; image processing; feature selection; object-based image analysis

1. Introduction

Shallow, coastal benthic habitats represent one of the most productive and valuable ecosystems on Earth [1]. The particular hydrodynamic conditions of these environments are responsible for the highly active exchange of nutrients, sediments, and biota. Their locations within euphotic zones make them an ideal place for the growth of macroalgae, which provide good settlements for benthic communities. Nearshore benthic habitats usually form complicated patterns, in which conducting spatial determination analysis is very important for ecosystem management and protection. Finally, precise mapping of the seafloor substratum and geomorphology is a fundamental task for marine spatial planning, especially with respect to marine protected areas (MPAs) or European Union (EU) legislative frameworks (e.g., Water Framework Directive 2000/60/EC, Habitats Directive 92/43/EEC, and Marine Strategy Framework Directive 2008/56/EC). In this study, we recognized and determined spatial areas occupied by valuable habitats that occur in the southern Baltic Sea. We evaluated our methods to obtain the most reliable maps of the studied area, which is one of the goals of the ECOMAP EU BONUS project, promoting Baltic Sea environmental assessments by opto-acoustic remote sensing, mapping, and monitoring.

The remote sensing methods used for seafloor mapping take advantage of sound propagation in marine environments. Over the last few decades, the rapid development of hydroacoustic methods utilizing single-beam echosounders, side-scan sonars, and multibeam echosounders (MBES) has occurred [2]. The quick growth of statistical techniques, which has taken place in recent years, has created great potential for precise mapping. Although global maps of the world's oceans' bathymetry based on gravity measurements are currently available, their low resolution makes them unusable for detailed analysis in such fields including benthic habitat mapping, mapping of sediments, underwater archeology, etc. [3].

Recently developed multibeam echosounders have allowed researchers to acquire three types of information: bathymetric data, which after processing is equivalent to interpolated digital elevation model (DEM) data, the angular dependency of the backscatter intensity of the acoustic signals from the seafloor, and the volume backscatter intensity of the water column. The spatial resolution of multibeam echosounder data, especially as applied in shallow water environments, can be compared to high-resolution LiDAR remote sensing data [4]. Up to now, only small areas of the world's oceans—much less than 15%—have been mapped with high-resolution bathymetry [5]. The availability of MBES backscatter data is even more limited. Seafloor acoustic reflectivity is a phenomenon that can be characterized as a measure of the acoustic energy coming back from the seafloor, reflecting the properties of the seafloor [6]. The determination of backscatter is therefore the most useful technique for creating categorical maps of the seabed. The backscatter of the water column is beyond the scope of this study.

Backscatter measurements from multibeam echosounders are not yet fully supervised and standardized [6]. For a better understanding of these phenomena, it is necessary to define the characteristic properties of backscatter intensity for particular benthic habitats in different areas. Seafloor substrata can be determined based on certain acquisition, processing, and interpretation techniques, which should be specified [7,8]. Considering the abovementioned objectives, we defined following research hypotheses: (1) different properties of backscatter intensity will allow us to distinguish habitat types in the southern Baltic Sea (the Rowy area); (2) the use of two frequencies significantly increases the amount of information gathered that will be useful for the correct classification of seafloor habitats; and (3) image processing methods, together with the application of statistical and textural analysis, will allow us to develop semi-automatic workflows to recognize and determine benthic habitats in the southern Baltic Sea.

Despite the fact that they were designed to gather deep water measurements, recent models of multibeam echosounders are capable of performing hydroacoustic surveys in shallow areas. Consequently, an increasing amount of research is being conducted in coastal areas (e.g., [9–12]). Nevertheless, hydroacoustic measurements in shallow water require especially careful sensor calibration, proper survey design, and experience to obtain accurate geospatial data.

Maps of benthic habitats can be created from hydroacoustic measurements using three types of analyses: manual expert interpretation of bathymetry and backscatter maps, acoustic signal parametrization, and image processing [13]. Knowledge-based expert interpretation has many disadvantages, such as lack of objectivity, high time consumption, and lack of repeatability; therefore, it is less frequently used in modern applications. Signal processing methods are usually related to unsupervised methods of classification and often work on one type of data (bathymetry or backscatter) [14]. They include, for example, angular range analysis (ARA, e.g., [15]), texture analysis [16,17], spectral analysis [18], and neural network analysis (e.g., [19,20]). The image processing approach benefits from different kinds of classification (often supervised) and allows researchers to apply many geomorphometric attributes (e.g., [21,22]). The approach presented here is based on object image analysis related to different acoustic products: backscatter and bathymetry combined in a relational database.

2. Materials and Methods

2.1. Study Site

This study focused on the nearshore shallow area located within the Polish Exclusive Economic Zone (EEZ). The detailed location of the aforementioned area is presented in Figure 1. The research area has dimensions of around 1.0 × 1.4 km, covering approximately 1.4 km^2. The outer boundary is located at a distance ranging between 0.5 and 2.0 km from the shoreline. The depth of the analyzed area varies from 4 to 20 m with a mean of 10 m. The geomorphology of the seabed is diversified, including valleys and crests of irregular shapes.

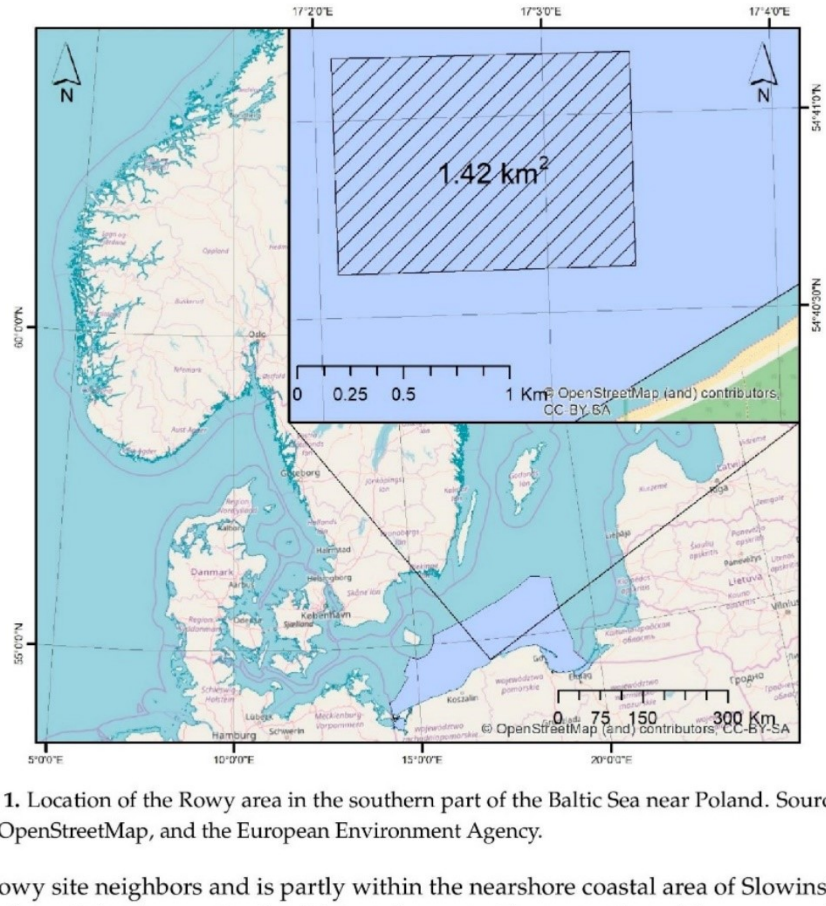

Figure 1. Location of the Rowy area in the southern part of the Baltic Sea near Poland. Sources: our study, OpenStreetMap, and the European Environment Agency.

The Rowy site neighbors and is partly within the nearshore coastal area of Slowinski National Park in northern Poland, near Gardno lake, at the coast. The protection of the surrounding marine environments has been established since 1995, when the borders of the National Park were expanded to marine areas up to a depth of 10 m as Ramsar site no. 757 [23]. The Rowy site is also located within the area of Natura 2000, no. PLB990002 [24].

The substratum of the study site is made of glacial tills that belong to a large moraine area occurring at the coast. The till outcrops represent relicts of postglacial structures that are crossed by valleys filled with modern marine sand and gravelly sand deposits, which form structures similar to ripple marks [25]. Glacial tills are often covered by large, dense boulder areas, and such terrain is rare within the Polish part of the southern Baltic Sea. Such a hard substratum provides a good base for various vegetation and benthic communities. Within the immediate surroundings of the Rowy area there is a lack of big urban or industrial areas, sources of contamination, and big river estuaries, so the environment maintains its relatively original nature. Previous research has confirmed the high biodiversity of the benthic communities within the analyzed area [26]. The presence of six species of red algae has been found there, such as *Bangiophyceae*, which is very rare in the Polish coast of the Baltic Sea, including unique *Furcellaria lumbricalis* and *Polysiphonia fucoides*. Moreover, boulder sites are often colonized by dense, cemented communities of *Mytilus trossulus* bivalves, with over 2500 individuals per m^2 in some locations [27]. The presence of large patches of such macroalgae is very valuable in terms of the functioning of the ecosystem and increasing the diversity of the phytophile fauna [28].

2.2. Hydroacoustic Data Acquisition and Processing

Hydroacoustic data were acquired during two surveys on 26–27 May 2018, using a small boat equipped with a multibeam echosounder (MBES) NORBIT iWBMS (model STX). The MBES was mounted on a pole and oriented vertically downwards during the measurements. The device allowed us to collect bathymetric data in a depth range of 2–150 m. Its angular spread across the ship's track was 150°, allowing us to collect 512 beams. The beam width had dimensions of $0.9 \times 0.9°$ at the working frequency of 400 kHz. The maximum angular coverage at the aforementioned frequency could be set up to 210°. The MBES worked with an integrated GNSS/INS navigation system (Wave Master, manufactured by Applanix: 85 Leek Crescent, Richmond Hill, ON Canada, L4B 3B3), including online RTK corrections for high positioning accuracy. During each survey, the working frequency of the MBES was set to a fixed value of 150 kHz or 400 kHz, depending on the day of the acquisition. In the case of a survey with the 150 kHz frequency, the maximum angular coverage was reduced to 160°. Our measurements were performed with a maximum ping rate of 30 Hz and a sweep time of 500 µs. To provide accurate profiles of the sound speed in the water column, the sound speed was measured consistently using a sound velocity profiler. Multibeam echosounder surveys were designed and performed to provide full spatial coverage (150%) of the area at a constant speed of 5.5–6 knots.

The hydroacoustic data were processed and cleaned using QPS Qimera 1.6.3 and Fledermaus Geocoder Toolbox (FMGT) 7.8.4 software. We gridded the bathymetric and backscatter data from the MBES with the maximum reliable resolution, which helped to avoid data gaps between the survey lines and to maintain consistency. Therefore, for the 150 kHz frequency, the data was gridded with a grid size of 0.75 m, and for the 400 kHz frequency, the grid size was 0.5 m. In order to determine the sensor errors, we utilized the combined uncertainty and bathymetric estimator (CUBE) algorithm, which obtains multiple estimations of depths related to the variation of the acoustic data [29]. We obtained standard deviations of the CUBE surface of lower than 30 cm. The backscatter mosaic was created using the 'flat' mode of the angle varying gain (AVG) correction tool with 'blend' mosaicking style and a window size of 300 [30]. The AVG correction in Fledermaus Geocoder Toolbox normalizes the backscatter data without angular dependency based on the calculations of the average backscatter response, between 20 and 60 degrees (or grazing angles [8]). 'Flat' mode is a standard type of AVG calculation, which smooths small variations of the backscatter signal and reduces its noise [31]. The window size indicates a series of a specified number of consecutive pings that is used for AVG normalization. The selected number of corrected curves (in our study, 300 pings) is used as a sliding window, moving along the survey lines (e.g., [32]). 'Blend' mosaicking style is a standard method for the management of overlapping lines in FMGT [8]. It blends nadir pixels with other overlapping pixels [31]. The bathymetric and backscatter data were created in reference coordinate system UTM 33 N based on WGS 84.

2.3. Ground-Truth Sampling and Analysis

The ground-truth samples were collected on 7 September 2018. They included sediment and video sampling using a Van Veen grab sampler and a remotely operated vehicle. The locations of the samples were carefully selected, chosen because of the particular characteristics of the seafloor based on prior knowledge of the research area [26]. Because of the difficulties of taking sediment samples from tills and boulders, of the total number of 31 samples, 29 were documented by video recordings and 14 were collected by the grab sampler. The sediment ground-truth data were analyzed using granulometric and sieve analysis, including the use of Folk and Ward parameters and Wentworth classification of the sediments [33,34]. A ROV was used in almost all the point locations, and apart from the video recordings in the target place, it was directed to carefully investigate the seafloor of each ground-truth point sampling area. Using mounted sensors, it obtained additional information, such as time, depth, direction, and temperature data, but its positioning and driving path were not capable of being precisely obtained during such seabed investigations. Therefore, despite having over 100 min of video recordings, we decided to generalize the obtained material and identify one class of ground-truth sample per specific point location. A deep investigation of the video recordings in conjunction with sediment analysis and hydroacoustic data distinguished six classes of habitats [6], which are presented in Table 1. The characteristic examples of the backscatter images shown in Table 1 occupy a spatial area of 9 m^2 and were presented using a false composite with R and G bands that corresponded to the backscatter intensity at 400 kHz and 150 kHz, respectively. The image descriptions shown in Table 1 also refer to fragments of backscatter images presented as false RGB composites. The geographic coordinates of the ground-truth samples with their descriptions are shown in Table A1. It should be noted that despite the fact that Samples 11 and 11b were acquired in similar locations, the distance between them was 15 m in a straight line, which was reflected in the different seafloor types at those locations. Because one class of acoustic facies represented artificial structures, such as a shipwreck located at a single, certain site of the area, we decided to perform classification algorithms for five distinct classes and assign the class of artificial structures manually at the end of the process.

2.4. Feature Extraction and Selection

We extracted 70 secondary features from the bathymetric and backscatter data, 35 for each of the two analyzed frequencies (150 kHz and 400 kHz). Together with the primary datasets (bathymetry 150 kHz, bathymetry 400 kHz, backscatter 150 kHz, and backscatter 400 kHz), we had 74 parameters in total. Table 2 presents all the extracted secondary features. The bathymetry-based features included the following: slope, aspect, eastness, northness, curvature, planar curvature, profile curvature, surface area to planar area (arc–chord ratio) [35], vector ruggedness measure (VRM) ruggedness [36], kurtosis, standard deviation of bathymetry, variance, fine-scale bathymetric position index (BPI), and broad-scale bathymetric position index [37]. While a majority of the features were calculated based on a sliding window size of 3×3 pixels, for some of them (slope, VRM ruggedness, bathymetry standard deviation, and kurtosis), we tested a multiscale approach [38]. For these features, we applied the following scales: 3×3, 5×5, 7×7, and 9×9. The backscatter secondary features included the following: backscatter standard deviation and various kinds of grey level co-occurrence matrices (GLCMs) [39], including homogeneity, contrast, dissimilarity, entropy, angular second moment, mean, standard deviation, and correlation. The backscatter secondary features were extracted based on object-based statistics. The spatial extent of all the secondary features (of both the bathymetric and backscatter data) was almost the same within the analyzed dataset (150 kHz or 400 kHz). The sizes of the sliding windows resulted in the occurrence of no data in some parts of the area, which slightly reduced its dimensions in the case of some secondary features, but it did not affect the further analysis.

Table 1. Acoustic facies, their descriptions, and the corresponding backscatter and seabed images

Class ID/Color	Backscatter Image (9 × 9 m)	Image Description	Seabed Image	Seabed Composition
VFS	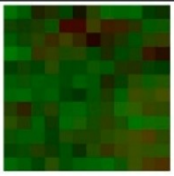	Dark green homogenous areas		Bare, flat area of very fine sand with worm burrows
S	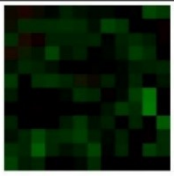	Very dark homogenous areas		Sand or slightly gravelly sand with ripple marks
SG_GS	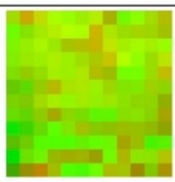	Green to orange areas		Slightly gravel or gravelly sand, rare boulders with barnacles and *Mytilus Trossulus*
B	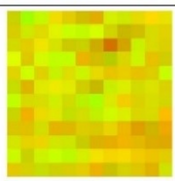	Light yellow to orange heterogenous areas with patchy patterns		A high concentration of *Mytilus Trossulus* on dense boulder substratum
R	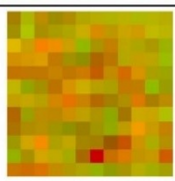	Dark orange areas with red patches		Large, dense patches of red algae with a high concentration of *Mytilus Trossulus* on boulder substratum
A	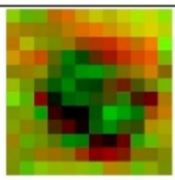	Very dark areas of undefined sharp transition with other areas		Artificial structures, such as a shipwreck

All the secondary features were imported (or created within the software in the case of the GLCMs) to eCognition software. The object-based statistics were extracted on the basis of the multiresolution segmentation of the backscatter intensity images with different 'scales' of segmentation (see Sections 2.4 and 3.4). The image objects were simply classified based on the point locations of the training samples (see Table A1). The mean scalar statistics of the classified objects, including all the investigated secondary features, were exported as georeferenced data.

All the secondary features were selected using the Boruta feature selection algorithm in the R software, using the 'Boruta' and 'rgdal' libraries [40,41]. Boruta is a wrapper function based on the random forest classifier, which selects the most important attributes after conducting multiple executions, evaluating performance by combining different subsets of input variables [22]. The result of the algorithm is expressed via feature importance (Z-score). The Z-score expresses a number of standard deviations between the result and the mean score. Features with the highest importance have Z-scores that are significantly higher than their shadow attributes and therefore are selected as confirmed [42]. Features without a decision at the end of the analysis are marked as tentative [43]. We used the 'rgdal' library to properly import the georeferenced data to the R software [41].

Table 2. List of extracted secondary features of the bathymetric and backscatter data for each of the analyzed frequencies (150 kHz and 400 kHz). VRM—vector ruggedness measure; BPI—bathymetric position index; and GLCM—grey level co-occurrence matrix.

ID	Bathymetry Feature	Window Size	ID	Backscatter Feature	Segmentation Scale
1–4	Slope	$3 \times 3, 5 \times 5, 7 \times 7, 9 \times 9$	27	Standard deviation	5/10
5	Aspect	3×3	28	GLCM Homogeneity	5/10
6	Eastness	3×3	29	GLCM Contrast	5/10
7	Northness	3×3	30	GLCM Dissimilarity	5/10
8	Curvature	3×3	31	GLCM Entropy	5/10
9	Planar curvature	3×3	32	GLCM Angular Second Moment	5/10
10	Profile curvature	3×3	33	GLCM Mean	5/10
11	Surface area to planar area (arc–chord ratio)	3×3	34	GLCM Standard Deviation	5/10
12–15	VRM ruggedness	$3 \times 3, 5 \times 5, 7 \times 7, 9 \times 9$	35	GLCM Correlation	5/10
16–19	Kurtosis	$3 \times 3, 5 \times 5, 7 \times 7, 9 \times 9$			
20–23	Standard deviation	$3 \times 3, 5 \times 5, 7 \times 7, 9 \times 9$			
24	Variance	3×3			
25	Fine scale BPI	3×3			
26	Broad scale BPI	3×3			

2.5. *Image Processing and Evaluation*

The backscatter mosaics created using the FMGT software were classified using image processing techniques. We evaluated pixel-based (PB) and object-based (OB) approaches. In our study, we used one unsupervised pixel-based (PB) method of image clustering—Jenks natural breaks classification. The algorithm works by maximizing the variance between the clusters and minimizing the variance within them [44]. We applied the method separately for grey-level backscatter images of different frequencies in the ArcGIS 10.4 software. According to our analysis of the ground-truth data, we computed the algorithm for the five classes of habitats.

The object-based image analysis (OBIA) of the acoustic facies was performed based on a multi-frequency, georeferenced backscatter image. We created objects in the eCognition Developer 9 software based on the multiresolution segmentation algorithm [45]. The technique creates images of objects using a bottom-up region merging method from one pixel based on a defined 'scale' of multiresolution segmentation. The merging process is based on the specific features of the relevant objects, such as their spectral properties or shapes. When the algorithm reaches the homogeneity criterion expressed by the 'scale' parameter, the fusion of neighboring objects stops [45]. Similarly, such as in other OB habitat mapping studies, we used the following multiresolution segmentation parameters: shape 0.1 and compactness 0.5 [46–49]. We tested the image objects created for the 'scales' of the multiresolution segmentation from 1 to 20 (with steps of 1).

The classifications of the image objects were performed based on a supervised approach using a few algorithms: classification and regression trees [50], support vector machines [51], random forests [52], and k-nearest neighbors. A supervised method assumes the utilization of a subset of ground-truth samples as training sites. Table A1 shows a description of all the ground-truth samples with separation for training and validation types. During the training process, the classifier computed the relationships between the image and the separated ground-truth data. The next step—application—used the inferred function to assign the unclassified areas implicitly [53].

The classification and regression tree (CART) technique generates a decision tree based on recursive partitioning. Decision trees are organized in branches and leaves (or nodes) that concentrate on similar groups of objects. Tree splitting increases the similarity within the groups until the terminal nodes are reached, and the splitting process stops [50]. The strength of the CART classifier is the easily interpreted result of the classification, which is explained as a series of questions. It does not assume any underlying relationships between the predictor and the response features. The weaknesses of the

CART classifier include the need for a primary estimation of the right size of the trees and the risk of overfitting due to a large number of splits [54].

The support vector machine (SVM) is machine learning algorithm based on the support vector approach. It partly belongs to the kernel-based classification methods [51]. The kernel is responsible for the transformation of datapoints from the input space to a higher dimensional feature space. The classifier creates the finest decision boundaries (called hyperplanes) that separate the feature vectors inside this feature space [55]. The feature vectors that are nearest (in terms of distance) to a hyperplane are called support vectors. The goal of the classifier is to obtain the largest possible margin that will separate the features in the best way.

Similarly to the CART method, random forest (RF) is a classification technique based on a decision tree approach [52]. The algorithm is responsible for the generation of many simple decision trees based on a random set of variables. The classifier considers an input feature vector, classifying it with all the trees in the forest and resulting in a class with the highest number of 'votes' [56]. One of the best advantages of the RF classifier is the high level of performance that can be achieved after the evaluation of many decision trees.

The k-nearest neighbors (KNN) algorithm is one of the simplest classifiers used in this study. The algorithm classifies a certain query object based on a specified number (K) of training samples located at the direct neighbor of the query point. To measure the influence of the neighbors, the classifier calculates the Euclidean distance between the query point and each instance. The value of K has a significant impact on the classification results. A number that is too small can cause a large variance in the prediction, whereas a number that is too large may result in large model bias. Therefore, it is typically recommended to choose a small value for K but to choose one that is large enough to avoid the probability of misclassification [57].

The performance of the chosen classifiers was evaluated based on an accuracy assessment. Error matrices were calculated for each classification result with cross-tabulation performed between the generated map and the validation subset of the ground-truth samples [58]. We calculated the common accuracy assessment statistics, such as the following: user's and producer's accuracy [59,60], overall accuracy, and kappa index of agreement (KIA) [61]. We anticipated the possibility of several good results related to different methods of classification. In such a case, we combined the best results to strengthen the accuracy, similar to the approach used in a previous study [12]. The general workflow of all the steps required to generate the predictive habitat maps in this study is presented in Figure 2.

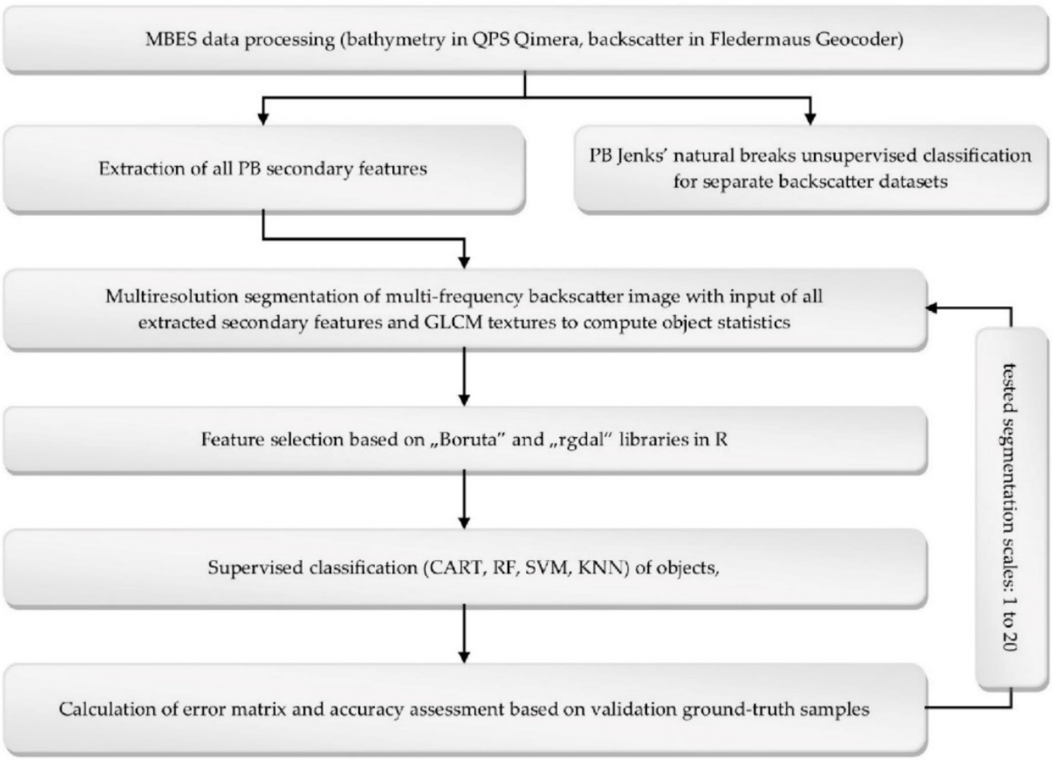

Figure 2. General workflow of the predictive habitat mapping developed in this study. MBES—multibeam echosounder; PB—pixel-based; GLCM—grey level co-occurrence matrix; CART—classification and regression trees; RF—random forest; SVM—support vector machine; and KNN—k-nearest neighbors.

3. Results

3.1. Discrimination of Ground-Truth Samples

Our analysis of the ground-truth sediment samples and the ROV video inspections distinguished 5 main habitat classes. One additional class of artificial structures, visible in Table 1 was assigned manually, so it was not considered as an input for the purposes of image processing. Figure 3A,B present the distribution of the mean backscatter intensity versus the specified habitat class for both of the frequencies used: 150 and 400 kHz. The values of the backscatter intensity were expressed as relative intensity values in the logarithmic scale in dB [6]. In general, the diagrams depicting the discrimination of the habitat classes showed a clear separation between the two groups of habitat classes. Sands and very fine sands were characterized by a low return of the acoustic signal, whereas the three remaining classes showed high backscatter. Moreover, the spread of the boxplots for the 150 kHz dataset was wider than the spread of the boxplots for the 400 kHz dataset. The thinner spread of the latter suggested that it could separate the habitat classes more clearly than the 150 kHz dataset.

3.2. Multibeam Echosounder Data Processing

The results of the multibeam data processing using the QPS Qimera and FMGT software are presented in Figure 4. The multi-frequency backscatter mosaic contained bands R (red) and G (green). We assigned the backscatter mosaic for the 400 kHz frequency to band R and backscatter grid of the 150 kHz frequency to band G. Figure 4B shows the location sites of the acquisition of the ground-truth samples. The bathymetric and backscatter datasets were used as a basis to compute 70 secondary features.

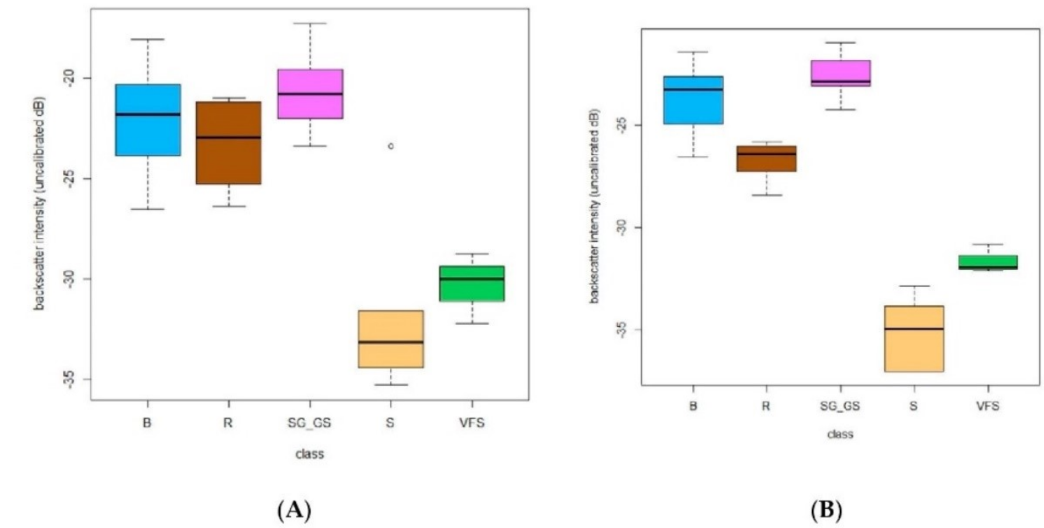

Figure 3. The distribution of the backscatter intensity in the five ground-truth classes: (**A**) for the 150 kHz frequency dataset, and (**B**) for the 400 kHz frequency dataset.

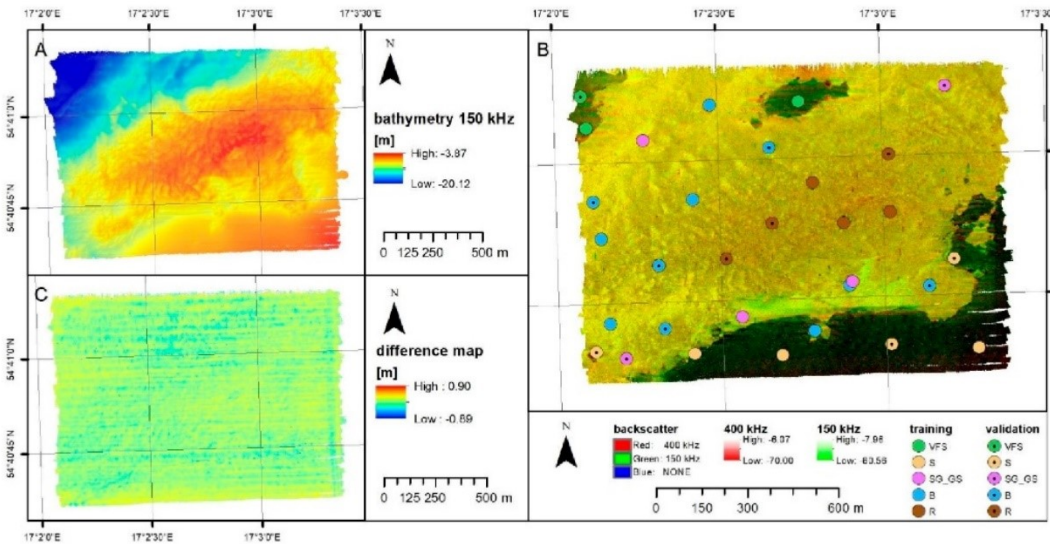

Figure 4. Results of the bathymetric and backscatter data processing: (**A**) bathymetry at 150 kHz; (**B**) multi-frequency backscatter at 150 kHz and 400 kHz; and (**C**) difference map between bathymetry 150 kHz and bathymetry 400 kHz.

3.3. Feature Selection

The Boruta feature selection algorithm was used as a basis for the supervised classifiers. For each scale of tested multiresolution segmentations, we extracted values of all the secondary features. We predicted the habitat maps using different sets of important and tentative attributes of the Boruta results. Figure 5A,B present the boxplots of the application of the feature selection algorithm for the best results in this study. For multiresolution segmentation scale 5, Boruta confirmed the importance of three features: backscatter 400 kHz, backscatter 150 kHz, and curvature 400 kHz. Three additional tentative features were suggested: bathymetry 150 kHz, GLCM homogeneity 400 kHz, and bathymetry 400 kHz. For multiresolution segmentation scale 10, the Boruta feature selection technique confirmed the importance of backscatter 400 kHz, backscatter 150 kHz, and bathymetry 400 kHz. It suggested three additional tentative attributes: slope 400 kHz, GLCM entropy 150 kHz, and the standard deviation of bathymetry 400 kHz created with sliding window size 9. Other secondary features were not relevant, so they were left for further analysis.

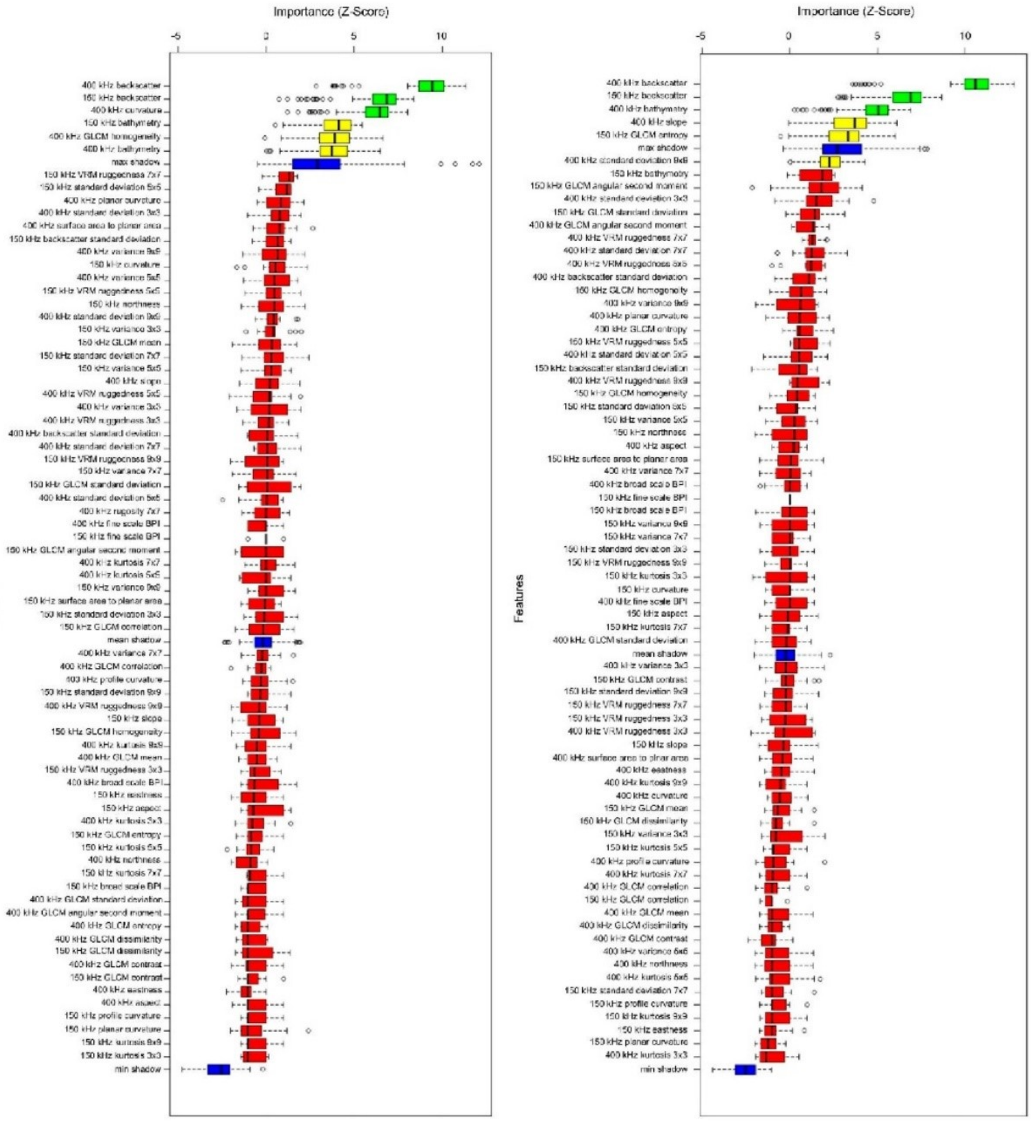

(A) **(B)**

Figure 5. Boxplot of the Boruta feature selection algorithm for the objects created with different 'scales' of multiresolution segmentation: (**A**) scale 5 and (**B**) scale 10.

3.4. Image Processing

As described above, object-based image analysis was performed based on multiresolution segmentation of different scales, from 1 to 20. The best classification results were obtained for image objects scales 5 and 10. For scale 5, the highest performance used the k-nearest neighbors classifier with K = 1, after applying six selected secondary features (with tentative attributes). Another best classification result was calculated using the random forest classifier for multiresolution segmentation scale 10. In this example, a set of four secondary features was applied: backscatter 400 kHz, backscatter 150 kHz, bathymetry 400 kHz, and slope 400 kHz.

Independently of the object-based image analysis, we performed pixel-based image processing using Jenks natural breaks clustering algorithm with unsupervised separation of single-frequency backscatter intensity images (150 kHz and 400 kHz) for the five classes. The results of all the applied methods of classification are presented in Figure 6.

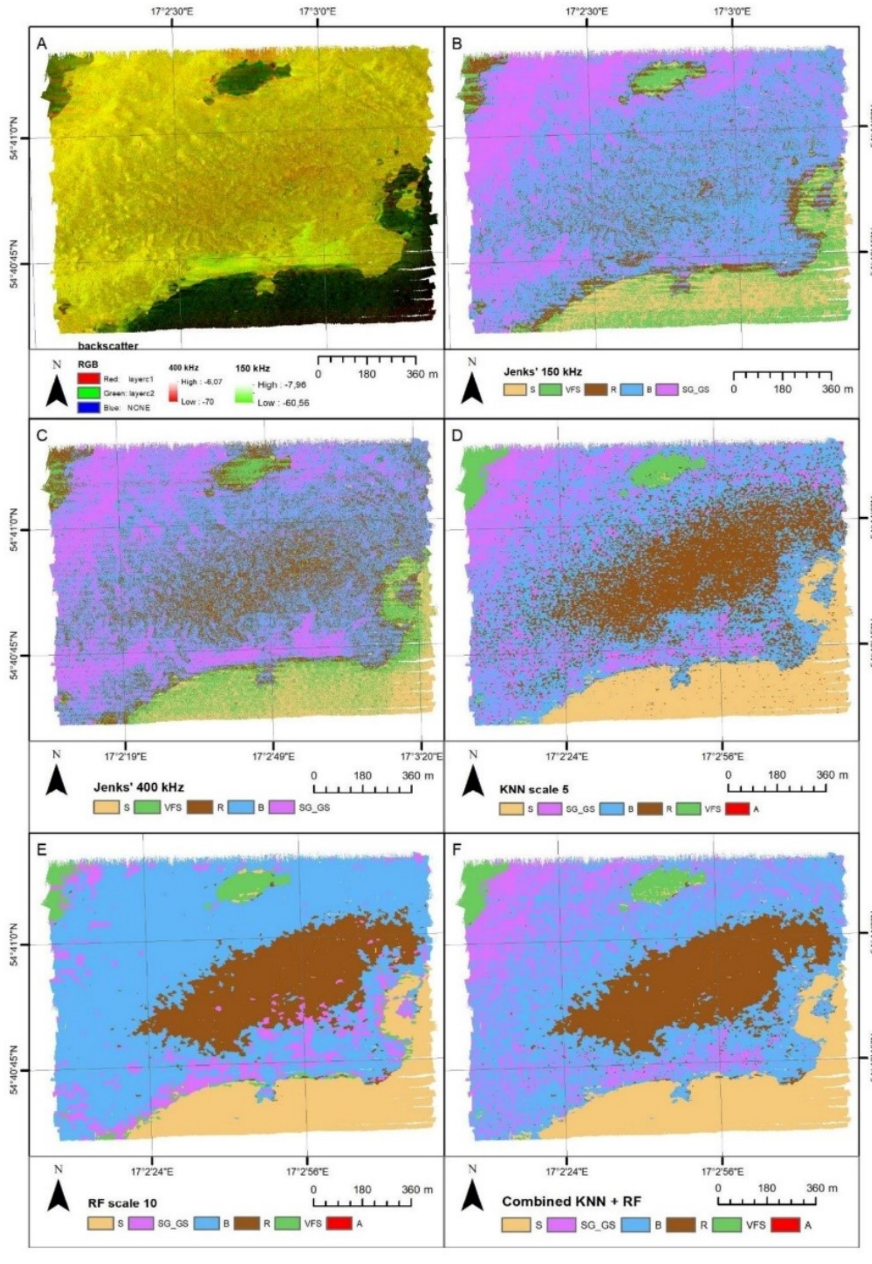

Figure 6. Results of the image analysis for the images of backscatter intensity from the Rowy area in the southern Baltic Sea: (**A**) multi-frequency backscatter of the analyzed area; (**B**) PB Jenks classification for the 150 kHz frequency; (**C**) PB Jenks classification for the 400 kHz frequency; (**D**) object-based (OB) KNN classification; (**E**) OB random forest (RF) classification; and (**F**) combined OB KNN and RF classification.

A visual inspection of the generated results supported by knowledge of the ground-truth samples allowed us to determine that both of the pixel-based results (Figure 6B,C) had difficulties with separating between the very fine sand (VFS) and sand (S) classes. These difficulties were visible in the pixel-based results as large noise in the areas with low backscatter return (the darkest areas in corresponding Figure 6A). It may have been caused by similar and slightly overlapping distribution of the backscatter intensity between these two classes (Figure 3). Moreover, the pixel-based results probably underestimated the class of red algae (R) and simultaneously overestimated the class of boulders (B). This was visible especially in the results of the Jenks natural breaks algorithm for the 150 kHz frequency, where the areas of red algae, represented in the backscatter false color composite by dark orange areas (see Figure 6A), were almost not separated from the boulder class (Figure 6C). The separation of the sandy gravel and gravelly sand (SG_GS) class was similar in both PB results (Figure 6B,C) and one OB result (KNN, see Figure 6D), and it was probably underestimated in the case of the random forest result (Figure 6E). For comparison with the PB results, it seems that the performance of both of the OB classifiers was good in separating between the very fine sand (VFS) and sand (S) classes. The noise within the areas of low backscatter intensity visible in both PB results was almost absent in the OB results. Between the two OB results there was, however, visible bias in the spatial separation between the boulder (B) and sandy gravel–gravelly sand (SG_GS) classes (compare Figure 6D,E).

3.5. Accuracy Assessment of Results

The performances of all the applied approaches of image analysis were evaluated based on error matrices and accuracy assessment statistics, shown in Tables A2–A5. Both object-based results had similar statistics with an overall accuracy of 86% and a kappa index of agreement of 0.81 (Tables A4 and A5). The accuracy assessment of the pixel-based results indicated much lower statistics with an overall accuracy of 42% and a kappa index of agreement of 0.24–0.27 (Tables A2 and A3). The error matrices confirmed our visual evaluations of the classifiers for certain classes suggested in the previous section. The highest user's and producer's accuracy per class indicated that apart from the VFS class, the KNN classifier perfectly determined the SG_GS class, while the RF method ideally separated the R class in comparison with all the other results. We took advantage of these perfect separations by combining both OB results. The predictive model that combines the object-based KNN and RF algorithms is presented in Figure 6F. This model increased the overall accuracy to 93% and the KIA measurement to 0.90. The error matrix of the combined model is shown in Table A6. Despite receiving high statistics in the accuracy assessment, we should note that the small number of ground-truth samples meant that each sample represented a high kappa value. This issue should be paid close attention as a potential source of errors when comparing this study with other marine habitat mapping studies.

4. Discussion

Multi-frequency, multibeam echosounder data is a promising new approach in the characterization of seabed habitats. Recent research confirms that the simultaneous analysis of many frequencies leads to a better understanding of seafloor properties [62]. Although we did not use a multibeam echosounder with multispectral mode (such as the R2Sonic 2026) for our measurements, we repeated the hydroacoustic surveys with different frequencies. Similar research has been presented in [62], where the surveys were repeated with three different frequencies: 200, 400, and 600 kHz. This approach helped us to make a detailed acoustic characterization of the seabed sediments. In our case, we performed hydroacoustic research at two frequencies: 150 kHz and 400 kHz. The additional information from the ground-truth data allowed us to define the distributions of the acoustic backscatter for all the classes of habitats, which differed depending on the frequency used. All the feature selection results confirmed that attributes of both frequencies were useful to explain the variability of the analyzed data.

The Boruta feature selection algorithm has been tested in the benthic habitat mapping literature a few times, giving promising results [22,63]. Our results confirmed the usefulness of the application of this feature selection method in habitat mapping. We recommend that if the algorithm would work on statistics gathered from object-based image analysis, then the classification should be performed on the same segmentation setting.

Our study confirmed that beyond the primary features, such as backscatter and bathymetry, some other secondary features were useful, such as slope, GLCM entropy, GLCM homogeneity, and the standard deviation of bathymetry. We suggest remembering such attributes for further feature selection actions. The list of suggested secondary features is not yet finished and may include, for example, spatial autocorrelation [63]; hue, saturation, and intensity [64]; angular range analysis [65], Q-values [66]; and maximum orbital velocity [64].

The scale of multiresolution segmentation is a very important setting of OBIA, which has an impact on further analysis, including the results of the classification [45]. Up to now, at least a few benthic habitat mapping studies have included the application of different scales of multiresolution segmentation [46,49]. To estimate the parameter in a proper way, we tested many scales from 1 to 20, with a step of 1—similar to the approach in [49]—for a wider range of the parameters. The best scale was chosen for the best accuracy assessment of the evaluated classification methods. Although the investigation of the dependency between the accuracy and the multiresolution segmentation scale used was not the aim of this study, we tested 80 sets of the OB segmentation–classification results (20 scales $\times$ 4 classifiers). Our attempts confirmed that the scale of the multiresolution segmentation was imperfect, and its incorrect determination may have led to poor results in the object-based classification. Future research should take a closer look at this phenomenon and investigate the changes in accuracy depending on the scale of the multiresolution segmentation parameter.

In this study, we performed a robust object-based methodology on a relatively small test area, characterized by diverse habitat conditions with the occurrence of unique red algae. Considering the regional conditions, there are no areas with similar characteristics within the Polish coast of the southern Baltic Sea. It should be noted that in the marine habitat mapping literature, there have been studies based on similar or smaller spatial extents, such as 0.056 km^2 [48] or 0.39 km^2 [12]. Other methods of benthic habitat mapping based on object-based image analysis were previously applied in various environments and areas, from smaller areas [48] to slightly less diverse areas within the Polish coast of the southern Baltic Sea [49] to larger areas [67]. Therefore, we can state that our methodology would be scalable.

In this study, we designed a ground-truth survey to encompass the representativeness of all kinds of habitats. It is necessary to keep in mind that a set of samples that is too small can lead to a falsified accuracy result [68]. Some studies have presented results of seabed mapping after analysis of similarly small but representative numbers of ground-truth samples [10,17,42,49]. In any such case, there is a possibility of errors, for which the sources have been described in detail (e.g., [69]). Despite the relatively small number of samples, we used varied methods of sampling, including Van Veen grabs and ROV video inspections within all the sites. Thus, our ground-truth survey was designed to obtain strict and diverse knowledge of the analyzed area.

Considering the unit of analysis, the methods of classification could be separated between pixel-based (PB) and object-based (OB) methods. The utilization of ground-truth samples allowed for further division between unsupervised and supervised techniques. The Jenks natural breaks method has been applied in habitat mapping studies several times [48,70]. In comparison with similar research, we obtained poor accuracy using this classification in this study. In our pixel-based classifications, there were visible 'salt and pepper' effects caused by the noise of the input data, which was obvious in comparison with the OB approaches [71]. The reason for the poor accuracy may be related to the overlapping distribution of the backscatter intensity for the habitat classes described in Section 3.1.

Different approaches of machine learning or decision trees have been widely used in recent predictive habitat mapping (e.g., [12,22,46,48,67,72,73]). Such approaches belong to both PB and OB techniques and supervised classification methods, executing top-down strategies: "assemble first, predict later" [13]. The OB approach of supervised classifiers has been developed over the last few years in marine habitat mapping (e.g., [12,46,48,65,67]). Many of the aforementioned studies concerned evaluations of classification methods. In particular, the random forest method seems to be a promising method for the automatic classification of benthic habitats. For example, in [65], the RF method achieved an excellent result of 94% overall accuracy and a KIA of 90%. Results with 80% overall accuracy are common in marine habitat mapping when using the random forest classifier [12,22,67].

The KNN classifier has been applied much less often in marine habitat mapping studies with other well-known examples [46,48]. In these studies, the KNN classifier separated classes with an overall accuracy from 52% to 66%. Considering the KIA value (from 0.38 to 0.43), the performance of the KNN classifier in these studies can be described as fair to moderate [46]. In our study, we obtained better accuracy using this method, but possible sources of errors should be kept in mind (see Section 3.5). We recommend continuing to evaluate this method of classification in further habitat mapping studies.

The application of two frequencies of MBES measurements is very interesting from the viewpoint of marine habitat mapping. The acoustic responses of the habitats are dependent on the frequency; therefore, distinct frequencies may reveal different attributes. With two frequencies, we have a better possibility of achieving habitat discrimination. One recent study has suggested that the combination of PB and OB methods can lead to a better separation of classes, resulting in better accuracy [12]. In the aforementioned study, the application of such an approach increased the overall accuracy by 5.1% and the kappa value by 0.06 (overall accuracy—83.6%, KIA—0.78). In comparison, the combination of two OB classifiers in our study allowed us to increase the overall accuracy by 7.1% and the KIA by 0.10. Both results suggest that the combination of the best classification outcomes might be useful and promising in future marine habitat mapping studies.

5. Conclusions

In this study, we developed a robust workflow for predictive habitat mapping based on multi-frequency, multibeam echosounder data. For the first time, we recognized and distinguished six nearshore habitats of the Rowy area in the southern Baltic Sea. The identified habitats included very rare seascapes for the Polish coast of the Baltic Sea, encompassing species of red algae and boulder sites colonized by *Mytilus Trossulus* bivalves. Future research will be conducted using the same model of multibeam echosounder device but with an acoustically calibrated option regarding the backscatter strength. Therefore, the composition of the seafloor will be represented from a physical point of view, which would create new perspectives in benthic habitat mapping, such as the ability to track spatial changes of habitats over time [42].

An important part of our workflow was the feature extraction and selection. We extracted 70 secondary features of the bathymetric and backscatter data. They included either pixel-based statistics or object-based GLCM textures. Some features were calculated based on multiscale or object-based approaches. The Boruta feature selection algorithm allowed us to choose relevant attributes, which included the following (beyond bathymetry and backscatter): slope, GLCM entropy, GLCM homogeneity, and the standard deviation of bathymetry. Our results confirmed the usefulness of the application of the Boruta feature selection method in habitat mapping. The proper feature selection helped us to discriminate habitat classes with similar distributions of backscatter intensity. However, the list of secondary features is not yet complete. We suggest expanding it for other attributes and a multiscale approach.

We tested different aspects of image processing, such as pixel-based and object-based image analysis, unsupervised and supervised methods of classification, and habitat mapping based on single-frequency and multi-frequency multibeam echosounder (MBES) datasets. Our results demonstrated the great usefulness of object-based image analysis and supervised classifiers, such as the random forest and k-nearest neighbors algorithms. Because, in our case, each classifier performed better with respect to specific classes of habitats, we took advantage of the best results and combined them, obtaining very good agreement—93% overall accuracy and a 0.90 Kappa coefficient. We applied such a combination based on two object-based results. In our study, the application of the multi-frequency, MBES dataset with the proper selection of secondary features significantly increased the accuracy of the habitat maps with respect to the single-frequency results.

Our workflow encouraged us to offer some additional suggestions. We recommend taking a closer look at the scale of multiresolution segmentation in object-based marine habitat mapping studies. A particularly interesting topic is the changes in accuracy depending on the scale of multiresolution segmentation parameter. We also recommend evaluating the k-nearest neighbors method of classification in future habitat mapping studies.

The rapid development of the hydroacoustic industry will bring about the greater availability of multi-frequency, multibeam echosounder data. Our predictive habitat mapping of shallow euphotic zones creates a new scientific perspective and provides relevant data for the management of natural resources.

Author Contributions: Conceptualization, L.J. and J.T.; Methodology, L.J.; Data acquisition, K.T., A.K., J.T., and P.P.; Data processing, L.J., K.T., A.K., P.P., and M.R.-Z.; Original draft preparation, L.J.; Review and editing of the manuscript, J.T.; and Supervision, J.T.

Funding: This research was funded by EU BONUS-185 ECOMAP project (Baltic Sea environmental assessments by opto-acoustic remote sensing, mapping, and monitoring) and co-financed by the National Centre for Research and Development no. BONUS-BB/ECOMAP/07/2017.

Acknowledgments: We would like to thank the crew of the research boat, Zelint, for their help in taking measurements in the Rowy area.

Conflicts of Interest: The authors declare no conflicts of interest.

Appendix A

Table A1. Specifications of the ground-truth samples with their ID numbers, types, and geographic coordinates. The symbols of the habitat classes correspond with those in Table 1.

ID	Habitat Class	Type [1]	Grab [2]	Latitude	Longitude
1	S	T	+	54.677560	17.054628
2	S	V	+	54.677732	17.050173
3	B	T		54.678197	17.046282
4	S	T	+	54.677502	17.044602
5	S	T	+	54.677612	17.040122
6	SG_GS	V	+	54.677525	17.036633
7	S	V	+	54.677740	17.035105
8	B	T		54.678568	17.035853
9	B	V		54.678383	17.038660
10	SG_GS	T	+	54.678663	17.042602
11	B	T		54.679515	17.048127
11b	SG_GS	T	++	54.679627	17.048258
12	B	V		54.679442	17.052195
13	S	V	+	54.680213	17.053486
14	R	T		54.681648	17.050273
15	R+A	T		54.681360	17.047902
16	R	V		54.680400	17.041873
17	B	T		54.681088	17.035512
18	B	V		54.682185	17.035162
19	VFS	V	+	54.685313	17.034647
20	VFS	T	++	54.684372	17.037770
21	SG_GS	T	+	54.683967	17.037770
22	VFS	T	+	54.684997	17.045757
23	SG_GS	V	+	54.685348	17.053240
24	R	V		54.683367	17.050290
25	R	T		54.682583	17.046350
26	B	V		54.683652	17.044187
27	B	T		54.682180	17.040230
28	R	V		54.681417	17.044258
29	R	T		54.684967	17.041220
30	B	V		54.680248	17.038418

[1] The types of samples are as follows: T—training and V—validation; [2] the methods of acquisition include the following: video recordings and grab samples (+), only video recordings (blank cells), or only grab samples (++).

Appendix B

Table A2. Error matrix and accuracy assessment statistics for the Jenks classification of the PB results based on the backscatter intensity grid of 150 kHz.

	Reference Class					
User	**S**	**SG_GS**	**B**	**R**	**VFS**	**Sum**
S	0	0	0	0	0	0
SG_GS	0	1	1	0	0	2
B	1	1	3	2	0	7
R	0	0	1	1	0	2
VFS	2	0	0	0	1	3
Sum	3	2	5	3	1	
Producer	0	0.5	0.6	0.333333	1	
User	0	0.5	0.428571	0.5	0.333333	
Overall Accuracy	0.428571					
KIA	0.243243					

Table A3. Error matrix and accuracy assessment statistics for the Jenks classification of the PB results based on the backscatter intensity grid of 400 kHz.

	Reference Class					
User	**S**	**SG_GS**	**B**	**R**	**VFS**	**Sum**
S	1	0	0	0	0	1
SG_GS	0	1	3	0	0	4
B	0	1	2	2	0	5
R	0	0	0	1	0	1
VFS	2	0	0	0	1	3
Sum	3	2	5	3	1	
Producer	0.333333	0.5	0.4	0.333333	1	
User	1	0.25	0.4	1	0.333333	
Overall Accuracy	0.428571					
KIA	0.272727					

Table A4. Error matrix and accuracy assessment statistics for the KNN classification of the results based on multiresolution scale 5.

	Reference Class					
User	**S**	**SG_GS**	**B**	**R**	**VFS**	**Sum**
S	2	0	0	0	0	2
SG_GS	0	2	0	0	0	2
B	1	0	5	1	0	7
R	0	0	0	2	0	2
VFS	0	0	0	0	1	1
Sum	3	2	5	3	1	
Producer	0.666667	1	1	0.666667	1	
User	1	1	0.714286	1	1	
Overall Accuracy	0.857143					
KIA	0.805556					

Table A5. Error matrix and accuracy assessment statistics for the RF classification of the results based on multiresolution segmentation scale 10.

	Reference Class					
User	**S**	**SG_GS**	**B**	**R**	**VFS**	**Sum**
S	2	0	0	0	0	2
SG_GS	1	1	0	0	0	2
B	0	1	5	0	0	6
R	0	0	0	3	0	3
VFS	0	0	0	0	1	1
Sum	3	2	5	3	1	
Producer	0.666667	0.5	1	1	1	
User	1	0.5	0.833333	1	1	
Overall Accuracy	0.857143					
KIA	0.808219					

Table A6. Error matrix and accuracy assessment statistics for the combined model of classification based on the KNN and RF results.

	Reference Class					
User	**S**	**SG_GS**	**B**	**R**	**VFS**	**Sum**
S	2	0	0	0	0	2
SG_GS	0	2	0	0	0	2
B	1	0	5	0	0	6
R	0	0	0	3	0	3
VFS	0	0	0	0	1	1
Sum	3	2	5	3	1	
Producer	0.666667	1	1	1	1	
User	1	1	0.833333	1	1	
Overall Accuracy	0.928571					
KIA	0.904110					

References

1. Barbier, E.B.; Hacker, S.D.; Kennedy, C.; Koch, E.W.; Stier, A.C.; Silliman, B.R. The value of estuarine and coastal ecosystem services. *Ecol. Monogr.* **2011**, *81*, 169–193. [CrossRef]
2. Brown, C.J.; Blondel, P. Developments in the application of multibeam sonar backscatter for seafloor habitat mapping. *Appl. Acoust.* **2009**, *70*, 1242–1247. [CrossRef]
3. Harris, P.T.; Baker, E.K. Why Map Benthic Habitats? In *Seafloor Geomorphology as Benthic Habitat*; Harris, P.T., Baker, E.K., Eds.; Elsevier: London, UK, 2012; pp. 3–22. [CrossRef]
4. Gao, J. Bathymetric mapping by means of remote sensing: Methods, accuracy and limitations. *Prog. Phys. Geogr.* **2009**, *33*, 103–116. [CrossRef]
5. Mayer, L.; Jakobsson, M.; Allen, G.; Dorschel, B.; Falconer, R.; Ferrini, V.; Lamarche, G.; Snaith, H.; Weatherall, P. The Nippon Foundation—GEBCO Seabed 2030 Project: The Quest to See the World's Oceans Completely Mapped by 2030. *Geosciences* **2018**, *8*, 1–18. [CrossRef]
6. Lamarche, G.; Lurton, X. Recommendations for improved and coherent acquisition and processing of backscatter data from seafloor-mapping sonars. *Mar. Geophys. Res.* **2017**, *39*, 5–22. [CrossRef]
7. Lucieer, V.; Roche, M.; Degrendele, K.; Malik, M.; Dolan, M.; Lamarche, G. User expectations for multibeam echo sounders backscatter strength data-looking back into the future. *Mar. Geophys. Res.* **2017**, *39*, 23–40. [CrossRef]
8. Schimel, A.C.G.; Beaudoin, J.; Parnum, I.M.; Le Bas, T.; Schmidt, V.; Keith, G.; Ierodiaconou, D. Multibeam sonar backscatter data processing. *Mar. Geophys. Res.* **2018**, *39*, 121–137. [CrossRef]
9. Ierodiaconou, D.; Laurenson, L.; Burq, S.; Reston, M. Marine benthic habitat mapping using Multibeam data, georeferenced video and image classification techniques in Victoria, Australia. *J. Spat. Sci.* **2007**, *52*, 93–104. [CrossRef]

10. Micallef, A.; Le Bas, T.P.; Huvenne, V.A.I.; Blondel, P.; Hühnerbach, V.; Deidun, A. A multi-method approach for benthic habitat mapping of shallow coastal areas with high-resolution multibeam data. *Cont. Shelf Res.* **2012**, *3–40*, 14–26. [CrossRef]
11. Madricardo, F.; Foglini, F.; Kruss, A.; Ferrarin, C.; Pizzeghello, N.M.; Murri, C.; Rossi, M.; Bajo, M.; Bellafiore, D.; Campiani, E.; et al. High resolution multibeam and hydrodynamic datasets of tidal channels and inlets of the Venice Lagoon. *Sci. Data* **2017**, *4*, 170121. [CrossRef]
12. Ierodiaconou, D.; Schimel, A.C.G.; Kennedy, D.; Monk, J.; Gaylard, G.; Young, M.; Diesing, M.; Rattray, A. Combining pixel and object based image analysis of ultra-high resolution multibeam bathymetry and backscatter for habitat mapping in shallow marine waters. *Mar. Geophys. Res.* **2018**, *39*, 271–288. [CrossRef]
13. Brown, C.J.; Smith, S.J.; Lawton, P.; Anderson, J.T. Benthic habitat mapping: A review of progress towards improved understanding of the spatial ecology of the seafloor using acoustic techniques. *Estuar. Coast. Shelf Sci.* **2011**, *92*, 502–520. [CrossRef]
14. Tegowski, J. Acoustical classification of the bottom sediments in the southern Baltic Sea. *Quat. Int.* **2005**, *130*, 153–161. [CrossRef]
15. Fonseca, L.; Brown, C.; Calder, B.; Mayer, L.; Rzhanov, Y. Angular range analysis of acoustic themes from Stanton Banks Ireland: A link between visual interpretation and multibeam echosounder angular signatures. *Appl. Acoust.* **2009**, *70*, 1298–1304. [CrossRef]
16. Blondel, P.; Gómez Sichi, O. Textural analyses of multibeam sonar imagery from Stanton Banks, Northern Ireland continental shelf. *Appl. Acoust.* **2009**, *70*, 1288–1297. [CrossRef]
17. Prampolini, M.; Blondel, P.; Foglini, F.; Madricardo, F. Habitat mapping of the Maltese continental shelf using acoustic textures and bathymetric analyses. *Estuar. Coast. Shelf Sci.* **2018**, *207*, 483–498. [CrossRef]
18. Tegowski, J.; Lubniewski, Z. Seabed Characterisation Using Spectral Moments of the Echo Signal. *Acta Acust. United Acust.* **2002**, *88*, 623–626.
19. Madricardo, F.; Tegowski, J.; Donnici, S. Automated detection of sedimentary features using wavelet analysis and neural networks on single beam echosounder data: A case study from the Venice Lagoon, Italy. *Cont. Shelf Res.* **2012**, *43*, 43–54. [CrossRef]
20. Marsh, I.; Brown, C. Neural network classification of multibeam backscatter and bathymetry data from Stanton Bank (Area IV). *Appl. Acoust.* **2009**, *70*, 1269–1276. [CrossRef]
21. Lecours, V.; Dolan, M.F.J.; Micallef, A.; Lucieer, V.L. A review of marine geomorphometry, the quantitative study of the seafloor. *Hydrol. Earth Syst. Sci.* **2016**, *20*, 3207–3244. [CrossRef]
22. Stephens, D.; Diesing, M. A comparison of supervised classification methods for the prediction of substrate type using multibeam acoustic and legacy grain-size data. *PLoS ONE* **2014**, *9*, e93950. [CrossRef] [PubMed]
23. Ramsar Sites Information Service. Available online: https://rsis.ramsar.org (accessed on 17 October 2018).
24. Natura 2000 Network Viewer. Available online: http://natura2000.eea.europa.eu/ (accessed on 17 October 2018).
25. Pieczka, F. Geomorfologia i Osady Denne Baltyku Poludniowego (Geomorphology and seabottom sediments of the Gdansk Basin, in Polish). *Perribalticum* **1980**, *1*, 79–118.
26. Tegowski, J.; Gorska, N.; Kruss, A.; Nowak, J.; Blenski, J. Analysis of single beam, multibeam and sidescan sonar data for benthic habitat classification in the southern Baltic Sea. In Proceedings of the 3rd International Conference and Exhibition on Underwater Acoustic Measurements: Technologies & Results, Nafplion, Greece, 21–26 June 2009; pp. 131–138.
27. Kendzierska, H. Stilo-Ustka. In *Atlas of Polish Marine Area Bottom Habitats*; Gic-Grusza, G., Kryla-Straszewska, L., Urbanski, J., Warzocha, J., Weslawski, J.M., Eds.; Broker-Innowacji: Gdynia, Poland, 2009; pp. 158–165.
28. Maritime Institute in Gdansk. *Roznorodnosc Biologiczna Przybrzeznego Glazowiska Rowy Przy Slowinskim Parku Narodowym (Biodiversity of Coastal Boulder Area Near the Slowinski National Park, in Polish)*; Zaklad Wydawnictw naukowych Instytutu Morskiego w Gdansku: Gdansk, Poland, 2006.
29. Calder, B.R.; Mayer, L.A. Automatic processing of high-rate, high-density multibeam echosounder data. *Geochem. Geophys. Geosyst.* **2003**, *4*. [CrossRef]
30. Fonseca, L.; Calder, B. Geocoder: A Efficient Backscatter Map Constructor. In Proceedings of the U.S. Hydrographic Conference, San Diego, CA, USA, 29–31 March 2009.
31. QPS. Fledermaus v7.8 Manual. Available online: https://confluence.qps.nl/dwnfledermaus/ (accessed on 15 October 2018).

32. Parnum, I.M.; Gavrilov, A.N. High-frequency multibeam echo-sounder measurements of seafloor backscatter in shallow water: Part 2—Mosaic production, analysis and classification. *Underw. Technol.* **2011**, *30*, 13–26. [CrossRef]
33. Wentworth, C.K. A Scale of Grade and Class Terms for Clastic Sediments. *J. Geol.* **1922**, *30*, 377–392. [CrossRef]
34. Folk, R.L.; Ward, W.C. Brazos River bar [Texas]; a study in the significance of grain size parameters. *J. Sediment. Res.* **1957**, *27*, 3–26. [CrossRef]
35. Du Perez, C. A new arc-chord ratio (ACR) rugosity index for quantifying three-dimensional landscape atructural complexity. *Landsc. Ecol.* **2014**, *30*, 181–192. [CrossRef]
36. Sappington, J.M.; Longshore, K.M.; Thompson, D.B. Quantifying Landscape Ruggedness for Animal Habitat Analysis: A Case Study Using Bighorn Sheep in the Mojave Desert. *J. Wildl. Manag.* **2007**, *71*, 1419–1426. [CrossRef]
37. Wilson, M.F.J.; O'Connell, B.; Brown, C.; Guinan, J.C.; Grehan, A.J. Multiscale Terrain Analysis of Multibeam Bathymetry Data for Habitat Mapping on the Continental Slope. *Mar. Geod.* **2007**, *30*, 3–35. [CrossRef]
38. Misiuk, B.; Lecours, V.; Bell, T. A multiscale approach to mapping seabed sediments. *PLoS ONE* **2018**, *13*, e0193647. [CrossRef]
39. Haralick, R.M.; Shanmugam, K.; Dinstein, I.H. Textural Features for Image Classification. *IEEE Trans. Syst. Man Cybern.* **1973**, *SMC-3*, 610–621. [CrossRef]
40. Kursa, M.B.; Rudnicki, W.R. Feature Selection with the Boruta Package. *J. Stat. Softw.* **2010**, *36*. [CrossRef]
41. Bivand, R.; Keitt, T.; Rowlingson, B.; Pebesma, E.; Sumner, M.; Hijmans, R.; Rouault, E. Package 'rgdal'. Bindings for the Geospatial Data Abstraction Library. Available online: https://cran.r-project.org/web/packages/rgdal/index.html (accessed on 15 October 2017).
42. Montereale-Gavazzi, G.; Roche, M.; Lurton, X.; Degrendele, K.; Terseleer, N.; Van Lancker, V. Seafloor change detection using multibeam echosounder backscatter: Case study on the Belgian part of the North Sea. *Mar. Geophys. Res.* **2017**, *39*, 229–247. [CrossRef]
43. Kursa, M.B.; Rudnicki, W.R. Package 'Boruta'. Wrapper Algorithm for All Relevant Feature Selection. 2016. Available online: https://notabug.org/mbq/Boruta/ (accessed on 29 October 2018).
44. Jenks, G. The Data Model Concept in Statistical Mapping. *Int. Yearbook Cartogr.* **1967**, *7*, 186–190.
45. Benz, U.C.; Hofmann, P.; Willhauck, G.; Lingenfelder, I.; Heynen, M. Multi-resolution, object-oriented fuzzy analysis of remote sensing data for GIS-ready information. *ISPRS J. Photogramm. Remote Sens.* **2004**, *58*, 239–258. [CrossRef]
46. Lucieer, V.; Hill, N.A.; Barrett, N.S.; Nichol, S. Do marine substrates 'look' and 'sound' the same? Supervised classification of multibeam acoustic data using autonomous underwater vehicle images. *Estuar. Coast. Shelf Sci.* **2013**, *117*, 94–106. [CrossRef]
47. Diesing, M.; Green, S.L.; Stephens, D.; Lark, R.M.; Stewart, H.A.; Dove, D. Mapping seabed sediments: Comparison of manual, geostatistical, object-based image analysis and machine learning approaches. *Cont. Shelf Res.* **2014**, *84*, 107–119. [CrossRef]
48. Montereale Gavazzi, G.; Madricardo, F.; Janowski, L.; Kruss, A.; Blondel, P.; Sigovini, M.; Foglini, F. Evaluation of seabed mapping methods for fine-scale classification of extremely shallow benthic habitats—Application to the Venice Lagoon, Italy. *Estuar. Coast. Shelf Sci.* **2016**, *170*, 45–60. [CrossRef]
49. Janowski, L.; Tegowski, J.; Nowak, J. Seafloor mapping based on multibeam echosounder bathymetry and backscatter data using Object-Based Image Analysis: A case study from the Rewal site, the Southern Baltic. *Oceanol. Hydrobiol. Stud.* **2018**, *47*, 248–259. [CrossRef]
50. Breiman, L.; Friedman, J.H.; Olshen, R.A.; Stone, C.J. *Classification and Regression Trees*; Wadsworth: Belmont, NY, USA, 1984.
51. Cortes, C.; Vapnik, V. Support-vector networks. *Mach. Learn.* **1995**, *20*, 273–297. [CrossRef]
52. Breiman, L. Random Forests. *Mach. Learn.* **2001**, *45*, 5–32. [CrossRef]
53. Mehryar, M.; Rostamizadeh, A.; Talwalkar, A. *Foundations of Machine Learning*; The MIT Press: Cambridge, UK, 2012.
54. Ripley, B.D. *Pattern Recognition and Neural Networks*; Cambridge University Press: Cambridge, UK, 1996.
55. Burges, C. A Tutorial on Support Vector Machines for Pattern Recognition. *Data Min. Knowl. Discov.* **1998**, *2*, 121–167. [CrossRef]

56. Rodriguez-Galiano, V.F.; Ghimire, B.; Rogan, J.; Chica-Olmo, M.; Rigol-Sanchez, J.P. An assessment of the effectiveness of a random forest classifier for land-cover classification. *ISPRS J. Photogramm. Remote Sens.* **2012**, *67*, 93–104. [CrossRef]
57. Bishop, C. *Neural Networks for Pattern Recognition*; University Press: Oxford, UK, 1995.
58. Foody, G.M. Status of land cover classification accuracy assessment. *Remote Sens. Environ.* **2002**, *80*, 185–201. [CrossRef]
59. Story, M.; Congalton, R.G. Accuracy assessment: A user's perspective. *Photogramm. Eng. Remote Sens.* **1986**, *52*, 397–399.
60. Congalton, R.G. A review of assessing the accuracy of classifications of remotely sensed data. *Remote Sens. Environ.* **1991**, *37*, 35–46. [CrossRef]
61. Cohen, J. A Coefficient of Agreement for Nominal Scales. *Educ. Psychol. Meas.* **1960**, *20*, 37–46. [CrossRef]
62. Feldens, P.; Schulze, I.; Papenmeier, S.; Schönke, M.; Schneider von Deimling, J. Improved Interpretation of Marine Sedimentary Environments Using Multi-Frequency Multibeam Backscatter Data. *Geosciences* **2018**, *8*. [CrossRef]
63. Diesing, M.; Stephens, D. A multi-model ensemble approach to seabed mapping. *J. Sea Res.* **2015**, *100*, 62–69. [CrossRef]
64. Rattray, A.; Ierodiaconou, D.; Womersley, T. Wave exposure as a predictor of benthic habitat distribution on high energy temperate reefs. *Front. Mater. Sci.* **2015**, *2*, 1–14. [CrossRef]
65. Hasan, R.; Ierodiaconou, D.; Laurenson, L.; Schimel, A. Integrating multibeam backscatter angular response, mosaic and bathymetry data for benthic habitat mapping. *PLoS ONE* **2014**, *9*, e97339. [CrossRef]
66. Brown, C.J.; Sameoto, J.A.; Smith, S.J. Multiple methods, maps, and management applications: Purpose made seafloor maps in support of ocean management. *J. Sea Res.* **2012**, *72*, 1–13. [CrossRef]
67. Hasan, R.; Ierodiaconou, D.; Monk, J. Evaluation of Four Supervised Learning Methods for Benthic Habitat Mapping Using Backscatter from Multi-Beam Sonar. *Remote Sens.* **2012**, *4*, 3427–3443. [CrossRef]
68. Carlotto, M.J. Effect of errors in ground truth on classification accuracy. *Int. J. Remote Sens.* **2009**, *30*, 4831–4849. [CrossRef]
69. Diesing, M.; Mitchell, P.; Stephens, D. Image-based seabed classification: What can we learn from terrestrial remote sensing? *ICES J. Mar. Sci.* **2016**, *73*, 2425–2441. [CrossRef]
70. Fogarin, S.; Madricardo, F.; Zaggia, L.; Kruss, A.; Montereale-Gavazzi, G.; Ferrarin, C.; Sigovini, M.; Lorenzetti, G.; Manfé, G. Benthic Morphologies and Habitats in a Shallow Highly Human Impacted Tidal Inlet. In Proceedings of the GeoHab 2016, Winchester, UK, 2–6 May 2016.
71. Lu, D.; Weng, Q. A survey of image classification methods and techniques for improving classification performance. *Int. J. Remote Sens.* **2007**, *28*, 823–870. [CrossRef]
72. Ierodiaconou, D.; Monk, J.; Rattray, A.; Laurenson, L.; Versace, V.L. Comparison of automated classification techniques for predicting benthic biological communities using hydroacoustics and video observations. *Cont. Shelf Res.* **2011**, *31*, S28–S38. [CrossRef]
73. Hasan, R.; Ierodiaconou, D.; Laurenson, L. Combining angular response classification and backscatter imagery segmentation for benthic biological habitat mapping. *Estuar. Coast. Shelf Sci.* **2012**, *97*, 1–9. [CrossRef]

Oświadczenia współautorów

Dr Łukasz Janowski
Maritime Institute,
Gdynia Maritime University,
(e-mail: ljanowski@im.umg.edu.pl)

Gdańsk, 07 February 2022
(city)

Author Contribution Statement

I declare that my contribution to the paper:

Janowski, L.; Trzcinska, K.; Tegowski, J.; Kruss, A.; Rucinska-Zjadacz, M.; Pocwiardowski, P. Nearshore benthic habitat mapping based on multi-frequency, multibeam echosounder data using a combined object-based approach: A case study from the Rowy Site in the Southern Baltic Sea. *Remote Sens*. 2018, 10, 1983. https://doi.org/10.3390/rs10121983

included:

- conceptualization,
- methodology,
- data processing,
- original draft preparation.

Overall, I estimate that my contribution to this work is **55%**.

Łukasz Janowski

Łukasz Janowski

Mgr Karolina Trzcińska
Department of Geophysics
Institute of Oceanography, University of Gdańsk
(e-mail: karolina.trzcinska@ug.edu.pl)

Gdańsk, 07 February 2022

Author Contribution Statement

I declare that my contribution to the paper:

Janowski, L.; Trzcinska, K.; Tegowski, J.; Kruss, A.; Rucinska-Zjadacz, M.; Pocwiardowski, P. Nearshore benthic habitat mapping based on multi-frequency, multibeam echosounder data using a combined object-based approach: A case study from the Rowy Site in the Southern Baltic Sea. *Remote Sens.* 2018, 10, 1983. https://doi.org/10.3390/rs10121983

included:

- data acquisition,
- data processing.

Overall, I estimate that my contribution to this work is **35%**.

I have done the following work:

- participation in research planning,
- participation in data recording,
- participation in data processing,
- participation in interpretation of results.

Karolina Trzcińska

Karolina Trzcińska

Prof. dr hab. Jarosław Tęgowski
Department of Geophysics
Institute of Oceanography, University of Gdańsk
(e-mail: jaroslaw.tegowski@ug.edu.pl)

Gdańsk, 07 February 2022

Author Contribution Statement

I declare that my contribution to the paper:

Janowski, L.; Trzcinska, K.; Tegowski, J.; Kruss, A.; Rucinska-Zjadacz, M.; Pocwiardowski, P. Nearshore benthic habitat mapping based on multi-frequency, multibeam echosounder data using a combined object-based approach: A case study from the Rowy Site in the Southern Baltic Sea. *Remote Sens*. 2018, 10, 1983. https://doi.org/10.3390/rs10121983

included:

- conceptualization,
- data acquisition,
- review and editing of the Manuscript,
- supervision.

Overall, I estimate that my contribution to this work is **4%**.

....

Jarosław Tęgowski

Dr Aleksandra Kruss
NORBIT-Poland Sp. z o.o.
(e-mail: aleksandra.kruss@norbit.com)

Sopot......................, 07 February 2022
(city)

Author Contribution Statement

I declare that my contribution to the paper:

Janowski, L.; Trzcinska, K.; Tegowski, J.; Kruss, A.; Rucinska-Zjadacz, M.; Pocwiardowski, P. Nearshore benthic habitat mapping based on multi-frequency, multibeam echosounder data using a combined object-based approach: A case study from the Rowy Site in the Southern Baltic Sea. *Remote Sens*. 2018, 10, 1983. https://doi.org/10.3390/rs10121983

included:

- data acquisition,
- data processing.

Overall, I estimate that my contribution to this work is **2%**.

Aleksandra Kruss
....

Aleksandra Kruss

Dr Maria Rucińska
Department of Geophysics
Institute of Oceanography, University of Gdańsk
(e-mail: maria.rucinska@ug.edu.pl)

Gdańsk, 07 February 2022

Author Contribution Statement

I declare that my contribution to the paper:

Janowski, L.; Trzcinska, K.; Tegowski, J.; Kruss, A.; Rucinska-Zjadacz, M.; Pocwiardowski, P. Nearshore benthic habitat mapping based on multi-frequency, multibeam echosounder data using a combined object-based approach: A case study from the Rowy Site in the Southern Baltic Sea. *Remote Sens*. 2018, 10, 1983. https://doi.org/10.3390/rs10121983

included:

- data processing.

Overall, I estimate that my contribution to this work is **2%**.

Rucińska
....

Maria Rucińska

Dr **Paweł Poćwiardow**ski
NORBIT-Poland Sp. z o.o.
(e-mail: pawel@norbit.com)

Santa Barbara, 07 February 2022
(city)

Author Contribution Statement

I declare that my contribution to the paper:

Janowski, L.; Trzcinska, K.; Tegowski, J.; Kruss, A.; Rucinska-Zjadacz, M.; Pocwiardowski, P. Nearshore benthic habitat mapping based on multi-frequency, multibeam echosounder data using a combined object-based approach: A case study from the Rowy Site in the Southern Baltic Sea. *Remote Sens*. 2018, 10, 1983. https://doi.org/10.3390/rs10121983

included:

- data acquisition,
- data processing.

Overall, I estimate that my contribution to this work is **2%**.

Paweł Poćwiardowski

PUBLIKACJA 2

Trzcinska K., Janowski L., Nowak J., Rucinska-Zjadacz M., Kruss A., Schneider von Deimling J., Pocwiardowski P., Tegowski J. Spectral features of dual-frequency multibeam echosounder data for benthic habitat mapping. *Mar. Geol*. 2020, 427, 106239. https://doi.org/10.1016/j.margeo.2020.106239

Marine Geology 427 (2020) 106239

Contents lists available at ScienceDirect

Marine Geology

journal homepage: www.elsevier.com/locate/margo

Invited Research Article

Spectral features of dual-frequency multibeam echosounder data for benthic habitat mapping

Karolina Trzcinska[a], Lukasz Janowski[a,b,*], Jaroslaw Nowak[c], Maria Rucinska-Zjadacz[a], Aleksandra Kruss[d], Jens Schneider von Deimling[e], Pawel Pocwiardowski[d], Jaroslaw Tegowski[a]

[a] Institute of Oceanography, University of Gdansk, al. Marszalka Pilsudskiego 46, 81-378 Gdynia, Poland
[b] Gdynia Maritime University, Morska 81-87 Str., 81-225 Gdynia, Poland
[c] MEWO S.A., Starogardzka 16, 83-010 Straszyn, Poland
[d] NORBIT-Poland Sp. z o.o., al. Niepodleglosci 813-815/24, 81-810 Sopot, Poland
[e] Institute of Geosciences Christian-Albrechts-Universität zu Kiel, Otto-Hahn-Platz 1, 24118 Kiel, Germany

ARTICLE INFO

Keywords:
Rough seafloor surface
Spectral features
Multibeam echosounder
Object-based image analysis
Benthic habitat mapping

ABSTRACT

Automatic methods of seafloor mapping are still in their early stage of development, despite the technical progress made in recent years. A serious imperfection is the limited types of predictor features available for seabed classification. It is therefore desirable to introduce new class of spectral features to benthic habitat mapping. In this study, we introduced eight spectral features of a rough seafloor surface that were indicative of better seabed classification. We compared them with traditional secondary features, like terrain variables and textural features. The suitability of 48 variables was tested, and the most important features were identified. The selected variables were used to perform a supervised object-based image analysis using four machine learning algorithms. We found that backscatter was the strongest predictor, followed by several spectral features from bathymetry that appeared more predictive than bathymetry itself. The highest overall accuracy of predictive model reached approximately 86% using the support vector machine classifier. The innovative results of this study suggest further application of the spectral features for predictive benthic habitat mapping, including research based on multi-frequency multibeam echosounder datasets. The utilisation of spectral features derived from bathymetry provide an important step towards more accurate maps of benthic habitats and seabed sediments composition.

1. Introduction

The ocean floor is the least explored surface of Earth. At present, it is estimated that less than 15% of the seafloor has been mapped in detail. On the other hand, the surfaces of the Moon and Mars have been mapped in significantly greater detail (Jones, 1999). Global initiatives, such as Seabed 2030 of the General Bathymetric Chart of the Oceans group, aim to change this state of knowledge by mapping the entire seabed by the year 2030 (Mayer et al., 2018).

Apart from side-scan based seafloor analyses, remote sensing measurements of the seabed surface have often employed multibeam echosounder (MBES) systems. Originally, MBES equipment was designed to collect measurements of the seafloor bathymetry, which allowed for the generation of digital elevation models (DEMs) of the seabed. In the early 1990s, an MBES was developed that could measure the backscattering strength from the seafloor based on its corresponding properties (Lamarche and Lurton, 2017). Recent recommendations have suggested concurrent acquisition of bathymetry and seafloor backscatter strength (or a related variable), as well as further generation of georeferenced grids of bathymetry and co-registered backscatter mosaics (Schimel et al., 2018).

1.1. Multibeam echosounder features and their impact on benthic habitat mapping studies

Terrestrial remote sensing studies often benefit from many features derived from different sensors, for instance, spectral or multi-spectral signatures, textural derivatives, or various indices (e.g. the Normalised Difference Vegetation Index). In this study, we used the term 'feature' in its typical sense with respect to remote sensing literature, as it is a predictor variable extracted from the remote sensing data for its usage in image classification (Diesing et al., 2016). Moreover, hereinafter, the

* Corresponding author at: Gdynia Maritime University, Morska 81-87 Str., 81-225 Gdynia, Poland
E-mail address: ljanowski@im.umg.edu.pl (L. Janowski).

https://doi.org/10.1016/j.margeo.2020.106239
Received 29 November 2019; Received in revised form 11 May 2020; Accepted 13 May 2020
Available online 19 May 2020

term 'spectral' has been used as a descriptor of the rough seafloor surface.

Recent benthic habitat mapping studies have underlined the utilisation of different features of MBES bathymetry and backscatter data (Diesing et al., 2016; Lecours et al., 2016; Held and Schneider von Deimling, 2019). Special attention has been paid to the geomorphometric analysis of bathymetry (Goff and Jordan, 1988; Wilson et al., 2007; Micallef et al., 2012; Li et al., 2016; Diesing and Thorsnes, 2018; Gafeira et al., 2018; Lucieer et al., 2018), textural analysis of backscatter (Montereale-Gavazzi et al., 2017; Prampolini et al., 2018; Samsudin and Hasan, 2017), and multi-scale analysis, including the geographic context of MBES datasets (Lecours et al., 2015; Misiuk et al., 2018; Porskamp et al., 2018). For example, Conti et al. (2019) used different feature categories (from bathymetry, texture, optical properties, and object-based shape) for the classification of a cold-water coral mound based on MBES and a high-resolution video mosaic. Additionally, Janowski et al. (2018a) extracted sixteen features of bathymetry and nine object-based features of backscatter to execute the mapping of seabed sediments in the Polish coastal area of the southern Baltic Sea. Furthermore, Rattray et al. (2015) introduced wave exposure as an oceanographic predictor variable for the mapping of high energy temperate reefs in Victoria, Australia.

Recent reviews of literature emphasise the need for new features for benthic habitat mapping (Diesing et al., 2016). It is known that environmental factors, such as light penetration in the water column, primary productivity, hydrodynamics, temperature, salinity, and oxygen concentration determine the distribution of habitats on the seabed (Brown et al., 2011). However, modelled features representing these factors are typically generated in spatial and temporal scales that are very different (e.g. often significantly larger) from those of MBES datasets, thereby limiting their applicability. On the other hand, secondary features extracted from MBES bathymetry and backscatter are directly related to the spatial and temporal extent of their counterparts. The development of new features may allow for a better understanding of the environmental processes occurring on and/or influencing the seabed, and proper application may increase predictive power and improve classification accuracy.

Spectral parameters have been successfully used to classify sediment types using single beam echosounder registrations (Tegowski et al., 2003). Previous research on spectral features of MBES bathymetry has indicated their utility for a detailed description of roughness and seafloor geomorphology, as well as the classification of seafloor sediments. Additionally, they have been used for benthic habitat mapping using Principal Components Analysis to reduce correlated data and the Fuzzy C-means clustering algorithm with a declared number of three classes (Tegowski et al., 2018). In this study, we presented and evaluated eight spectral features derived from bathymetry and applied them for the classification of the seabed using object-based image analysis (OBIA). These parameters originated from two-dimensional fast Fourier transformation (2D FFT). Lyons et al. (2002) described one of the first applications of this method for seabed characterisation with high-resolution, in which the photogrammetric method (stereoscopic photograph) was utilised; a three-dimensional model of the bottom surface was generated using this approach. Application of the 2D FFT allowed for the spatial distribution of the power spectral density of the surface heights to be obtained. The same technique has been applied in several other studies (e.g. Briggs et al., 2005). Moreover, this method was improved upon and applied to the analysis of high-resolution bathymetry from modern hydroacoustic measurements, including the application of a MBES (e.g. Cazenave et al., 2008; Lefebvre et al., 2009). Schönke et al. (2017) used 2D Fourier transform to describe the microroughness of the seabed based on underwater laser line scanning in the southeastern North Sea.

Classification of the seabed substrata and benthic habitats is one of the main tasks necessary for the spatial planning of the marine environment. In addition to providing crucial information for the establishment of Marine Protected Areas, such actions are within the main aims of Descriptor 6 of the Marine Strategy Framework Directive 2008/56/EC, which is related to seafloor integrity. In general, these actions assume the development of standardised methods for seabed mapping and monitoring. Although recent studies include proposals for the working procedures of benthic habitat mapping or the development of habitat classification schemes, diversity of specific environmental conditions (e.g. depth or sediment types), causes that they are still only valid for strict spatial areas (Strong et al., 2019).

1.2. Multi-frequency multibeam echosounder studies

A recent trend in benthic habitat mapping is the use of multi-frequency MBES data. Bottom backscattering strength registered by echosounder strongly depends on the frequency of the emitted signal, its true incidence angle, seabed roughness, and geo-acoustic properties of the seafloor. The dependency of backscatter strength on frequency has been observed in laboratory and field studies with various responses from different sediment types exhibited (e.g. Jackson et al., 1986; Urick, 1983). Recent habitat mapping studies have emphasised the use of multi-frequency MBES datasets for better discrimination between seabed types (Feldens et al., 2018; Gaida et al., 2018; Janowski et al., 2018b; Fakiris et al., 2019).

High-frequency pulses allow for the detecting smaller objects and seabed structures; however, such pulses are strongly attenuated, thus limiting the sonar range. Low-frequency signals are not as attenuated; they can penetrate deeper into the sediments below the seafloor, but they are less sensitive to small features and weak boundaries with a slight change in acoustic impedance, such as the boundary between water and mud. Overall, acoustic images (especially of seafloor sediments) that are recorded at several frequencies often provide more information with respect to the physical and biological characteristics of seabed habitats compared with that of a single-frequency (Feldens et al., 2018; Gaida et al., 2018; Janowski et al., 2018b; Fakiris et al., 2019). Finer sediments, such as sands and silts, are more sensitive to acoustic frequencies than coarser sediments, such as gravel, shells, or boulders (Jackson et al., 1986; Williams et al., 2009; Hefner et al., 2010; Gaida et al., 2018).

In this study, we focused on the spectral features derived from bathymetry, which was considered independent of the frequency. Most applicable for this approach were MBES, which delivered bathymetry, as well as co-registered and geolocated backscatter of the seabed. In this study, we did not focus on multi-spectral MBES, although we used several frequencies to enlarge our feature space. Our objectives were as follows: (1) to introduce eight spectral features of a rough seafloor surface, (2) to evaluate the importance of spectral features for benthic habitat mapping, and (3) to classify benthic habitats and estimate the accuracy of classification, including the input from spectral features.

2. Materials and methods

2.1. Study site

The study site was situated in a shallow area off the Polish coast of the southern Baltic Sea. The water depth ranged between 3.8 and 20.1 m below sea level (Fig. 1). The site was in direct proximity to Slowinski National Park and partially located within a Natura 2000 area, which protects marine areas up to 10 m below sea level. In the research area, six classes of benthic habitats were present, including flat areas of very fine sand with traces of worm burrows (VFS), sands with ripple marks (S), sandy gravels or gravelly sands (SG_GS), boulders covered with a large concentration of *Mytilus trossulus* bivalves (B), boulders covered with *Mytilus trossulus* and large patches of red algae (R), and artificial structures (A), such as a shipwreck located in the centre of the study area (Kendzierska, 2009; Tegowski et al., 2009; Janowski et al., 2018b).

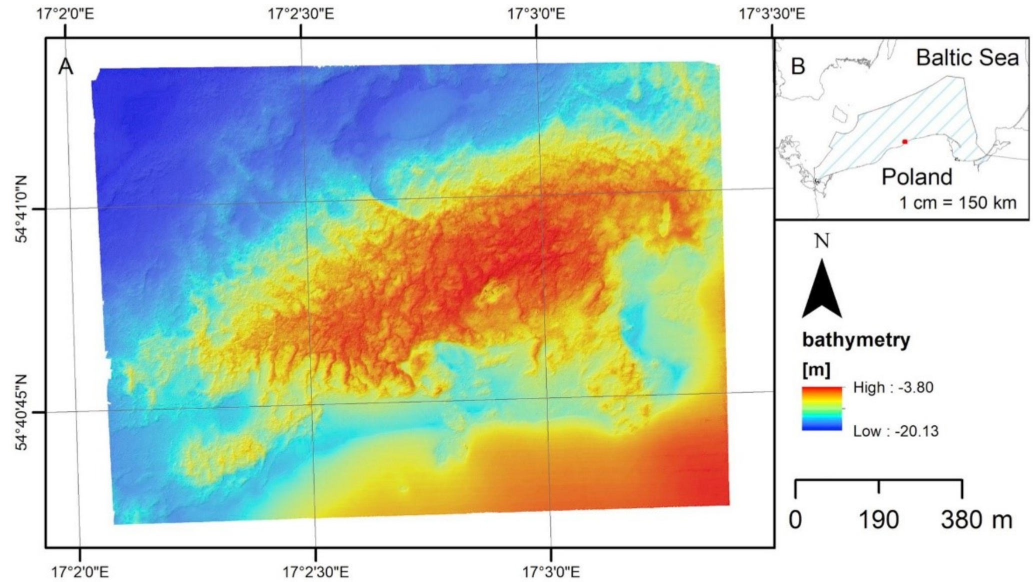

Fig. 1. (A) Bathymetry and (B) location of the Rowy Site in the southern Baltic Sea. For visualisation and processing purposes, multibeam echosounder (MBES) coverage is clipped to a regular shape, omitting vessel track lines that extend beyond the rectangular area.

The seabed consisted of valleys and crests with depths of approximately 2 m and lengths of dozens of metres to approximately 180 m. The main geomorphologic structure was a large 1100 m × 500 m moraine outcrop located in the centre of the area. Filled with glacial tills, it was covered with areas comprising numerous boulders with red algae vegetation. Such a hard substratum has not been typical along the Polish coast of the Baltic Sea; however, it allowed for conditions necessary for the development of unique benthic communities, such as *Mytilus trossulus* bivalves and *Furcellaria lumbricalis* or *Polysiphonia fucoides* red algae. Previous studies of this site have confirmed its high ecological relevance (Kendzierska, 2009; Tegowski et al., 2009). The area surrounding the moraine shoal appeared inhomogeneous and consisted of sands of different grain sizes and occasional gravel admixtures. The bio- and geodiversity of this area has made it highly suitable for the evaluation of non-invasive research methods of the seafloor, including the determination of different acoustic characteristics.

2.2. Data acquisition and processing

MBES datasets were acquired using a NORBIT iWBMS STX system (manufactured by Norbit ASA: Po box 1858, Lade 7440, Trondheim, Norway) mounted on a portable pole on the 'Zelint' research vessel. The MBES device was manufactured especially for use in shallow marine areas and typically reserved for hydroacoustic measurements from 0.2 to 160 m below sea level. At a maximum frequency of 400 kHz, the receiving beam width was 0.9° x 0.9° and allowed for the collection of 512 beams. The MBES had an integrated WaveMaster (manufactured by Applanix: 85 Leek Crescent, Richmond Hill, ON Canada, L4B 3B3) Global Navigation Satellite System/Inertial Navigation System that was supported by Real Time Kinematic/Global Positioning System corrections for precise positioning and altitude measurements. Using the Polish Active Geodetic Network - European Position Determination System NAWGEO service (www.asgeupos.pl), we received real-time positioning with an accuracy of 3 cm horizontally and 5 cm vertically. In this study, the influence of acoustic absorption on the recorded signals was initially ignored; however, it was considered during post-processing. To fulfil our research purposes, the frequency was set to either 150 or 400 kHz, and the swath range covered 150–160°. The maximum ping rate for both frequencies was 20 Hz, and we applied a 200 µs (for 150 kHz) and 500 µs (for 400 kHz) modulated chirp with a bandwidth of 6 and 80 kHz, respectively. Surveys were designed in respect to the systematic collection of five sound velocity profiles. A constant vessel speed 2.83–3.09 m/s was maintained.

The MBES datasets were processed using QPS Qimera 1.6.3 and Fledermaus Geocoder Toolbox 7.8.4 software, which allowed for bathymetry and backscatter data processing, cleaning, and mosaicking. After registration, a patch test was applied. A bathymetric grid with a pixel size of 0.25 m × 0.25 m was calculated for both frequencies. Because we did not find any significant differences in the MBES measurements recorded at 150 and 400 kHz, we combined the frequencies to obtain the bathymetry from a dense point cloud. The Qimera software allowed for the manual cleaning of any outliers and/or acoustic spikes. Backscatter grids were generated based on beam time series (snippets) with resolutions of 0.75 m and 0.5 m for 150 kHz and 400 kHz, respectively, using a mosaicking method with an Angle Varying Gain (AVG) correction included in the Geocoder engine (Fonseca et al., 2009). The AVG method has been commonly utilised for the correction of MBES angular dependency and to obtain a normalised seafloor backscatter dataset. We applied the default settings of the AVG, which were 'flat' (mode), 'blend' (mosaicking style), and '300' (size of processing window). The flat mode was responsible for reducing backscatter signal noise and smoothing fine variations. The blend mosaicking style was responsible for the management of overlapping MBES swaths. This allowed for the blending of the pixels along the nadir track line of the vessel with other overlapping pixels (Schimel et al., 2018). The window size corresponded to a specific number of consecutive MBES pings considered for AVG correction (e.g. see Parnum and Gavrilov, 2011). All the MBES datasets were extracted as surface floating point files in a Universal Transverse Mercator (zone 33 N) projected coordinate system.

We applied the general workflow for benthic habitat mapping developed by Janowski et al. (2018b) to the MBES data. Hence, we extracted statistical and geomorphometric features of bathymetry, for

Table 1
List of bathymetry and backscatter features extracted in this study.

ID	Feature of bathymetry	Window size	ID	Feature of backscatter	Scale of objects
1–4	Standard deviation	3 × 3, 5 × 5, 7 × 7, 9 × 9	40	Standard deviation	1–20
5–8	Kurtosis	3 × 3, 5 × 5, 7 × 7, 9 × 9	41	GLCM Homogeneity	1–20
9–12	VRM ruggedness	3 × 3, 5 × 5, 7 × 7, 9 × 9	42	GLCM Entropy	1–20
13	Slope	3 × 3	43	GLCM Contrast	1–20
14	Variance	3 × 3	44	GLCM Standard Deviation	1–20
15	Curvature	3 × 3	45	GLCM Dissimilarity	1–20
16	Profile curvature	3 × 3	46	GLCM Correlation	1–20
17	Planar curvature	3 × 3	47	GLCM Angular Second Moment	1–20
18	Aspect	3 × 3	48	GLCM Mean	1–20
19	Eastness	3 × 3			
20	Northness	3 × 3			
21	Surface area to planar area (arc-chord ratio)	3 × 3			
22	BPI 50	3 × 3			
23	BPI 250	3 × 3			
24–25	Fractal dimension (Dfft)	20 × 20, 35 × 35			
26–27	Spectral moment m_0	20 × 20, 35 × 35			
28–29	Spectral moment m_2	20 × 20, 35 × 35			
30–31	Mean frequency (ω_0)	20 × 20, 35 × 35			
32–33	Spectral width (v^2)	20 × 20, 35 × 35			
34–35	Spectral skewness ($\tilde{\gamma}_s$)	20 × 20, 35 × 35			
36–37	Quality factor (*Q*-factor)	20 × 20, 35 × 35			
38–39	Spectral skewness defined for central moments (γ_{s_centr})	20 × 20, 35 × 35			

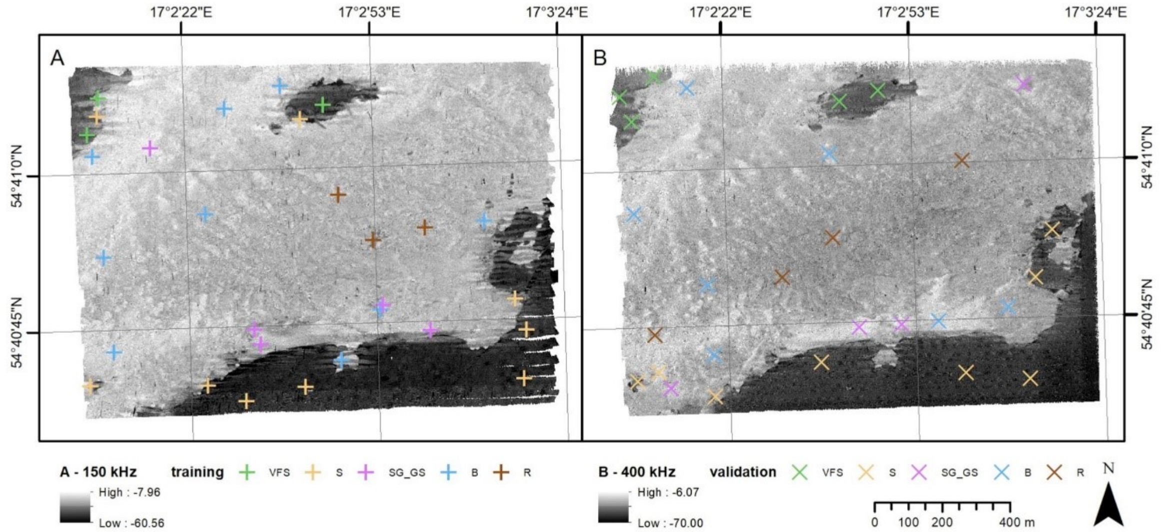

Fig. 2. Locations of ground-truth training and validation samples on multibeam echosounder (MBES) backscatter image for (A) 150 kHz and (B) 400 kHz frequencies; S - sand, B - boulders, R - red algae on boulders, SG_GS - sandy gravel or gravelly sand, and VFS - very fine sand. (For interpretation of the references to colour in this figure legend, the reader is referred to the web version of this article.)

instance, slope and vertical ruggedness measure (Sappington et al., 2007), bathymetric position index (Wilson et al., 2007), as well as textural features of backscatter, such as different types of grey level co-occurrence matrices (Haralick et al., 1973). Additionally, we derived first- and second-order 2D spectral parameters of bathymetry. A list of all extracted features is presented in Table 1. Features 1–23 were created using the Benthic Terrain Modeler toolbox for ArcGIS (Walbridge et al., 2018), features 24–39 were calculated using algorithms coded in MATLAB, and features 40–48 were created using OBIA workflows in Trimble eCognition software (Janowski et al., 2018b). When possible, we tested various sizes of rectangular moving windows or scales of image-based objects (Table 1), which enabled us to perform multi-scale analysis of geospatial datasets to a certain extent (Misiuk et al., 2018).

2.3. Bathymetric 2D spectral parameters

Utilising 2D FFT of the bathymetric grid allowed us to generate eight spectral parameters, which will be discussed in respect to their predictive power for the description of seafloor geomorphology and classification. The eight spectral parameters were zero-order spectral moment (m_0), second-order spectral moment (m_2), mean frequency (ω_0), spectral width (ν^2), spectral skewness (γ_s), spectral skewness defined for central moments (γ_{s_centr}), quality factor (*Q*-factor), and fractal dimension (Dfft).

2.3.1. Considerations of 2D seabed spectral parameters

Assuming that the height values of the bottom surface are normally distributed, and the surface is isotropic, the power spectral density can

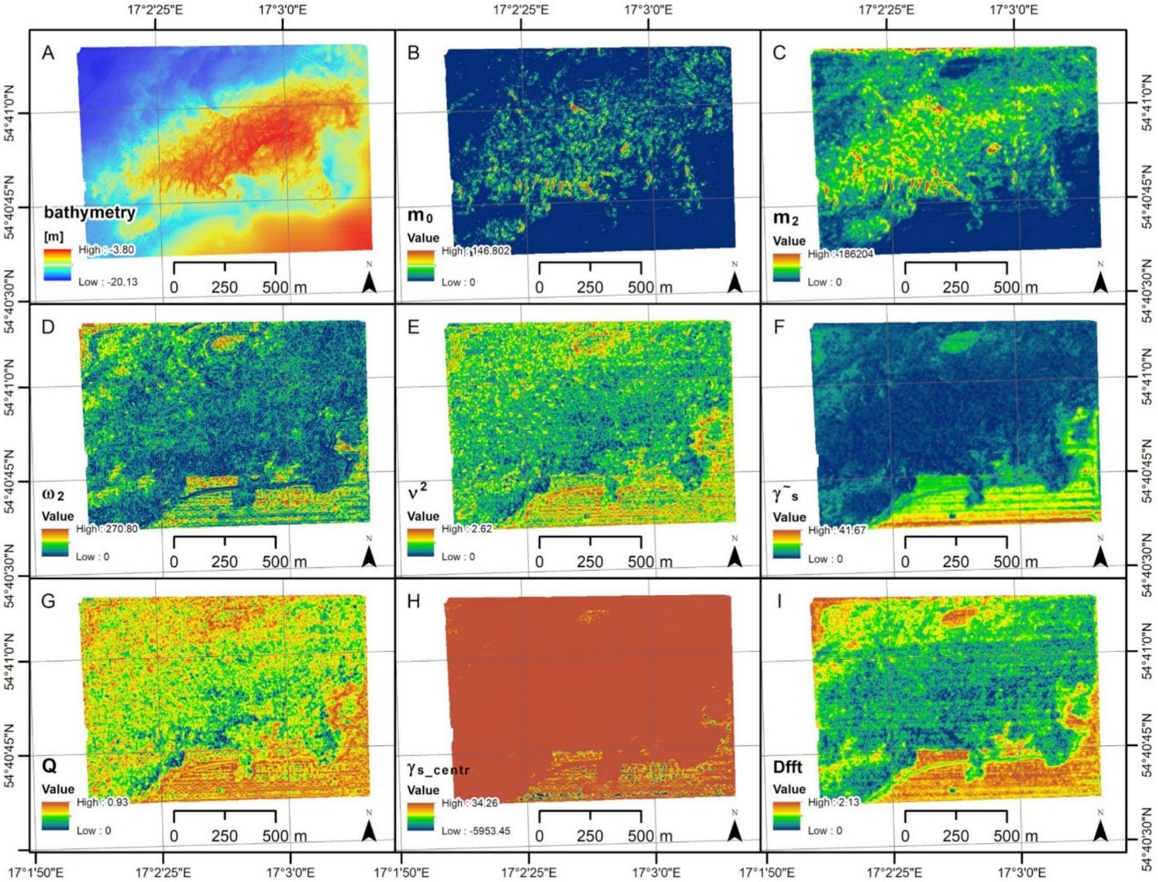

Fig. 3. Bathymetry and corresponding spectral parameters created using moving window with dimensions of 20 m × 20 m; (A) bathymetry; (B) zero-order spectral moment; (C) second-order spectral moment; (D) mean frequency; (E) spectral width, (F) spectral skewness; (G) quality factor; (H) spectral skewness defined for central moments; (I) fractal dimension.

be expressed as the following power function (Jackson et al., 1986; Jackson and Richardson, 2007):

$$W(\vec{k}) = W(k_x, k_y) = w_2 k^{-\gamma_2}, \tag{1}$$

where $\vec{k}\,(k_x, k_y)$ is the wave vector of surface inequalities, γ_2 is the exponent of the spectrum, and w_2 is the spectral power of the rough seabed surface expressed in cm^4. Both the γ_2 and w_2 spectral parameters comprehensively characterise the scale and degree of surface roughness in that they are basic parameters of the physical models of sound scattering at the bottom (APL, 1994). Measurements of the γ_2 using different techniques, such as stereophotography, laser scanning, acoustic scanning, and mechanical stylus scanning, indicated that the value of this parameter ranges from 2.4 to 3.9 (in most instances), whereas the mean value is 3.25 (APL, 1994). The values of the parameters w_2 and γ_2 can be determined from the Fourier spectrum of a rough surface, and such a method was adopted in this study.

The 2D normalised bathymetric cross spectrum *s(x,y)* can be represented by Fourier transformation as follows:

$$P(K_x, K_y) = \int_{-\infty}^{\infty}\int_{-\infty}^{\infty} s(x,y)e^{-i2\pi(K_x x, K_y y)}dxdy, \tag{2}$$

where K_x and K_y are the spatial wave numbers expressed in the cycle·m^{-1}. The result of the transformation is a spatial spectrum of the surface height. The 2D FFT requires subtraction of the average height and trend removal to avoid spectral leakage. Further reduction of the spectral leakage effect requires additional multiplication of the transformed bathymetric surface by a function of the discrete prolate spheroidal sequences spectral window, or in our case, a first-order parameter in which NW (Slepian bandwidth parameter) = two window widths. Our algorithm was performed on the basis of a moving window with the dimensions of 20 m × 20 m or 35 m × 35 m with a 90% overlap. After executing the 2D FFT, we extracted one-dimensional (1D) cross-sections spectra from 0° to 180° (every 5°) for which we calculated spectral parameters.

To find the specific features of the tested surface of the bottom, 1D spectra were parameterized, and the results were averaged. For each of the 37 spectra, spectral moments m_r (Clough and Penzien, 1975) were calculated as follows:

$$m_r = \int_0^{\infty} \omega^r S(\omega)d\omega, \tag{3}$$

where r is the order of the moment, ω is the circular frequency, and $S(\omega)$ is the density of the power spectrum.

The mean frequency is defined as the following equation:

$$\omega_0 = m_1/m_0. \tag{4}$$

The spectral width is calculated according to the following equation:

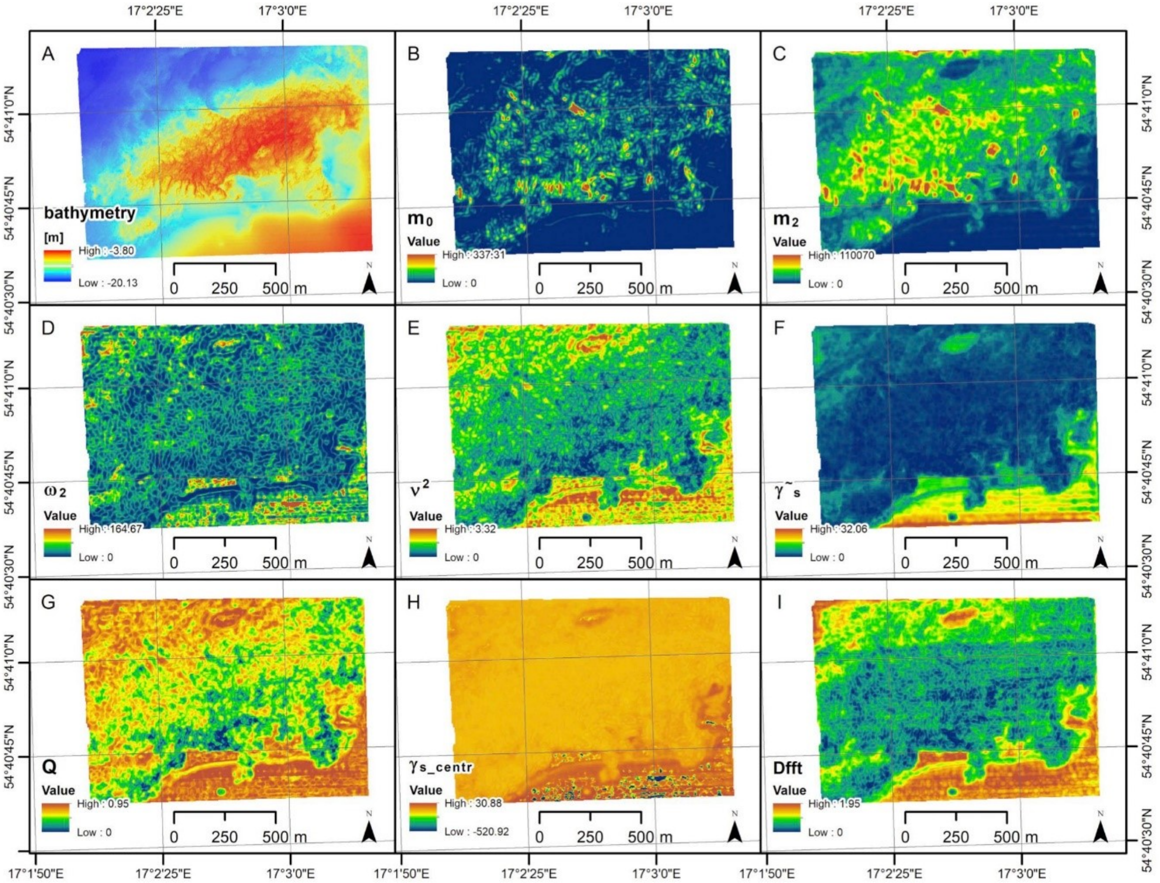

Fig. 4. Bathymetry and corresponding spectral parameters created using moving window with dimensions of 35 m × 35 m; (A) bathymetry; (B) zero-order spectral moment; (C) second-order spectral moment; (D) mean frequency; (E) spectral width, (F) spectral skewness; (G) quality factor; (H) spectral skewness defined for central moments; (I) fractal dimension.

$$\nu^2 = \frac{m_0 m_2}{m_1^2} - 1. \tag{5}$$

It is defined as the concentration of the spectral energy density around the mean frequency. The higher the value of average frequency, the lower the parameter value. Furthermore, the parameter value is higher for a wider spectrum and lower when the opposite is true. A very sensitive parameter for changes in the shape of the surface is the spectral skewness defined for central moments (Davidson and Louglin, 2000), which is calculated as follows:

$$\widetilde{\gamma}_s = \frac{\widetilde{m}_3}{\widetilde{m}_2^{3/2}}. \tag{6}$$

Another parameter based on 1D spectral density of power is the Dfft. If the rough surface of the bottom has fractal properties, the ratio between the spectrum $S(f)$ and the frequency f takes the form of an exponential relation for the frequency interval f (Mandelbrot, 1982) as follows:

$$S(f) = K{\cdot}f^{-\beta}, \tag{7}$$

where K is a constant, and β is the exponent of the power function. The spectrum slope is calculated by linear regression. The Dfft is defined as follows:

$$D_{FFT} = \frac{5-\beta}{2}. \tag{8}$$

Additionally, the Q-factor, which is a combination of spectral moments, can be also calculated with the following equation:

$$Q = \left(1 - \frac{m_1^2}{m_0 \bullet m_2}\right)^{0.5}. \tag{9}$$

The Q-factor is a measure of spectrum peak 'sharpness'. For the 1D spectra obtained in this way, the eight spectral parameters defined above were calculated. Whereas spectral parameters created with a moving window size of 20 m × 20 m had a resulting pixel resolution of 2 m × 2 m, parameters generated with the larger window size (35 m × 35 m) had a pixel resolution of 3.5 m × 3.5 m.

2.4. Ground-truth data acquisition and processing

Ground-truth samples were acquired with a remotely operated vehicle (ROV) and a Van Veen grab sampler. Samples were retrieved during three surveys on 7 September 2018, 20–23 November 2018, and 21–25 January 2019. Based on previous research in this area, as well as backscatter acoustic characteristics, the locations were carefully chosen in a representative way to capture all the properties of the seabed (Tegowski et al., 2009). ROV video recordings were collected in more

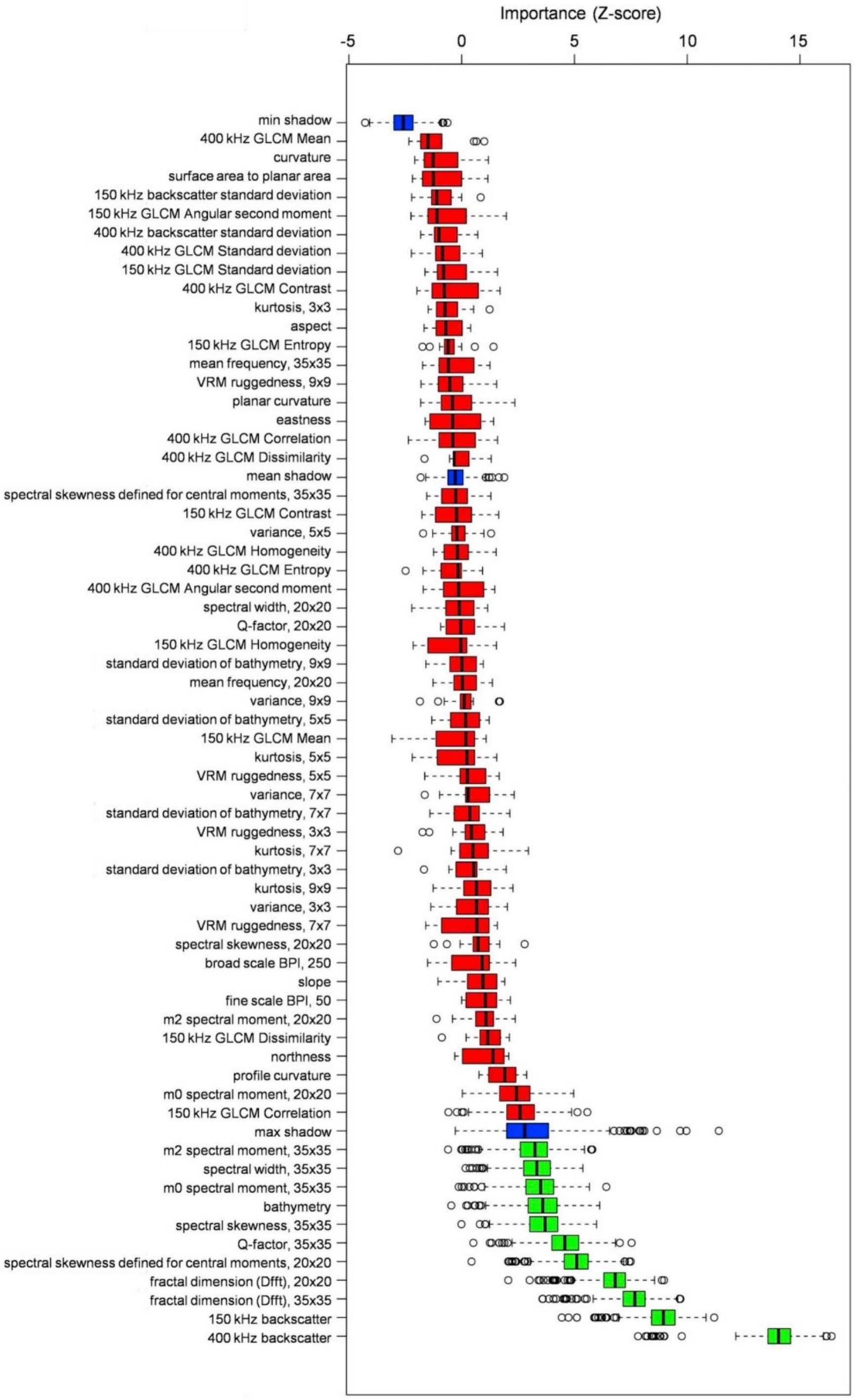

Fig. 5. Results of Boruta feature selection algorithm for all parameters used in this study.

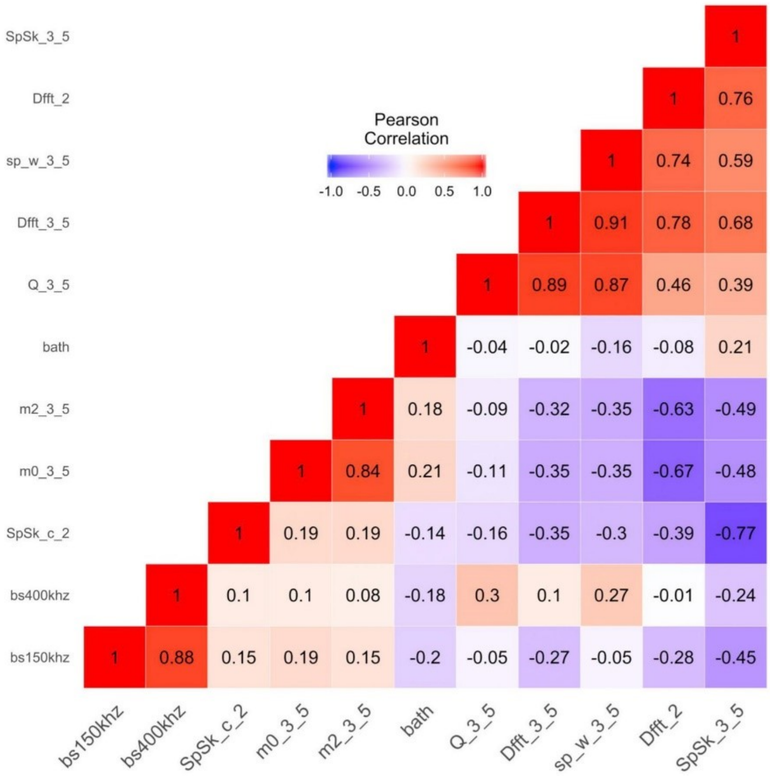

Fig. 6. Results of correlation matrix for features selected in this study; backscatter 150 kHz (bs150khz); backscatter 400 kHz (bs400khz); spectral skewness defined for central moments (20; SpSk_c_2); spectral moment m_0 (35; m_0_3_5); spectral moment m_2 (35; m_2_3_5); bathymetry (bath); *Q*-factor (35; Q_3_5); fractal dimension (35; Dfft_3_5); spectral width (35; sp_w_3_5); fractal dimension (20; Dfft_2); spectral skewness (35; SpSk_3_5).

than half the sites, allowing for the investigation of the locations and surrounding areas. Sediment samples were collected from 46 sites, and they were classified using the methods of Folk and Ward (1957), as well as the Wentworth method (Wentworth, 1922).

From the 57 ground-truth samples, 29 were chosen for the training of supervised classifiers, and 28 were used to test the classification performance. The split was performed based on random single splitting. Our split for the training/test samples was targeted to obtain better prediction performance than that of model fitting. Fig. 2 presents the locations of the ground-truth samples used for training and validation with reference to the MBES backscatter. Note that the A benthic habitat class is omitted in Fig. 2 because of its presence in only one specific site. It was, therefore, classified manually at the conclusion of the supervised classification process, based on the exact location of the shipwreck visible on the MBES bathymetry and ROV video datasets.

2.5. Image analysis for predictive habitat mapping

To evaluate the importance of individual features we applied the Boruta feature selection algorithm (Kursa and Rudnicki, 2010) based on the random forest (RF) machine learning algorithm by Breiman (2001). The algorithm belongs to the wrapper feature selection methods that evaluate the performance of a certain model after searching for all possible feature selections. Typically, wrapper methods aim to minimise prediction error, and because of this, they belong to common minimal-optimal feature selection methods as well (Kursa, 2016). The wrapper is implemented in R software using the 'Boruta' library. The wrapper method iteratively evaluates sets of different input features and calculates a *Z*-score, which is indicative of feature importance. Each evaluation is done by the introduction of other irrelevant features that are treated as a reference for the assessment of the original features. The Z-score is calculated based on the RF method during the training of the classifier (Breiman, 2001). Based on the feature importance measure, feature selection is performed iteratively, successively removing irrelevant features. To exclude tentative (unallocated) features, the maximum number of Boruta iterations was set to 5000. Although our aim was to identify all relevant features, including weakly relevant ones (Nilsson et al., 2007), we allowed the possibility of refinement if some were correlated. To remove highly correlated features, a correlation analysis was performed in the R software using a 'caret' package. Features with an absolute Pearson's correlation of 0.75 or higher were removed.

In this study, we used Trimble eCognition software to conduct an OBIA. This image processing technique was developed in the 2000s to manage an increasing number of high-resolution remote sensing images containing larger amounts of heterogenous information (Blaschke, 2010). Through a multiresolution segmentation (MS) algorithm, the OBIA merged similar pixels of an image into groups of uniform shapes and sizes (Benz et al., 2004). MS had various parameters that we defined and tested to generate meaningful image objects. Whereas the colour parameter corresponded to the relative values of the MBES backscatter intensity, the associated parameter (shape) was related to the ratio between compactness and smoothness. Compactness referred to the ratio between the segment border length and the square root of the pixel count within. Smoothness was related to the ratio between the border length of the segment and its bounding box (Benz et al., 2004). Both weighted pairs of parameters were determined with values of 0.1 to 0.9, and the total value of each pair was 1. The MS parameters of shape and compactness were defined as 0.1 and 0.5, respectively. We also tested 1–20 scale parameters of MS that were responsible for the termination of the merging process of the image objects. Segmentation was performed to delineate image objects based equally on two

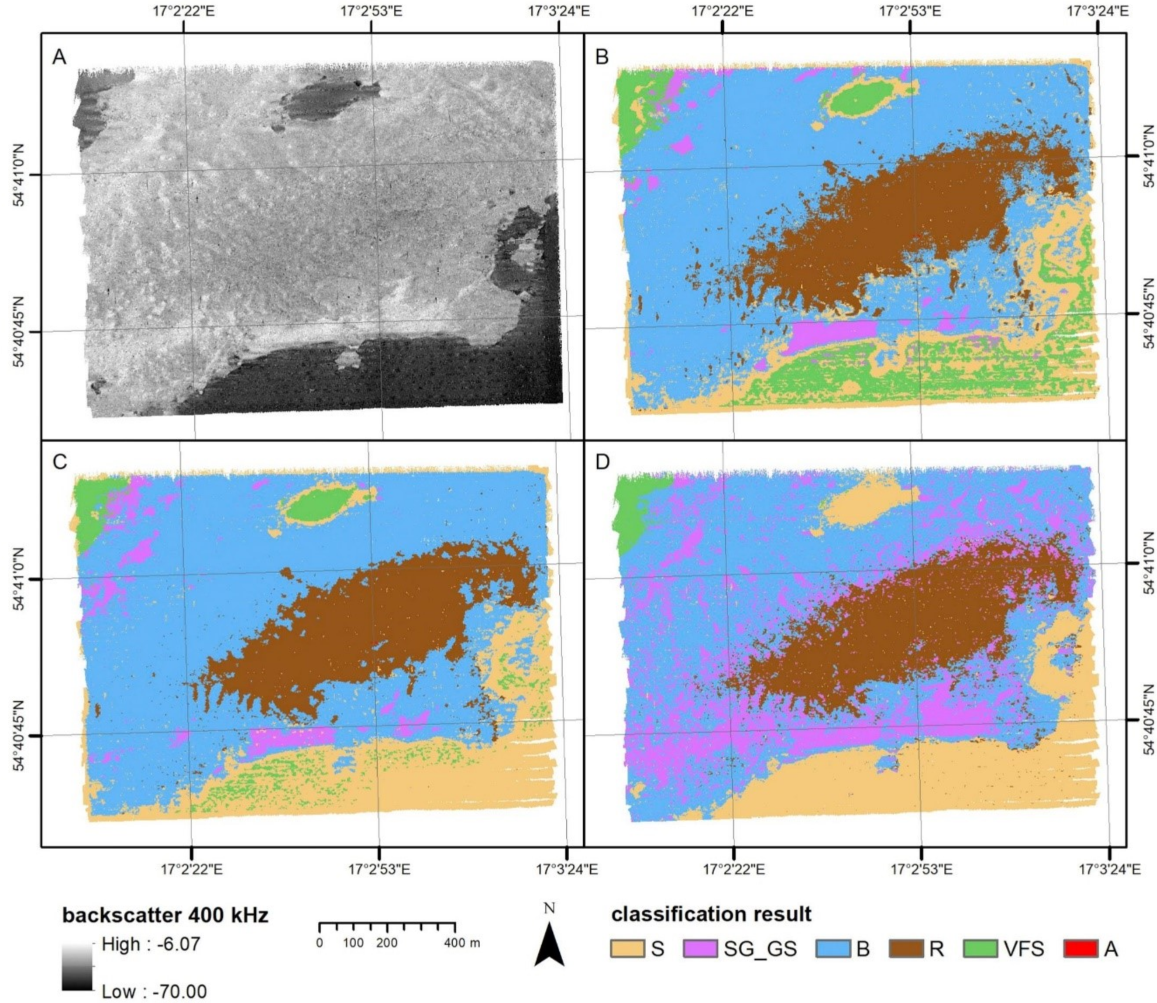

Fig. 7. Comparison between (A) backscatter 400 kHz grid and (B) classification results for all relevant features; (C) uncorrelated features; and (D) only primary features. S - sand, B - boulders, R - red algae on boulders, SG_GS - sandy gravel or gravelly sand, and VFS - very fine sand. (For interpretation of the references to colour in this figure legend, the reader is referred to the web version of this article.)

backscatter derivatives, namely, 150 kHz and 400 kHz.

Similar to other benthic habitat mapping studies, a few supervised classification approaches were tested to generate predictive outcomes based on ground-truth samples (Diesing et al., 2014; Hasan et al., 2012; Montereale Gavazzi et al., 2016). In this study, they included k-nearest neighbours (KNN), classification and regression trees (CART), RF, and support vector machines (SVM). We implemented these algorithms, which were available in the eCognition software. The KNN classified a specified object (query point) by a certain number (K) of known training samples that were located at the nearest neighbour around the query point. Euclidean distances (between the object and each instance) were calculated in the feature space to estimate the influence area of the neighbours. The KNN classification algorithm has been described in detail by Bremner et al. (2005). CART makes classification rules by recursively partitioning the data into increasingly homogenous groups. The algorithm created a decision tree that was associated with a system of questions and answers, thereby allowing the determination of the final classification (Breiman et al., 1984). RF was the machine learning method used for classification, regression, and other tasks, which consisted of constructing multiple decision trees that generated the class dominant or predicted average of individual trees (Breiman, 2001). SVM based on the machine learning technique used an algorithm that transformed datasets into a multidimensional feature space to find the appropriate boundary between them. Data points were called vectors, and the vectors that supported border selection were called support vectors. Machine learning models that use support vectors have been called SVM (Cortes and Vapnik, 1995).

We used validation ground-truth samples to create error matrices and calculate accuracy assessment statistics (Foody, 2002). These included the accuracy of the user and producer (Congalton, 1991; Story and Congalton, 1986), overall accuracy, and kappa index of agreement (Cohen, 1960).

Table 2
Error matrices and accuracy assessment statistics for three benthic habitat models.

All relevant features		Reference					
		S	SG_GS	B	R	VFS	Sum
Prediction	S	7	0	0	0	0	7
	SG_GS	0	2	0	0	0	2
	B	1	2	7	1	0	11
	R	0	0	0	3	0	3
	VFS	0	0	0	0	5	5
	Sum	8	4	7	4	5	
	Producer's	0.875	0.5	1	0.75	1	
	User's	1	1	0.636	1	1	
	Overall Accuracy	0.857					
	KIA	0.815					
Uncorrelated		S	SG_GS	B	R	VFS	Sum
Prediction	S	6	0	0	0	0	6
	SG_GS	0	2	0	0	0	2
	B	2	2	7	1	0	12
	R	0	0	0	3	0	3
	VFS	0	0	0	0	5	5
	Sum	8	4	7	4	5	
	Producer's	0.75	0.5	1	0.75	1	
	User's	1.000	1.000	0.583	1	1	
	Overall Accuracy	0.821					
	KIA	0.769					
Only primary features		S	SG_GS	B	R	VFS	Sum
Prediction	S	6	0	0	0	2	8
	SG_GS	1	2	3	1	0	7
	B	1	2	4	0	0	7
	R	0	0	0	3	0	3
	VFS	0	0	0	0	3	3
	Sum	8	4	7	4	5	
	Producer's	0.75	0.5	0.571	0.75	0.6	
	User's	0.75	0.286	0.571	1	1	
	Overall Accuracy	0.643					
	KIA	0.545					

3. Results

3.1. Spectral parameters of bathymetry

The processed MBES bathymetry was presented in Fig. 1, and the co-registered backscatter for both frequencies was shown in Fig. 2. Figs. 3 and 4 show the bathymetry and its eight derived spectral parameters for moving windows of 20 m × 20 m and 35 m × 35 m, respectively.

Visual insight for the created parameters demonstrated that several could match the geomorphologic features of bathymetry, especially a few spectral parameters (e.g. m_0, m_2, and spectral skewness defined for central moments) redrawn with specific features such as valleys and crests (Figs. 3 and 4). Moreover, the comparison of MBES backscatter (Fig. 2) showed a rough similarity to seabed areas of strong absorption or backscattering (visible as Dfft).

3.2. Ground-truth data processing

Six benthic habitat classes were determined, and they included VFS, S, SG_GS, B, R, and, A. The extensive identification of the benthic habitats with reference to MBES backscatter in this area was described by Janowski et al. (2018b).

3.3. Feature selection

The results of the Boruta feature selection are presented in Fig. 5. The algorithm performed 612 iterations and confirmed 11 features as important. The most important feature in this study was 400 kHz backscatter; this was followed by 150 kHz backscatter, Dfft (35), Dfft (20), spectral skewness defined for central moments (20), *Q*-factor (35), spectral skewness (35), bathymetry, spectral moment m_0 (35), spectral width (35), and spectral moment m_2 (35). The Boruta results indicated that certain spectral parameters were of greater significance than bathymetry, from which they were derived. This was especially visible in the Dfft parameter, which had a importance score approximately twice as great as that of bathymetry. It was also noteworthy that all the other extracted features (including the geomorphometric, statistical, and textural features) of the MBES bathymetry and backscatter were not considered important. Our initial results suggested the relevance of multi-frequency MBES; in other words, the first and second most important features were backscatter collected at different frequencies. The correlation analysis removed six highly correlated features, as shown in Fig. 6. The retained features were 400 kHz backscatter, bathymetry, spectral skewness defined for central moments (20), *Q*-factor (35), and spectral moment m_2 (35).

From the twenty scales of MS and four methods of supervised classification, the best classification performance was found with MS 8 and the SVM classifier. We adopted the following properties of the SVM classifier: radial-basis function kernel with C factor 100 and gamma 0.1. We created three predictive models using the following sets of features: (1) all relevant; (2) uncorrelated; and (3) only primary features (backscatter 400 kHz and bathymetry). The predictive benthic habitat maps generated using this approach are shown in Fig. 7.

The error matrix and accuracy assessment of the predictive habitat mapping method are presented in Table 2. Based on the validation subset of the ground-truth samples, the model with all relevant features confirmed a high performance that achieved a prediction accuracy of 86% and a Kappa index of agreement of 0.82. The second model, which considered only uncorrelated features, also achieved high accuracy; however, in comparison with the previous map, it misclassified one validation sample. The reference model without spectral features had an overall accuracy of 64% and a Kappa index of agreement of 0.55. Taking the accuracy of the user and producer into consideration, the two best-performing models were in reasonable agreement for specific classes, such as VFS, S, and R. We performed McNemar's chi-squared test for the statistical significance of differences in overall accuracy between the three models (Foody, 2004). The test result for differences between all relevant and uncorrelated features was 0.0. It means that the difference between these two models is statistically insignificant at the 5% level of significance. The McNemar's chi-squared test for differences between all relevant and only primary features models was 4.17 with p-value = .04, while the same test between uncorrelated and only primary features was 3.2 with p-value = .07. Mentioned results mean that there was a significant difference in the accuracy between all relevant and only primary features models and lack of significant difference between uncorrelated and only primary features models at the 5% level of significance.

4. Discussion

In this study, we introduced eight spectral features of a rough seafloor surface. The significance of the spectral features was evaluated and expressed using an importance score. We built and estimated the accuracy of three models of benthic habitat mapping, thereby demonstrating that the majority of introduced spectral features (i.e. seven out of eight) could improve the predictive power of supervised classifiers.

This study emphasised the importance of spectral parameters derived from bathymetry for predictive benthic habitat mapping based on multi-frequency MBES measurements. We did not observe significant differences in the bathymetry between both datasets (150 and 400 kHz). However, moderate differences existed in the backscatter of both frequencies, thus supporting the usefulness for a multi-frequency approach. We assumed that consistency in the bathymetry gathered with different frequencies was valid for sandy and gravelly sediments, as well as hard substrates. However, substantial depth differences in softer sediments could occur when significant acoustic penetration occurs (Schneider von Deimling et al., 2013). Furthermore, the beam resolution was linked with the frequency using one acoustic array with lower beam resolution when using lower frequencies. This could have affected the bathymetric results presented in this study.

A visual comparison of the spectral parameters (particularly Dfft) indicated a high similarity between certain features of the multibeam backscatter datasets. Remarkably, the Boruta results showed that the spectral parameters of bathymetry, in general, had a greater significance than bathymetry itself. If the spectral parameters could match certain types of seabeds, they could be very useful for benthic habitat mapping at times when only MBES bathymetry is available. This study highlighted that the implementation of these spectral parameters could significantly improve supervised classification and benthic habitat mapping.

Other research of the Rowy Site demonstrated high applicability of the KNN and RF methods of classification (Janowski et al., 2018b). On the other hand, in this study, we obtained the best prediction performance with the SVM technique. Additional ground-truth samples were available for this study, thereby doubling the amount in relation to previous research (Janowski et al., 2018b). Increasing the number of samples provided a more realistic reference. Therefore, the predictions presented in this study could be considered as more robust.

The spectral analyses of surfaces, including Dfft, have already been applied in the analyses of seafloor data (Goff et al., 1999; Wilson et al., 2007) for morphological description. However, geomorphometry has been applied to the terrestrial environment very intensely (e.g. Sofia et al., 2016). Spectral analysis of the land surface has been used by geomorphologists; for example, Hutchinson and Gallant (2000) explored the usefulness of using numerical geomorphometric methods in terrain shape analysis. In the marine realm, studies using the autocovariance function of multibeam bathymetry successfully characterised the widths of morphological structures such as abyssal hills and continental slope canyons (Goff and Jordan, 1988; Goff, 2001). However, it was not determined as to what the size of the processing window of the spectral parameters should be for useful classification. This issue should be investigated further. The analysis of the spectral features, such as lidar data, from other sources of DEMs would be another topic worth exploring.

An MBES currently allows for the registration of absolute (calibrated) backscattering strength values; however, uncalibrated backscattering is still the most commonly used of these two measurement types. There is a need for calibrated systems with accurate hydroacoustic measurements so that data from different registrations can be compared. Because backscatter is dependent upon frequency, it can also be a disadvantage when compiling various datasets. In turn, the bathymetric spectral features represent absolute values, and therefore, they are reliable and easy to compare with measurements from other datasets. Spectral parameters are generally not dependent on the operating frequency of the MBES when the effects of sediment penetration can be excluded. However, taking such spectral features into account requires a high quality MBES bathymetry dataset and precise motion compensation. Any vessel motion artefacts can interfere, or 'leak', into the spectral features when they are not compensated. However, modern motion compensation systems work well correcting these errors. The dataset presented in this study was recorded on a vessel with a length of 8 m and width of 3 m at a sea state between 2 and 4. Despite unfavourable weather conditions for such a small vessel, the surveys yielded valuable results.

Because our study site was characterised by complex geomorphological features, we can ascertain that the presented method of predictive benthic habitat mapping could be especially valuable in other areas with diverse morphology (e.g. reefs). Considering a broader perspective, the spectral analysis of seafloor bathymetry could provide new insight into the analyses of DEMs of other sources, such as gravity models (Smith and Sandwell, 1997), which would allow for the exploration and interpretation of large scale complex geomorphological features, including volcanic structures, seamounts, or mid-ocean ridges.

Funding

This work resulted from the BONUS ECOMAP project, supported by BONUS (Art 185), funded jointly by the EU and the Federal Ministry of Education and Research of Germany (BMBF), the National Centre for Research and Development of Poland (NCBR) [grant number BONUS-BB/ECOMAP/07/2017], and the Innovation Fund Denmark (Innovationsfonden).

Declaration of Competing Interest

None.

References

APL, 1994. APL-UW High-Frequency Ocean Environmental Acoustic Models Handbook (Technical report APL-UW TR9407 AEAS 9501), Seattle. Applied Physics Laboratory, University of Washington, pp. 210.

Benz, U.C., Hofmann, P., Willhauck, G., Lingenfelder, I., Heynen, M., 2004. Multi-resolution, object-oriented fuzzy analysis of remote sensing data for GIS-ready information. ISPRS J. Photogramm. Remote Sens. 58, 239–258. https://doi.org/10.1016/j.isprsjprs.2003.10.002.

Blaschke, T., 2010. Object based image analysis for remote sensing. ISPRS J. Photogramm. Remote Sens. 65, 2–16. https://doi.org/10.1016/j.isprsjprs.2009.06.004.

Breiman, L., 2001. Random forests. Mach. Learn. 45, 5–32. https://doi.org/10.1023/a:1010933404324.

Breiman, L., Friedman, J.H., Olshen, R.A., Stone, C.J., 1984. Classification and Regression Trees. Wadsworth, Belmont.

Bremner, D., Demaine, E., Erickson, J., Iacono, J., Langerman, S., Morin, P., Toussaint, G., 2005. Output-sensitive algorithms for computing nearest-neighbour decision boundaries. Discret. Comput. Geom. 33, 593–604. https://doi.org/10.1007/s00454-004-1152-0.

Briggs, K.B., Lyons, A.P., Pouliquen, E., Mayer, L.A., Richardson, M.D., 2005. Seafloor Roughness, Sediment Grain Size and Temporal Variability, in Underwater Acoustic Measurements: Technologies and Results. Heraklion, Crete, Greece, pp. 29–37.

Brown, C.J., Smith, S.J., Lawton, P., Anderson, J.T., 2011. Benthic habitat mapping: a review of progress towards improved understanding of the spatial ecology of the seafloor using acoustic techniques. Estuar. Coast. Shelf Sci. 92, 502–520. https://doi.org/10.1016/j.ecss.2011.02.007.

Cazenave, P.W., Lambkin, D.O., Dix, J.K., 2008. Quantitative bedform analysis using decimetre resolution swath bathymetry. In: CARIS 12th International User Group Conference. United Kingdom, Bath.

Clough, R.W., Penzien, J., 1975. Dynamics of Structure. McGraw-Hill, New York.

Cohen, J., 1960. A coefficient of agreement for nominal scales. Educ. Psychol. Meas. 20, 37–46. https://doi.org/10.1177/001316446002000104.

Congalton, R.G., 1991. A review of assessing the accuracy of classifications of remotely sensed data. Remote Sens. Environ. 37, 35–46. https://doi.org/10.1016/0034-4257(91)90048-b.

Conti, L.A., Lim, A., Wheeler, A.J., 2019. High resolution mapping of a cold water coral mound. Scientific Reports 9, 1016. https://doi.org/10.1038/s41598-018-37725-x.

Cortes, C., Vapnik, V., 1995. Support-vector networks. Machine Learning 20, 273–297. https://doi.org/10.1007/bf00994018.

Davidson, K.L., Louglin, P.J., 2000. Instantaneous spectral moments. Journal of The Franklin Institute 337, 421–436. https://doi.org/10.1016/S0016-0032(00)00034-X.

Diesing, M., Thorsnes, T., 2018. Mapping of cold-water coral carbonate mounds based on geomorphometric features: an object-based approach. Geosciences 8 (2), 34. https://doi.org/10.3390/geosciences8020034.

Diesing, M., Green, S.L., Stephens, D., Lark, R.M., Stewart, H.A., Dove, D., 2014. Mapping seabed sediments: Comparison of manual, geostatistical, object-based image analysis and machine learning approaches. Cont. Shelf Res. 84, 107–119. https://doi.org/10.1016/j.csr.2014.05.004.

Diesing, M., Mitchell, P., Stephens, D., 2016. Image-based seabed classification: what can we learn from terrestrial remote sensing? ICES Journal of Marine Science: Journal du Conseil 73, 2425–2441. https://doi.org/10.1093/icesjms/fsw118.

Fakiris, E., Blondel, P., Papatheodorou, G., Christodoulou, D., Dimas, X., Georgiou, N., Kordella, S., Dimitriadis, C., Rzhanov, Y., Geraga, M., Ferentinos, G., 2019. Multi-frequency, Multi-sonar mapping of shallow habitats—Efficacy and management implications in the National Marine Park of Zakynthos, Greece. Remote Sens. 11, 461.

Feldens, P., Schulze, I., Papenmeier, S., Schönke, M., Schneider von Deimling, J., 2018. Improved interpretation of marine sedimentary environments using multi-frequency multibeam backscatter data. Geosciences 8 (6), 214. https://doi.org/10.3390/geosciences8060214.

Folk, R.L., Ward, W.C., 1957. Brazos River bar [Texas]; a study in the significance of grain size parameters. Journal of Sedimentary Research 27, 3–26.

Fonseca, L., Brown, C., Calder, B., Mayer, L., Rzhanov, Y., 2009. Angular range analysis of acoustic themes from Stanton Banks Ireland: a link between visual interpretation and multibeam echosounder angular signatures. Appl. Acoust. 70, 1298–1304. https://doi.org/10.1016/j.apacoust.2008.09.008.

Foody, G.M., 2002. Status of land cover classification accuracy assessment. Remote Sens. Environ. 80, 185–201. https://doi.org/10.1016/s0034-4257(01)00295-4.

Foody, G.M., 2004. Thematic map comparison: evaluating the statistical significance of differences in classification accuracy. Photogramm. Eng. Remote Sens. 70, 627–633.

Gafeira, J., Dolan, M., Monteys, X., 2018. Geomorphometric characterization of pockmarks by using a GIS-based semi-automated toolbox. Geosciences 8 (5), 154. https://doi.org/10.3390/geosciences8050154.

Gaida, T., Tengku Ali, T., Snellen, M., Amiri-Simkooei, A., van Dijk, T., Simons, D., 2018. A multispectral bayesian classification method for increased acoustic discrimination of seabed sediments using multi-frequency multibeam backscatter data. Geosciences 8 (12), 455. https://doi.org/10.3390/geosciences8120455.

Goff, J.A., 2001. Quantitative classification of canyon systems on continental slopes and a possible relationship to slope curvature. Geophys. Res. Lett. 28, 4359–4362. https://doi.org/10.1029/2001GL013300.

Goff, J.A., Jordan, T.H., 1988. Stochastic modelling of seafloor morphology: Inversion of Sea Beam data for second-order statistics. Journal of Geophysical Research: Solid Earth 93, 13589–13608. https://doi.org/10.1029/JB093iB11p13589.

Goff, J.A., Orange, D.L., Mayer, L.A., Hughes Clarke, J.E., 1999. Detailed investigation of continental shelf morphology using a high-resolution swath sonar survey: the Eel margin, northern California. Mar. Geol. 154, 255–269. https://doi.org/10.1016/S0025-3227(98)00117-0.

Haralick, R.M., Shanmugam, K., Dinstein, I.H., 1973. Textural Features for image Classification. IEEE Transactions on Systems, Man, and Cybernetics SMC-3, 610–621. https://doi.org/10.1109/tsmc.1973.4309314.

Hasan, R., Ierodiaconou, D., Monk, J., 2012. Evaluation of four Supervised Learning Methods for Benthic Habitat Mapping using Backscatter from Multi-Beam Sonar. Remote Sens. 4, 3427–3443. https://doi.org/10.3390/rs4113427.

Hefner, B.T., Jackson, D.R., Ivakin, A.M., Tang, D., 2010. High frequency measurements of backscattering from heterogeneities and discrete scatterers in sand sediments. In: Proceedings of the Tenth European Conference on Underwater Acoustics (ECUA2010), Istanbul, Turkey, 5–9 July 2010. 3. pp. 1386–1390.

Held, P., Schneider von Deimling, J., 2019. New feature classes for acoustic habitat mapping—a multibeam echosounder point cloud analysis for mapping submerged aquatic vegetation (SAV). Geosciences 9 (5), 235. https://doi.org/10.3390/geosciences9050235.

Hutchinson, M.F., Gallant, J.C., 2000. Digital elevation models and representation of terrain shape. In: Wilson, J.P., Gallant, J.C. (Eds.), Terrain Analysis. John Wiley and Sons, Principles and Applications. New York, pp. 29–49.

Jackson, D.R., Richardson, M.D., 2007. High-frequency Seafloor Acoustics. Springer, pp. 557.

Jackson, D.R., Baird, A.M., Crisp, J.J., Thomson, P.A.G., 1986. High-frequency bottom backscatter measurements in shallow water. The Journal of the Acoustical Society of America 80, 1188–1199. https://doi.org/10.1121/1.393809.

Janowski, L., Tegowski, J., Nowak, J., 2018a. Seafloor mapping based on multibeam echosounder bathymetry and backscatter data using Object-based image Analysis: a case study from the Rewal site, the Southern Baltic. Oceanol. Hydrobiol. Stud. 47, 248–259. https://doi.org/10.1515/ohs-2018-0024.

Janowski, L., Trzcinska, K., Tegowski, J., Kruss, A., Rucinska-Zjadacz, M., Pocwiardowski, P., 2018b. Nearshore Benthic Habitat Mapping based on Multi-Frequency, Multibeam Echosounder Data using a combined Object-based Approach: a Case Study from the Rowy Site in the Southern Baltic Sea. Remote Sens. 10, 1983. https://doi.org/10.3390/rs10121983.

Jones, E.J.W., 1999. Marine geophysics. In: Chichester. Wiley, New York.

Kendzierska, H., 2009. Stilo-Ustka. In: Gic-Grusza, G., Kryla-Straszewska, L., Urbanski, J., Warzocha, J., Weslawski, J.M. (Eds.), Atlas of Polish Marine Area Bottom Habitats. Broker-Innowacji, Gdynia, pp. 158–165.

Kursa, M., 2016. Robust and Efficient Approach to Feature Selection with Machine Learning, Faculty of Mathematics. University of Warsaw, Informatics and Mechanics.

Kursa, M.B., Rudnicki, W.R., 2010. Feature selection with the Boruta Package. Journal of Statistical Software 36 (11). https://doi.org/10.18637/jss.v036.i11.

Lamarche, G., Lurton, X., 2017. Recommendations for improved and coherent acquisition and processing of backscatter data from seafloor-mapping sonars. Mar. Geophys. Res. 39, 5–22. https://doi.org/10.1007/s11001-017-9315-6.

Lecours, V., Devillers, R., Schneider, D.C., Lucieer, V.L., Brown, C.J., Edinger, E.N., 2015. Spatial scale and geographic context in benthic habitat mapping: review and future directions. Marine Ecology Progress Series 535, 259–284. https://doi.org/10.3354/meps11378.

Lecours, V., Dolan, M.F.J., Micallef, A., Lucieer, V.L., 2016. A review of marine geomorphometry, the quantitative study of the seafloor. Hydrology and Earth System Sciences 20, 3207–3244. https://doi.org/10.5194/hess-20-3207-2016.

Lefebvre, A., Thompson, C.E.L., Collins, K.J., Amos, C.L., 2009. Use of a high-resolution profiling sonar and a towed video camera to map a Zostera marina bed, Solent, UK. Estuar. Coast. Shelf Sci. 82, 323–334. https://doi.org/10.1016/j.ecss.2009.01.027.

Li, J., Tran, M., Siwabessy, J., 2016. Selecting optimal random forest predictive models: a case study on predicting the Spatial distribution of Seabed Hardness. PLoS One 11, e0149089. https://doi.org/10.1371/journal.pone.0149089.

Lucieer, V., Lecours, V., Dolan, M., 2018. Charting the course for future developments in marine geomorphometry: an introduction to the special issue. Geosciences 8 (12), 477. https://doi.org/10.3390/geosciences8120477.

Lyons, A.P., Fox, W.L.J., Hasiotis, T., Pouliquen, E., 2002. Characterization of the two-dimensional roughness of wave-rippled sea floors using digital photogrammetry. IEEE J. Ocean. Eng. 27, 515–524. https://doi.org/10.1109/JOE.2002.1040935.

Mandelbrot, B.B., 1982. The Fractal Geometry of Nature. Freeman, San Francisco.

Mayer, L., Jakobsson, M., Allen, G., Dorschel, B., Falconer, R., Ferrini, V., Lamarche, G., Snaith, H., Weatherall, P., 2018. The Nippon Foundation—GEBCO Seabed 2030 PROJECT: the quest to See the World's oceans completely mapped by 2030. Geosciences 8 (2), 1–18. https://doi.org/10.3390/geosciences8020063.

Micallef, A., Le Bas, T.P., Huvenne, V.A.I., Blondel, P., Hühnerbach, V., Deidun, A., 2012. A multi-method approach for benthic habitat mapping of shallow coastal areas with high-resolution multibeam data. Cont. Shelf Res. 39–40, 14–26. https://doi.org/10.1016/j.csr.2012.03.008.

Misiuk, B., Lecours, V., Bell, T., 2018. A multiscale approach to mapping seabed sediments. PLoS One 13, e0193647. https://doi.org/10.1371/journal.pone.0193647.

Montereale Gavazzi, G., Madricardo, F., Janowski, L., Kruss, A., Blondel, P., Sigovini, M., Foglini, F., 2016. Evaluation of seabed mapping methods for fine-scale classification of extremely shallow benthic habitats – Application to the Venice Lagoon, Italy. Estuar. Coast. Shelf Sci. 170, 45–60. https://doi.org/10.1016/j.ecss.2015.12.014.

Montereale-Gavazzi, G., Roche, M., Lurton, X., Degrendele, K., Terseleer, N., Van Lancker, V., 2017. Seafloor change detection using multibeam echosounder backscatter: case study on the Belgian part of the North Sea. Mar. Geophys. Res. 39, 229–247. https://doi.org/10.1007/s11001-017-9323-6.

Nilsson, R., Peña, J.M., Björkegren, J., Tegnér, J., 2007. Consistent feature selection for pattern recognition in polynomial time. J. Mach. Learn. Res. 8, 589–612.

Parnum, I.M., Gavrilov, A.N., 2011. High-frequency multibeam echo-sounder measurements of seafloor backscatter in shallow water: Part 2 – Mosaic production, analysis and classification. Underw. Technol. 30, 13–26. https://doi.org/10.3723/ut.30.013.

Porskamp, P., Rattray, A., Young, M., Ierodiaconou, D., 2018. Multiscale and hierarchical classification for benthic habitat mapping. Geosciences 8 (4), 119. https://doi.org/10.3390/geosciences8040119.

Prampolini, M., Blondel, P., Foglini, F., Madricardo, F., 2018. Habitat mapping of the Maltese continental shelf using acoustic textures and bathymetric analyses. Estuar. Coast. Shelf Sci. 207, 483–498. https://doi.org/10.1016/j.ecss.2017.06.002.

Rattray, A., Ierodiaconou, D., Womersley, T., 2015. Wave exposure as a predictor of benthic habitat distribution on high energy temperate reefs. Front. Mar. Sci. 2, 1–14. https://doi.org/10.3389/fmars.2015.00008.

Samsudin, S.A., Hasan, R.C., 2017. Assessment of Multibeam Backscatter Texture Analysis for Seafloor Sediment Classification. *ISPRS - International Archives of the Photogrammetry*. Remote Sensing and Spatial Information Sciences XLII-4 (W5), 177–183. https://doi.org/10.5194/isprs-archives-XLII-4-W5-177-2017.

Sappington, J.M., Longshore, K.M., Thompson, D.B., 2007. Quantifying Landscape Ruggedness for Animal Habitat Analysis: a Case Study Using Bighorn Sheep in the Mojave Desert. J. Wildl. Manag. 71, 1419–1426. https://doi.org/10.2193/2005-723.

Schimel, A.C.G., Beaudoin, J., Parnum, I.M., Le Bas, T., Schmidt, V., Keith, G., Ierodiaconou, D., 2018. Multibeam sonar backscatter data processing. Mar. Geophys. Res. 39, 121–137. https://doi.org/10.1007/s11001-018-9341-z.

Schneider von Deimling, J., Weinrebe, W., Tóth, Z., Fossing, H., Endler, R., Rehder, G., Spieß, V., 2013. A low frequency multibeam assessment: Spatial mapping of shallow gas by enhanced penetration and angular response anomaly. Mar. Pet. Geol. 44, 217–222. https://doi.org/10.1016/j.marpetgeo.2013.02.013.

Schönke, M., Feldens, P., Wilken, D., Papenmeier, S., Heinrich, C., Schneider von Deimling, J., Held, P., Krastel, S.J.G.-M.L., 2017. Impact of Lanice conchilega on seafloor microtopography off the island of Sylt (German Bight, SE North Sea). Geo-Mar. Lett. 37, 305–318. https://doi.org/10.1007/s00367-016-0491-1.

Smith, W.H.F., Sandwell, D.T., 1997. Global sea floor topography from satellite altimetry and ship depth soundings. Science 277, 1956–1962. https://doi.org/10.1126/science.277.5334.1956.

Sofia, G., Hillier, J.K., Conway, S.J., 2016. Frontiers in geomorphometry and earth surface dynamics: possibilities, limitations and perspectives. Earth Surface Dynamics 4, 721–725. https://doi.org/10.5194/esurf-4-721-2016.

Story, M., Congalton, R.G., 1986. Accuracy assessment: a user's perspective. Photogramm. Eng. Remote. Sens. 52, 397–399.

Strong, J.A., Clements, A., Lillis, H., Galparsoro, I., Bildstein, T., Pesch, R., 2019. A review of the influence of marine habitat classification schemes on mapping studies: inherent assumptions, influence on end products, and suggestions for future developments. ICES J. Mar. Sci. 76, 10–22. https://doi.org/10.1093/icesjms/fsy161.

Tegowski, J., Gorska, N., Klusek, Z., 2003. Statistical analysis of acoustic echoes from underwater meadows in the eutrophic Puck Bay (southern Baltic Sea). Aquat. Living Resour. 16, 215–221. https://doi.org/10.1016/S0990-7440(03)00015-9.

Tegowski, J., Gorska, N., Kruss, A., Nowak, J., Blenski, J., 2009. Analysis of single beam, multibeam and sidescan sonar data for benthic habitat classification in the southern Baltic Sea. In: Papadakis, J., Bjorno, L. (Eds.), 3rd International Conference and Exhibition on Underwater Acoustic Measurements: Technologies and Results. Nafplion, Greece, pp. 131–138.

Tegowski, J., Trzcińska, K., Janowski, Ł., Kruss, A., Kusek, K., Nowak, J., 2018. Comparison of backscatter and seabed topographic characteristics recorded by multibeam echosounder at rewal Area - Southern Baltic Sea. In: *2018 Joint Conference - Acoustics* (pp. 1-4), https://doi.org/10.1109/ACOUSTICS.2018.8502330.

Urick, R.J., 1983. Principles of Underwater Sound. McGraw-Hill, New York.

Walbridge, S., Slocum, N., Pobuda, M., Wright, D., 2018. Unified geomorphological analysis workflows with benthic terrain modeler. Geosciences 8 (3), 94. https://doi.org/10.3390/geosciences8030094.

Wentworth, C.K., 1922. A Scale of Grade and Class Terms for Clastic Sediments. The Journal of Geology 30, 377–392.

Williams, K.L., Jackson, D.A., Tang, D., Briggs, K.B., Thorsos, E.I., 2009. Acoustic backscattering from a sand and a sand/mud environment: experiments and data/model comparisons. IEEE J. Ocean. Eng. 34, 388–398. https://doi.org/10.1109/joe.2009.2018335.

Wilson, M.F.J., O'Connell, B., Brown, C., Guinan, J.C., Grehan, A.J., 2007. Multiscale terrain analysis of multibeam bathymetry data for habitat mapping on the continental slope. Mar. Geod. 30, 3–35. https://doi.org/10.1080/01490410701295962.

Oświadczenia współautorów

Mgr Karolina Trzcińska
Department of Geophysics
Institute of Oceanography, University of Gdańsk
(e-mail: karolina.trzcinska@ug.edu.pl)

Gdańsk, 07 February 2022

Author Contribution Statement

I declare that my contribution to the paper:

Trzcinska, K.; Janowski, L.; Nowak, J.; Rucinska-Zjadacz, M.; Kruss, A.; Schneider von Deimling, J.; Pocwiardowski, P.; Tegowski, J. Spectral features of dual-frequency multibeam echosounder data for benthic habitat mapping. *Mar. Geol.* 2020, 427, 106239. https://doi.org/10.1016/j.margeo.2020.106239

included:

- conceptualization,
- data curation,
- formal analysis,
- investigation,
- methodology,
- software,
- validation,
- writing—original draft,
- writing—review and editing.

Overall, I estimate that my contribution to this work is **80%**.

I have done the following work:

- participation in research planning,
- participation in data recording,
- to propose the application of spectral parameters to the classification method in eCogniton software,
- preparing maps of spectral parameters,
- interpretation of results.

Karolina Trzcińska

Karolina Trzcińska

Dr Łukasz Janowski
Maritime Institute,
Gdynia Maritime University,
(e-mail: ljanowski@im.umg.edu.pl)

Gdańsk, 07 February 2022
(city)

Author Contribution Statement

I declare that my contribution to the paper:

Trzcinska, K.; Janowski, L.; Nowak, J.; Rucinska-Zjadacz, M.; Kruss, A.; Schneider von Deimling, J.; Pocwiardowski, P.; Tegowski, J. Spectral features of dual-frequency multibeam echosounder data for benthic habitat mapping. *Mar. Geol*. 2020, 427, 106239. https://doi.org/10.1016/j.margeo.2020.106239

included:

- conceptualization,
- data curation,
- investigation,
- methodology,
- software,
- validation,
- visualization,
- writing—original draft,
- writing—review and editing.

Overall, I estimate that my contribution to this work is **8%**.

Łukasz Janowski

Łukasz Janowski

Dr Jarosław Nowak
MEWO S.A.,

Straszyn, 07 February 2022
(city)

Author Contribution Statement

I declare that my contribution to the paper:

Trzcinska, K.; Janowski, L.; Nowak, J.; Rucinska-Zjadacz, M.; Kruss, A.; Schneider von Deimling, J.; Pocwiardowski, P.; Tegowski, J. Spectral features of dual-frequency multibeam echosounder data for benthic habitat mapping. *Mar. Geol.* 2020, 427, 106239. https://doi.org/10.1016/j.margeo.2020.106239

included:

- methodology,
- software.

Overall, I estimate that my contribution to this work is **2%**.

....

Jarosław Nowak

Dr Maria Rucińska
Department of Geophysics
Institute of Oceanography, University of Gdańsk
(e-mail: maria.rucinska@ug.edu.pl)

Gdańsk, 07 February 2022

Author Contribution Statement

I declare that my contribution to the paper:

Trzcinska, K.; Janowski, L.; Nowak, J.; Rucinska-Zjadacz, M.; Kruss, A.; Schneider von Deimling, J.; Pocwiardowski, P.; Tegowski, J. Spectral features of dual-frequency multibeam echosounder data for benthic habitat mapping. *Mar. Geol.* 2020, 427, 106239. https://doi.org/10.1016/j.margeo.2020.106239

included:

- data curation,
- writing—review and editing.

Overall, I estimate that my contribution to this work is **1%**.

Rucińska
....

Maria Rucińska

Dr Aleksandra Kruss
NORBIT-Poland Sp. z o.o.
(e-mail: aleksandra.kruss@norbit.com)

Sopot, 07 February 2022
(city)

Author Contribution Statement

I declare that my contribution to the paper:

Trzcinska, K.; Janowski, L.; Nowak, J.; Rucinska-Zjadacz, M.; Kruss, A.; Schneider von Deimling, J.; Pocwiardowski, P.; Tegowski, J. Spectral features of dual-frequency multibeam echosounder data for benthic habitat mapping. *Mar. Geol.* 2020, 427, 106239. https://doi.org/10.1016/j.margeo.2020.106239

included:

- data curation,
- writing—review and editing.

Overall, I estimate that my contribution to this work is **1%**.

Aleksandra Kruss

Aleksandra Kruss

Dr Jens Schneider von Deimling,
Marine Geophysics and Hydroacoustics
Christian-Albrechts-Universität zu Kiel, Germany
(e-mail: jens.schneider@ifg.uni-kiel.de)

Kiel, 07 February 2022
(city)

Author Contribution Statement

I declare that my contribution to the paper:

Trzcinska, K.; Janowski, L.; Nowak, J.; Rucinska-Zjadacz, M.; Kruss, A.; Schneider von Deimling, J.; Pocwiardowski, P.; Tegowski, J. Spectral features of dual-frequency multibeam echosounder data for benthic habitat mapping. *Mar. Geol*. 2020, 427, 106239. https://doi.org/10.1016/j.margeo.2020.106239

included:

- project administration,
- supervision.

Overall, I estimate that my contribution to this work is **2 %**.

……………………………………………..

Jens Schneider von Deimling

Dr Paweł Poćwiardowski
NORBIT-Poland Sp. z o.o.
(e-mail: pawel@norbit.com)

Santa Barbara, 07 February 2022
(city)

Author Contribution Statement

I declare that my contribution to the paper:

Trzcinska, K.; Janowski, L.; Nowak, J.; Rucinska-Zjadacz, M.; Kruss, A.; Schneider von Deimling, J.; Pocwiardowski, P.; Tegowski, J. Spectral features of dual-frequency multibeam echosounder data for benthic habitat mapping. *Mar. Geol*. 2020, 427, 106239. https://doi.org/10.1016/j.margeo.2020.106239

included:

- data curation.

Overall, I estimate that my contribution to this work is **1%**.

Pocwiardowski.
………………………………

Paweł Poćwiardowski

Prof. dr hab. Jarosław Tęgowski
Department of Geophysics
Institute of Oceanography, University of Gdańsk
(e-mail: jaroslaw.tegowski@ug.edu.pl)

Gdańsk, 07 February 2022

Author Contribution Statement

I declare that my contribution to the paper:

Trzcinska, K.; Janowski, L.; Nowak, J.; Rucinska-Zjadacz, M.; Kruss, A.; Schneider von Deimling, J.; Pocwiardowski, P.; Tegowski, J. Spectral features of dual-frequency multibeam echosounder data for benthic habitat mapping. *Mar. Geol.* 2020, 427, 106239. https://doi.org/10.1016/j.margeo.2020.106239

included:

- conceptualization,
- data curation,
- formal analysis,
- methodology,
- project administration,
- software,
- supervision.

Overall, I estimate that my contribution to this work is **5 %**.

....

Jarosław Tęgowski

PUBLIKACJA 3

Trzcinska K., Tegowski J., Pocwiardowski P., Janowski L., Zdroik J., Kruss A., Rucinska M., Lubniewski Z., Schneider von Deimling J. Measurement of Seafloor Acoustic Backscatter Angular Dependence at 150 kHz Using a Multibeam Echosounder. *Remote Sens*. 2021, 13, 4771. https://doi.org/10.3390/rs13234771

remote sensing

MDPI

Article

Measurement of Seafloor Acoustic Backscatter Angular Dependence at 150 kHz Using a Multibeam Echosounder

Karolina Trzcinska [1], Jaroslaw Tegowski [1,*], Pawel Pocwiardowski [2], Lukasz Janowski [3], Jakub Zdroik [1], Aleksandra Kruss [2], Maria Rucinska [1], Zbigniew Lubniewski [4] and Jens Schneider von Deimling [5]

1 Institute of Oceanography, University of Gdansk, Al. Marszalka Pilsudskiego 46, 81-378 Gdynia, Poland; karolina.trzcinska@ug.edu.pl (K.T.); jakub.zdroik@ug.edu.pl (J.Z.); maria.rucinska@ug.edu.pl (M.R.)
2 NORBIT-Poland Sp. z o.o., Al. Niepodleglosci 813-815/24, 81-810 Sopot, Poland; pawel@norbit.com (P.P.); aleksandra.kruss@norbit.com (A.K.)
3 Maritime Institute, Gdynia Maritime University, Morska 81-87 Str., 81-225 Gdynia, Poland; ljanowski@im.umg.edu.pl
4 Department of Geoinformatics, Faculty of Electronics, Telecommunications and Informatics, Gdansk University of Technology, Narutowicza 11/12, 80-233 Gdansk, Poland; zbigniew.lubniewski@eti.pg.edu.pl
5 Marine Geophysics and Hydroacoustics, Christian-Albrechts-Universität zu Kiel, Christian-Albrechts-Platz 4, 24118 Kiel, Germany; jens.schneider@ifg.uni-kiel.de
* Correspondence: jaroslaw.tegowski@ug.edu.pl

Abstract: Acoustic seafloor measurements with multibeam echosounders (MBESs) are currently often used for submarine habitat mapping, but the MBESs are usually not acoustically calibrated for backscattering strength (BBS) and cannot be used to infer absolute seafloor angular dependence. We present a study outlining the calibration and showing absolute backscattering strength values measured at a frequency of 150 kHz at around 10–20 m water depth. After recording bathymetry, the co-registered backscattering strength was corrected for true incidence and footprint reverberation area on a rough and tilted seafloor. Finally, absolute backscattering strength angular response curves (ARCs) for several seafloor types were constructed after applying sonar backscattering strength calibration and specific water column absorption for 150 kHz correction. Thus, we inferred specific 150 kHz angular backscattering responses that can discriminate among very fine sand, sandy gravel, and gravelly sand, as well as between bare boulders and boulders partially overgrown by red algae, which was validated by video ground-truthing. In addition, we provide backscatter mosaics using our algorithm (BBS-Coder) to correct the angle varying gain (AVG). The results of the work are compared and discussed with the published results of BBS measurements in the 100–400 kHz frequency range. The presented results are valuable in extending the very sparse angular response curves gathered so far and could contribute to a better understanding of the dependence of backscattering on the type of bottom habitat and improve their acoustic classification.

Keywords: multibeam echosounder; bottom backscattering strength angular response; backscatter correction

Citation: Trzcinska, K.; Tegowski, J.; Pocwiardowski, P.; Janowski, L.; Zdroik, J.; Kruss, A.; Rucinska, M.; Lubniewski, Z.; Schneider von Deimling, J. Measurement of Seafloor Acoustic Backscatter Angular Dependence at 150 kHz Using a Multibeam Echosounder. *Remote Sens.* **2021**, *13*, 4771. https://doi.org/10.3390/rs13234771

Academic Editor: Danilo Orlando

Received: 12 October 2021
Accepted: 22 November 2021
Published: 25 November 2021

1. Introduction

Ocean shelves and shallow waters are exposed to increasing anthropogenic pressure and economic exploitation. Marine areas offer potential for raw material exploitation and offshore energy production sites that require infrastructure such as pipelines and cables on the seabed. Shallow areas are also intensively exploited by fishing using bottom trawls. Human activities such as intensive fishing and polluting the oceans with sewage may have a destructive effect on the benthic flora and fauna and cause secondary harm through, e.g., reef and habitat destruction. Mapping and monitoring the individual habitats and identifying potential harm or even destruction imply a need for reliable remote sensing of the seafloor. Satellites have become commonly used devices for mapping land areas, whereas, for investigating the marine environment, acoustic measurements are more suitable because, among other reasons, they are not limited by the depth of the euphotic layer. Hydroacoustic swath devices are very efficient tools for underwater spatial remote sensing, enabling large-scale high-resolution mapping and detection of objects in the water column and on the seafloor, thus supporting environmental monitoring of benthic areas. There are well-established methodologies for acoustic-based mapping with confirmed reliability (e.g., [1–3]). High-frequency MBES recordings have been suggested and proven to be a valuable tool for this type of research [4–6]. In recent years (2017–2020), the ECOMAP project has been exploring the use of swath devices and shallow marine seismic and LIDAR measurements to study the seabed environment (e.g., [7–9]).

The main task of industrial MBES measurements is bathymetry, but systems have improved with regard to backscattering strength measurements of both the water column and the seafloor [10]. Especially in shallow water less than 20 m in water depth, ship-based MBES offers great potential for recording sidescan-like snippets [11]. The intensity of backscattered signals depends on many parameters, such as the geoacoustic properties of the seabed, but it is also controlled by the sonar-target geometry, including the individual beam incidence angles and varying bottom reverberation areas (Figure 1) modulated by the local slope of the seabed.

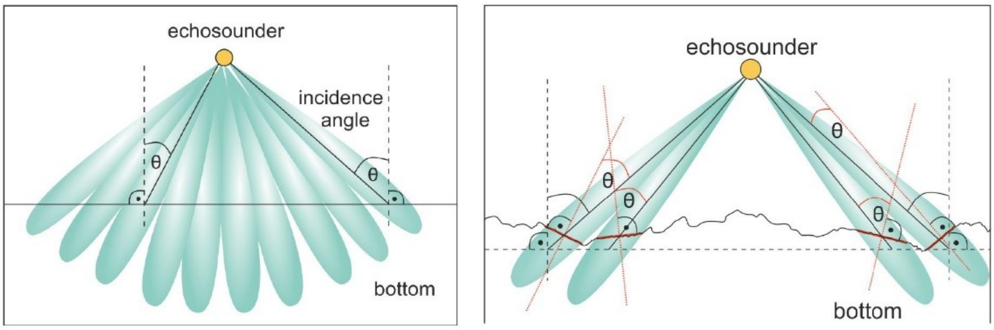

(**a**) (**b**)

Figure 1. MBES receiving beam pattern with indicated angle (θ) between axes of individual beams and normal angle to reverberation area: (**a**) at flat bottom and (**b**) at rough bottom.

The slope of the seabed has an effect on the BBS [12], due not only to modifications of the reflection angle but also to differences in footprint area. A flat bottom assumption can cause misinterpretation of acoustic signals in the description and classification of bottom habitats, especially when an offset of a few degrees appears unnoted [7]. The impact of slope on signals recorded by multibeam echosounders is even more pronounced in very shallow environments and those with significant topographic variations (Figure 1b).

We can divide parameters that influence registered echo signal into three groups: (i) device-based parameters (e.g., frequency, transducer sensitivity, directivity patterns), (ii) environmental parameters, i.e., acoustic absorption of water during two-way travel (e.g., salinity, temperature), and (iii) seafloor parameters modulating backscattering strength, i.e., physical interaction processes between signal and scattering objects (e.g., roughness of seabed, sediment porosity). To use both absolute backscattering strength and incident-specific echo shape bottom characteristics (ARC), we must know how the parameters in the first two groups modulate the acoustic signals.

MBES measurement with corrected backscattering strength is generally sparse, although affordable [13]. Some companies (e.g., Kongsberg, NORBIT) provide calibration files based on tank measurements and, thus, offer the ability to record absolute backscattering strength values on the fly. In this work, we also outline how we performed the calibration, which was one goal of the EU-funded project BONUS ECOMAP, where we used a calibrated NORBIT STX prototype sonar.

Acoustic measurements of the seafloor with various incidence and corrected backscattering strength are extremely rare [13–18]. In this study, we intended to deliver a set of specific records of this kind, the first ones gathered in the Baltic Sea so far. In addition, we discuss how such measurements can improve acoustic seafloor classification and compare absolute backscattering strength and ARCs to the few reports published so far.

The recorded echoes of acoustic signals scattered on the seabed (backscatter) together with bathymetry are often used to classify benthic habitats [8,19–21]. The backscatter parameter is not the real BBS value, but the relative signal intensity recorded by the receiver, which is modified so that the relative intensity values correspond to one angle of incidence of the acoustic beam on the bottom. A popular and commercially used tool for preparing such backscatter mosaics is Geocoder, presented by Fonseca and Calder [22]. Geocoder uses the data recorded by MBESs, performs radiometric and geometric correction, and interpolates the intensity values into the final backscatter mosaic.

1.1. Models, Classification, and Calibration

The purpose of using corrected backscattering intensity is to provide an absolute value of the bottom backscattering strength of the seafloor. This requires the use of sonar, whose response on the seafloor is accurately known with regard to the sensitivity during transmission and reception of the signal and taking into account the frequency and angle of incidence. Moreover, this requires applying accurate compensations for transmission losses related to medium and beam geometry and footprint extent to recorded BBS values [16,23].

In most applications for MBES data collection and processing, it is possible to apply environmental parameters measured by, e.g., CTD. This procedure adjusts backscatter data to compensate refraction and attenuation of acoustic signals while traveling in the water. For the calculations presented in this paper, we used an absorption coefficient, which is the result of absorption calculations from a formula given by Francois and Garrison using averaged environmental parameters [24]. The last step to correct intensity signals for propagation and attenuation losses is to refer their value to the beam footprint area on the bottom. Most of the time, a flat bottom assumption is used to calculate this value [23,25].

A compendium of good practices for backscatter collection and processing prepared by the BSWG GeoHab group is the first document of its kind focusing on the quality of MBES acoustic intensity data [23]. Whereas IHO hydrographic standards [26] adequately described MBES bathymetry measurements, standards related to MBES backscatter measurements are rarely standardized in the literature. Ideally, backscatter should be based on full calibration of the sonar sensitivity in transmission and reception, giving access to absolute backscatter strength levels [16,23].

The methods of benthic habitat classification can be divided into two groups: empirical approaches [27] and approaches based on physical modeling of the seabed with various geoacoustic parameters [28]. In the case of MBES, the empirical approach uses the registered backscattered intensity from areas with ground-truth samples and, optionally, bathymetry to assign segmented seabed data to habitat types, creating classified polygons [8,19–21]. The physical model-based approach predicts backscattering strength by modeling the acoustic propagation given the respective geoacoustic properties of the seabed, compares measured values with modeled values, and, on this basis, differentiates classes. This approach depends on the model used to describe backscattering from the seabed and the quality of MBES data. The popular APL model was developed for frequencies from 10 to 100 kHz [29]. Backscattering models are not well recognized for frequencies above 100 kHz [15,30]. Modern MBESs for shallow water are usually operated at higher frequencies (typically 150–400 kHz). In the authors' opinion, difficulties in understanding the phenomenon of backscattering on the seabed are largely due to there being only a small quantity of published calibrated hydroacoustic measurements [15]. A more advanced solution is to prepare a catalog of backscatter parameters for different seabed types at different frequencies and environmental parameters, such as bottom roughness, volume reverberation (including the presence of gas bubbles in the sediment), and grain size, as well as the difference in acoustic impedance between sea water and bottom materials [31]. Measuring the absolute values of angular dependence of the BBS is also necessary to assess the variability of the characteristics of benthic habitats in space and time. Measuring the absolute BBS values may support the development of unsupervised classification methods for previously identified benthic habitats, such as angular range analysis presented by Fonseca et al. [32].

MBES backscatter was the most important parameter for classification of benthic habitats in several works [8,19–21]. This highlights the importance of MBES backscatter and the need to measure it as accurately as possible. There is a need to better recognize and investigate the characteristics of backscatter in order to be able to use it for research in the most efficient way [23]. A few studies were conducted recently on calibrating MBESs in reference areas [13,33–35]. The most common calibration methods are listed as follows:

1. MBES cross-calibration by comparing field data recorded by calibrated SBES, which is based on comparing data recorded in the same place by an acoustically calibrated SBES and an uncalibrated MBES [36]. The SBES transmitter is tilted at different angles to test the angular dependence of the recorded backscatter signal. Correction of MBES recordings is performed on the basis of the measured difference between SBES and MBES measurements. An example is calibration of a Kongsberg EM 2040 MBES using a reference Simrad EK60 in areas located in the Bay of Brest, France [16].
2. Calibration with sound sources of known characteristics. This method uses sources with known levels. The aim of the method is to determine receiver and transmitter sensitivities with a defined measurement angle and signal frequency [16,37]. This method has been applied to sonar (Mesotech SM2000/SM20 [38], Kongsberg EM3002 [39], Reson SeaBat T50 [13], Reson SeaBat 7125 [40]). This approach is possible at only a few specialized laboratories worldwide. Foote et al. [41] suggested applying this calibration method to MBES. However, the method contains many difficulties, including the large number of receiving beams, often several hundred.

For the measurements provided in this paper, we utilized the second calibration approach with hydrophones and sound sources of known characteristics. We used a NORBIT iWBMSh (model STX) MBES calibrated in the manufacturer's laboratory in Trondheim, Norway. In this paper, we present the angular dependencies of absolute values of BBS for specific habitats of the southern Baltic Sea obtained with the acoustically calibrated MBES.

1.2. Goals

Acoustic measurements of the seafloor with various incidence angles and absolute BBS are extremely rare [13,16]. In this study, we provide a set of specific records of this kind, the first ones gathered in the Baltic Sea so far. In addition, we discuss how such measurements can improve acoustic seafloor classification and compare absolute backscattering strength and ARCs to the few cases published so far [13–17]. The main objectives of the work are to develop and discuss (i) the angular dependence of absolute BBS value measurement results for several benthic habitats in the Baltic Sea using transmitted signals of 150 kHz, and (ii) the BBS-Coder applied during the work to achieve an easy-to-interpret backscatter mosaic.

2. Materials and Methods

2.1. Calibration of Multibeam Echosounder

NORBIT's laboratory tank was used to perform all calibration procedures. They were conducted in order to evaluate the actual detailed MBES characteristics, knowledge of which is necessary to measure physical quantities of the seafloor, such as backscattering strength.

Bottom backscattering strength BBS is defined as

$$BBS = 10 \log_{10} \sigma, \tag{1}$$

where σ is the bottom backscattering coefficient [23,30,42]. It denotes the ratio of insonified wave energy backscattered by the seabed with respect to a unit bottom surface.

Bottom backscattering strength is dependent on the frequency of the scattered wave and its angle of incidence to the bottom. It is strongly associated with the physical properties of various types of bottom habitats. BBS depends on many seabed parameters, including density, sound velocity, surface roughness of the seabed surface, and heterogeneity of sediment volume. For most echosounders, the attenuation is so high that the input from volume scattering of the sediment can be described as a function of the reverberation area [23]. Therefore, when considering seafloor backscatter, an interface cross-section is often used, and, when considering the volume scattering, the cross-section for scatterers within the sediment is omitted [43].

With the given measured target strength *TS*, *BBS* can be calculated as

$$BBS = TS - BAC, \tag{2}$$

and the bottom area correction *BAC* is equal to

$$BAC = 10\ \log_{10}(A), \tag{3}$$

where *A* is the reverberation area insonified by an echosounder.

We can refer to the following classical sonar equation [43]:

$$EL = SL - 2TL + TS, \tag{4}$$

where *EL* denotes the received echo signal level, *SL* (source level) is the emitted signal level, *TL* is the one-way transmission loss describing the signal attenuation due to spreading and absorption in the water column, and *TS* is target strength describing the backscattering introduced by an investigated object. It should be pointed out that, in an underwater acoustic system, *EL* is not measured directly, but rather as the level of voltage in the receiving module circuit after energy is transformed from acoustic to electric form. When a set of separate MBES beams is used, instead of *EL*, we apply the term of beam level *BL*, which is the received voltage signal level for a particular beam. Moreover, the MBES operation cannot be described by a single value of *SL*, as it contains specialized signal processing, such as beamforming and matched filtering, each characterized by its own gain, and the directivity properties of particular beams must also be taken into account.

To show all factors that influence *TS* and *BBS* measured by the multibeam echosounder, by introducing the device gain *DG* instead of *SL* and using the relationship between *TS* and *BBS* (Equation (2)), the sonar equation for a given MBES receive beam can be written as

$$BBS = BL - DG + 2TL - BAC, \tag{5}$$

where the device gain *DG* is the superposition of several factors describing the MBES operation, in both its transmitting and receiving segments, i.e.,

$$DG = OCR + VGA(t) + PG(Rx_{set}) + SL_0(Tx_{set}) + Dir_{Rx}(\theta,\varphi) + Dir_{Tx}(\theta,\varphi). \tag{6}$$

OCR is the open circuit response of the receiving array itself, which is defined as the ratio of the RMS voltage produced by the received plane wave to the RMS pressure p of this wave at the transducer face; *VGA* is the gain of the time-dependent variable gain amplifier applied in the sonar in order to compensate the spherical spreading of the acoustic wave in the water column; *PG* is the processing gain related to the analog-to-digital conversion, beamformer, and applied matched filter specific to a given transmitted pulse length and shape; SL_0 is the source level characterizing the transmission array Tx_{set}; $Dir_{Tx}(\theta,\varphi)$ and $Dir_{Rx}(\theta,\varphi)$ are the directivity patterns of the transmission and receiving arrays, respectively, as functions of an azimuth angle θ and elevation angle φ.

The transmission loss TL is expressed as

$$2TL = 40\log_{10}(R) + 2A_bR/1000, \quad (7)$$

where A_b is the absorption coefficient (dB/km), and R is the range from the device to the bottom (m) and can be derived from the two-way travel time as measured by a sonar. Lastly, the bottom area correction BAC is defined as in Equation (3), where A is the bottom reverberation area corresponding to a given beam. It can be shown that A for long and short pulse regimes [23] can be expressed as

$$A = min[c\tau/2/sin(\theta),\ \theta_{RX\ 3dB}\ R/cos(\theta)]\cdot\varphi_{TX\ 3dB}\ R, \quad (8)$$

where $\theta_{RX\ 3dB}$, $\varphi_{TX\ 3dB}$ are 3 dB beam widths of the receiving and transmitting beams, respectively, τ is the inverse of the signal bandwidth, and θ is the incident angle. Footprint A is related to the actual inclination of the bottom; hence, it is corrected when the complete bathymetry is known.

In Equation (5), the DG term depends only on the MBES characteristics. TL and BAC depend on environmental features such as the absorption coefficient and seabed inclination; however, as shown in Equation (8), reverberation area A is also influenced by the device characteristics. The aim of the calibration is to measure, in different conditions, all of the terms described above related to MBES characteristics that influence the measured BBS values.

The calibration was performed in the NORBIT laboratory tank, with a size of 10 m × 6 m × 5 m. NORBIT also provided all calibration equipment. The standard calibration method utilizing external hydrophones, as well as sound sources of known characteristics, was used.

Figure 2 shows the transmitter path calibration setup. According to given Tx settings, the sounding pulse waveform is generated in the sonar transmitter segment and projected into the water column in the laboratory tank toward the hydrophones. The hydrophone pointed at (θ, φ) with respect to the center of the projector array registers the source level for this direction.

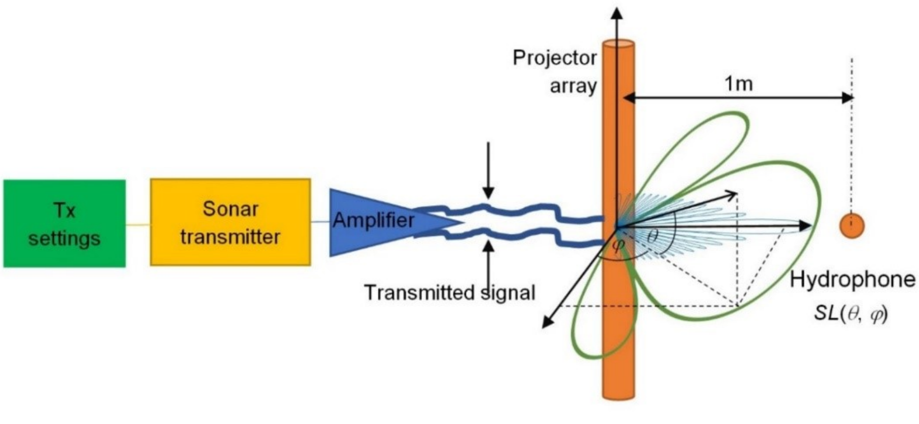

Figure 2. Transmitter path calibration scheme.

Figure 3 shows the receiver path calibration setup. The independent sound source pointed at (θ, φ) and situated at a given distance generates an acoustic wave of known characteristics $p(\theta, \varphi)$. After being received by the echosounder receiver array and transformed into the electric domain, then into digital form, the appropriate signal processing is done in the sonar receiver segment, including VGA, beamforming, and matched filter processing, resulting in beam data.

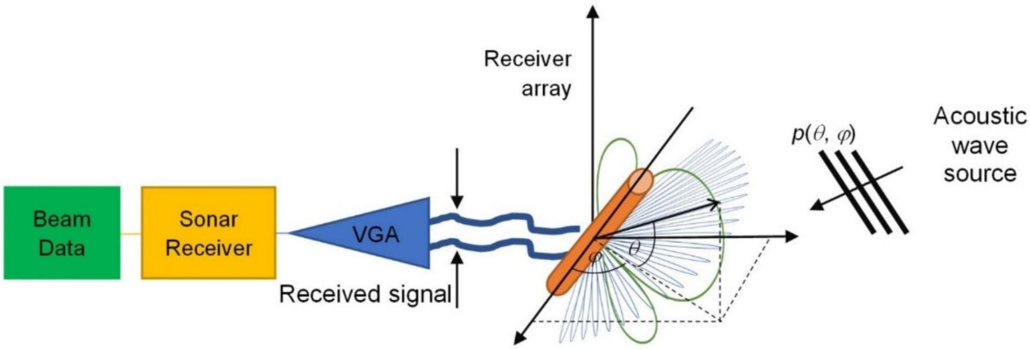

Figure 3. Receiver path calibration scheme.

The quantities and characteristics measured during the calibration included the following:

- Source level (SL_0) of the transmitting sector Tx;
- Two-dimensional directivity patterns Dir_{Tx} and Dir_{Rx} for the set of transmitting and receiving transducers;
- Receiver sensitivity, including the antenna component OCR and the gains related to signal processing, VGA and PG;
- Actual characteristics of transmitted signals, i.e., pulse duration and shape.

The measurements were conducted in a wide range of transmitter settings and conditions, including power, frequency, pulse duration, and pulse type (continuous wave or chirp) with different bandwidths.

It should be noted that not all quantities mentioned in the above equations can be measured separately, but the complete results of measurements allowed us to evaluate and appropriately compensate for the joint influence of the sonar component characteristics on the obtained BBS values.

The calibration results described above were written in XML files, which were used by the NORBIT software to generate corrected records. The files contain all corrections of the system, such as multifrequency beam patterns, gains, and frequency responses for all parts of the system in the entire operating frequency range from 150 to 700 kHz. These data, along with the applied models of particular terms in the sonar equation, allow us to compensate for sonar characteristics and to base the bottom classification or habitat mapping on measurements of physical quantities such as backscattering strength.

2.2. Research Area and Data Collection

The measurements with the NORBIT MBES were conducted in the Rowy seafloor area, located approximately 1.5 km off the southern coast of the Baltic Sea (Figure 4). This area is characterized by post-glacial sedimentation and local current transport. The seafloor deepens from the coast toward the northwest with a gentle slope [8]. The study area in the central part is built by glacial till covered by boulders and pebbles. In the southern and northwestern parts of the area, a cover of fine-grained sands occurs on the bottom surface (Figure 5). The research area ranges between 4 and 20 m water depth and is morphologically diverse. Numerous pebbles and boulders are covered with *Mytilus trossulus* bivalves [8,44]. In the study area, there are red algae, such as Bangiophyceae, including *Furcellaria lumbricalis* and *Polysiphonia fucoides*. The northwestern and southern parts of the area are relatively flat and covered with very fine sands [8] (Figure 5).

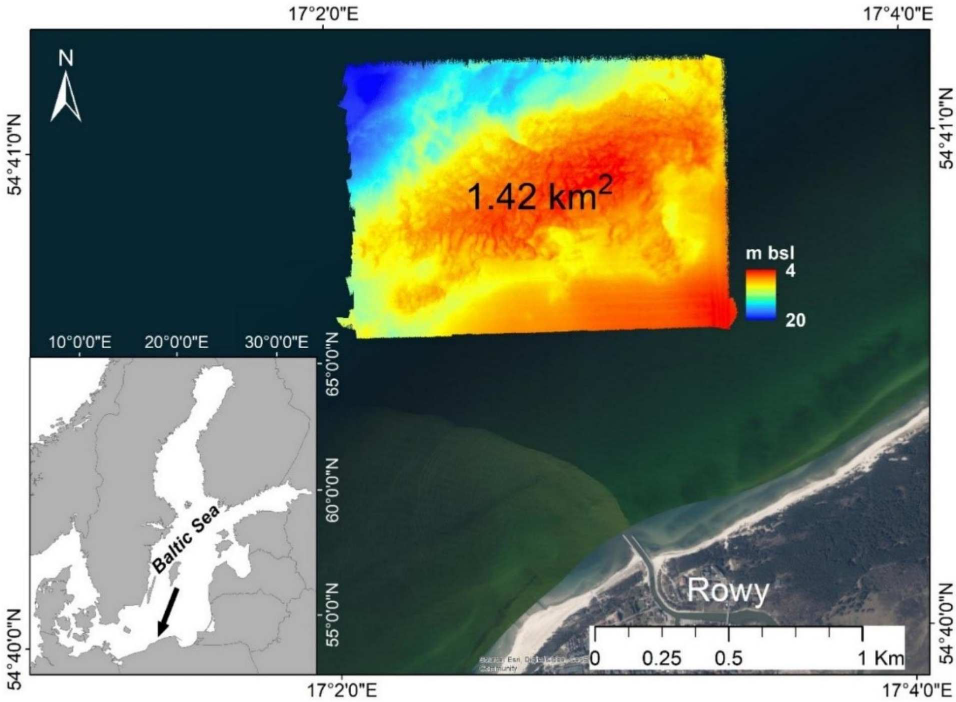

Figure 4. Location of Rowy area, southern part of Baltic Sea.

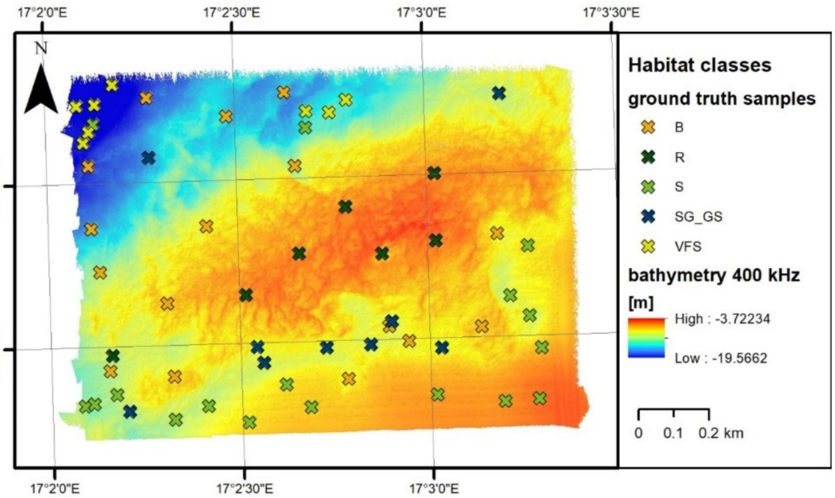

Figure 5. Bathymetry of research area with samples of sediments: S, sand; SG-GS, sandy gravel or gravelly sand; B, boulders; R, red algae on boulders; VFS, very fine sand.

A test version of the NORBIT MBES was used during the measurements. The NORBIT iWBMSh STX is a compact, high-resolution, tightly integrated, broadband multibeam sonar with a curved array. Its small form factor, low power draw, and tight integration allow installation on any survey platform. The MBES was equipped with an integrated Applanix OceanMaster inertial navigation system (INS) with two Trimble antennas for the global navigation satellite system (GNSS) pole mounted on a frame attached to the side of the boat. Two GPS antennas were mounted on the roof of the boat cabin. We used real-time kinematic/global positioning system (RTK-GPS) corrections from the ASG-EUPOS NAWGEO service, with an accuracy of 3 cm horizontally and 5 cm vertically [45]. A Valeport sound velocity profiler was used to provide accurate profiles of the sound speed in the water column. The NORBIT iWBMSh is dedicated for use in shallow-water research between 0.2 and 160 m depth. It can collect 512 beams at frequencies ranging between 150 and 700 kHz. We used a swath coverage of 150–160° to maintain the density of our bottom detections. The maximum ping rate was 20 Hz. The measurements were made at a vessel speed of 3 m/s, and data were recorded in Qinsy software and NORBIT's GUI software. To maintain homogeneous data density, the equiangle mode was used, i.e., a beamforming mode with a constant distance in angles between consecutive beams. We applied a pulse length of 200 μs for 150 kHz. At a frequency of 150 kHz, the receiving beam width is $2.4° \times 2.4°$, and, at the maximum available frequency of 700 kHz, it is $0.5° \times 0.5°$. A full patch test was conducted, and offsets were applied in order to achieve accurate positioning. Only acoustically calibrated iWBMSh STX MBES data were used to prepare the resulting ARCs in order to obtain absolute backscattering strength values.

In the studied area, 57 samples of bottom sediments were collected [9], and benthic habitats were separated into five classes [46,47]: S, sand; SG-GS, sandy gravel or gravelly sand; B, boulders; R, red algae on boulders; VFS, very fine sand (Figure 5). The area was divided into six classes using object-based image analysis (OBIA) classification [8], presented in Figure 6. We also considered samples on artificial structures (wrecks), but since they were not representative in the later part of data analysis and statistics calculation, this class was omitted. Grab samples were collected from aboard the University of Gdansk research vessels Oceanograf and Zelint.

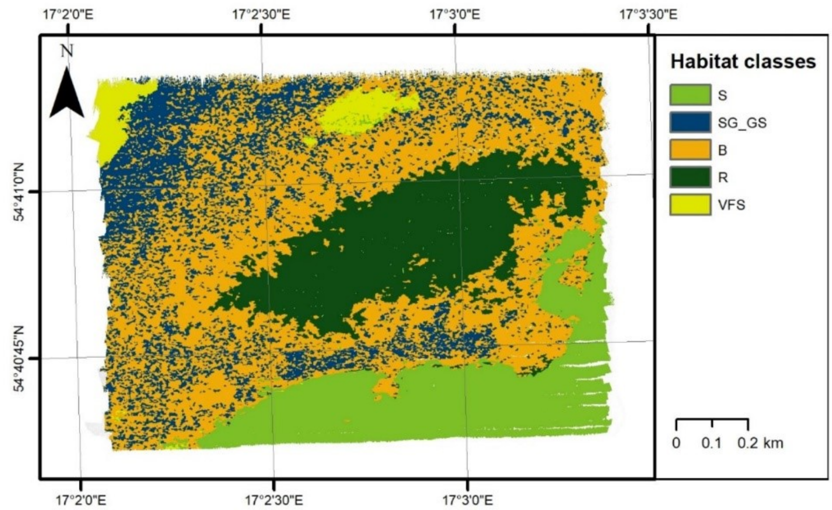

Figure 6. Habitat map from Janowski et al. [8] (object-based, combined k-nearest neighbor + random forest methods of supervised classification).

2.3. Postprocessing of Backscatter Data

Data were recorded in a shallow water area, and we applied environmental parameters 10 °C, 7 PSU, depth 0, and pH 8.

The data were replayed in the NORBIT GUI software applying the correction described in Section 2.1. The replayed BBS was corrected for acoustic absorption in the water body, where a constant absorption value of 15 dB/km for 150 kHz was calculated after Francois and Garrison's equation [24].

Bathymetry was processed in Qimera software with standard corrections, including ray path correction, cleaning and spike removal, and application of roll, pitch, and yaw offsets from calibration. Information about the position of each sounding for all pings was exported from Qimera as a txt file with a location in the UTM WGS 84 33N projected coordinate system. We developed our own software combining s7k (MBES data format) and txt files to access corrected BBS and position information (Figure 7). Then, we implemented a correction to compensate for the effect of a sloping seabed and true incidence on BBS in order to know the angular relationships of absolute BBS values for different types of seabed. First, we removed the correction used in the NORBIT GUI based on the flat bottom assumption correction from the calculated surface area A of the reverberation. Then, we adjusted the resulting values by our calculated BAC values (Equation (3)), where we considered the slope of the seafloor and the depth and distance from the transducer at each measurement point when calculating the reverberation area. These values were averaged and are presented in the results section as angular response curves of BBS values. In the next step, we ran our AVG correction, BBS-Coder, to remove the angular response as an intrinsic property of the seabed for the sake of generating a backscatter map that is easy to interpret and suitable for image-based classification. The correction algorithms were written in the D programming language [48].

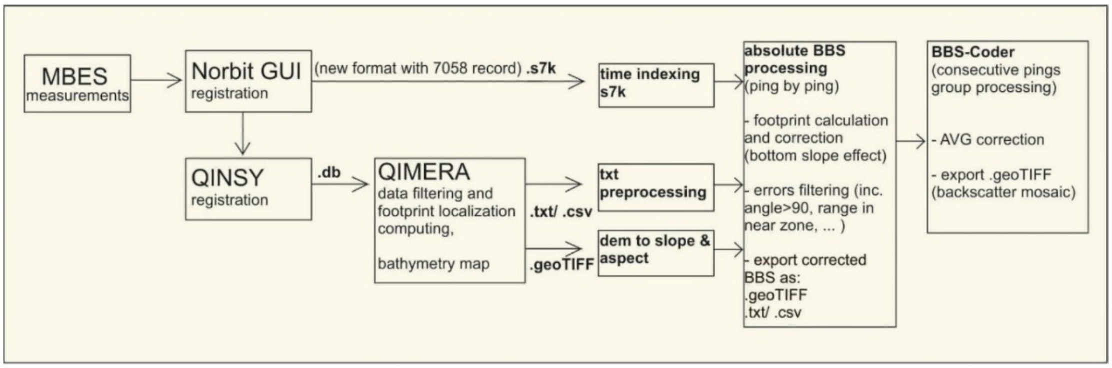

Figure 7. Data processing workflow from MBES raw data toward absolute BBS and fully georeferenced mosaic including corrections for intensity values corresponding to angle of incidence on the bottom (BBS-Coder).

2.3.1. Reverberation area and Bottom Slope Correction

The BBS value depends on the surface area A of the reverberation (Equations (2) and (3)). Significant changes in the BBS value are introduced by considering the actual distance of the acoustic transducer from the point measured at the bottom (R (range) in Equation (8)). The reverberation area on a flat bottom can be calculated from the angle of the receiving beam of the multibeam echosounder, the distance from the transducer to the bottom, and the angle of incidence. However, on a hummocky seabed, the true reverberation area can only be calculated in postprocessing after a 2D bathymetric model has been generated. In fact, the surface of the seabed is hardly ever perfectly flat, thus requiring calculation of the true angle of incidence. As a result, the individual beam reverberation area is not only controlled by the beam angle but also by the slope of the seabed. In order to calculate the reverberation area, it is necessary to consider the actual angle of incidence on the corrugated bottom and the angle of inclination of the bottom in relation to the transducer's center beam of the sonar [49–51]. It is, therefore, necessary to use roll/pitch vessel movement correction to obtain a more precise calculation.

In our study, the roll/pitch vessel movement was applied in Qimera to set the ship's location and orientation and to calculate the resulting positions of all soundings on the seabed. Seafloor slope was calculated using a bathymetric map with a resolution of 0.5 m, with most of the area, A, being less than 0.5 m^2. After the bathymetry was calculated, the received beam orientation of the survey was back-calculated again to obtain the true incidence of each beam on the tilted seafloor. For all recorded data and all angles of incidence, the reverberation area A was calculated, and further BBS was calculated using Equation (2). Consideration of the bottom slope gently changed the BBS values.

2.3.2. BBS-Coder: AVG Correction, and Backscatter Map Preparation

The backscattering strength recorded by the MBES depends on the angle of incidence of the acoustic pulse to the bottom. High BBS values near 0° incidence angles are primarily related to Lambert's law describing characteristics of the backscattered sound, which depends on the cosine of the angle of incidence [31,42].

To implement BBS-Coder, we used the averaged values of the measured BBS in a sliding window with averaging of neighboring pings. All BBS measurements in the studied area were brought down to values corresponding to the backscattering for an angle of 40° in order to generate a uniform backscatter map. We selected 40° as the center of the far angular range defined by Fonseca and Mayer [52]. There is no standard for the choice of reference angle [12], but backscattering from 40° is less angle-variant and more distinct for discriminating between various benthic habitats; therefore, this is often the angle of reference. Fonseca et al. [32] used 20–30° and Lamarche et al. [27] chose 45° as the discriminant value.

The applied BBS-Coder procedure was based on the division of recorded MBES data into subsets, with each subset containing a sequence of 50 pings, and each ping having 512 beams. It was assumed that the bottom backscattering properties were constant within each subset. From all recorded data in a given subset, we calculated the average BBS values for the angle of incidence, as shown in Figure 8a. Each registered beam was assigned to an appropriate half-degree interval of the angle of incidence (having a center value of 0°, 0.5°, 1°, 1.5°, 2°, 2.5°, etc.).

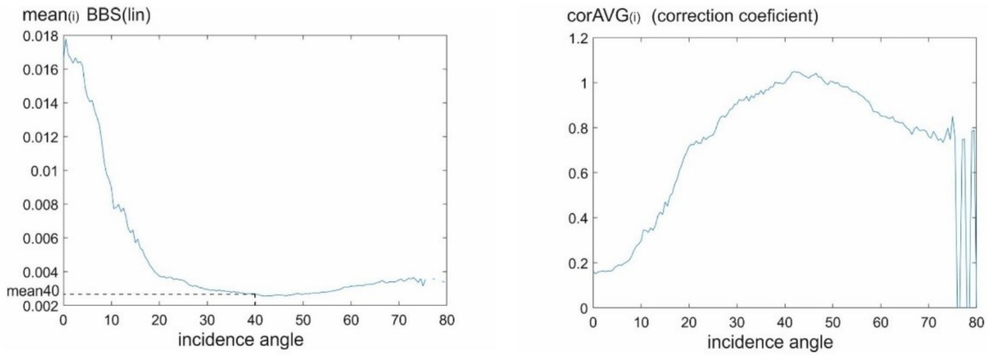

(a) (b)

Figure 8. Calculated BBS_lin in linear scale values for different incidence angles in 50 ping subsets: (**a**) average values of linear BBS; (**b**) correction coefficients (corAVG).

The correction coefficients, $corAVG_{(i)}$, were then calculated for each angle of incidence as follows:

$$corAVG_{(i)} = \frac{\text{mean40}}{\text{mean}_{(i)}}, \quad (9)$$

where $corAVG_{(i)}$ is the value of correction for i incidence angle, i = 0°, 0.5°, 1°, 1.5°, 2°, 2.5°, ... 90°, mean40 is the average value of 10^(BBS/10) for an angle of incidence of 40°, and $\text{mean}_{(i)}$ is the average value of 10^(BBS/10) for angle of incidence i.

Averaging and multiplication were performed for linear values.

An example of the correction coefficients calculated for one of the 50 ping packages is shown in Figure 8b. In the right part of Figure 8, we can see large changes in values; this is due to zero correction values for angles that were not present in the analyzed packet of 50 pings, as seen in Figure 8a. Then, each BBS value in the dataset (50 pings × 512 beams) was multiplied by the *corAVG* value appropriate for the angle of incidence of a given beam.

$$BS40_{(j)} = 10log_{10}(10^{(\frac{BBS_{(j)}}{10})}\ corAVG_{(i)}), \tag{10}$$

where $BS40_{(j)}$ is the value after correction for j number of beams in the data package, j = 1, 2, 3, … 25,600 (50 pings × 512 beams). In fact, the maximum value of j is slightly lower because some of the measuring points were removed during the cleaning process.

Backscatter maps presented in the results section were generated from the calculated BS40 values. A single 0.5 × 0.5 m grid element often contains several calculated BS40 values. In such a situation, the values in a single grid element are averaged in order to prepare a map of the studied area.

3. Results

3.1. Angular Response Curves of BBS Values for Specific Habitat of the Baltic Sea

We calculated the angular response curves of absolute BBS for the specific habitat of the Baltic Sea occurring in the studied area: S, sand; SG-GS, sandy gravel or gravelly sand; B, boulders; R, red algae on boulders; VFS, very fine sand. Figure 9a shows the dependence of BBS on the angle of incidence, for which the values are averaged for the measurements made in the areas where homogeneous habitats occur, according to the separations from the map of habitats according to Janowski et al. [8] (Figure 6) for 150 kHz. Figure 9b shows the angular response curves of BBS values. The values are averaged for measurements made within a 3 m radius of the sampling points for 150 kHz.

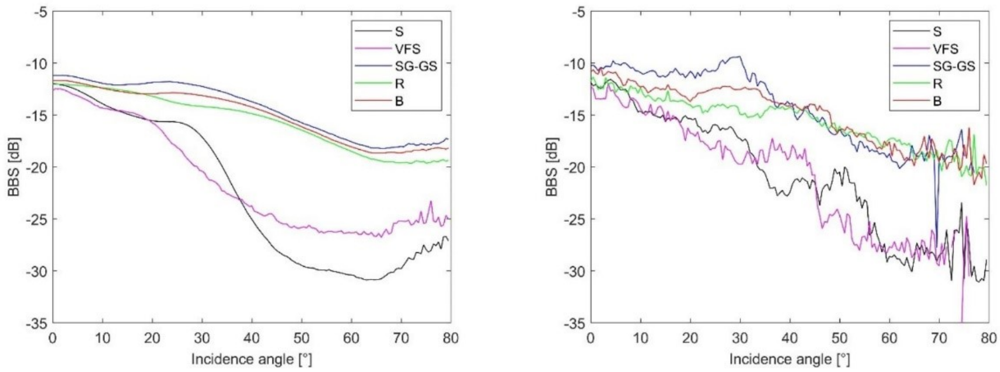

(**a**) (**b**)

Figure 9. Dependence of BBS for 150 kHz on incidence angle for different classes (S, sand; VFS, very fine sand; SG-GS, sandy gravel or gravelly sand; R, red algae on boulders; B, boulders): (**a**) averaging over habitat classification shown in Figure 6 and (**b**) from ground-truth samples.

Table 1 presents the acoustic characteristics of habitat types occurring in the research area. The dependence of BBS values on the angle of incidence was determined for two situations:

- Black line: angular response curves of BBS with values averaged for measurements made within 3 m radius of the sampling points for registration using 150 kHz signal frequency;
- Dashed black line: angular response curves of BBS with values averaged for measurements made in areas where homogeneous habitats occur, according to the separations from the map of habitats according to Janowski et al. [8] (Figure 6) for registration using 150 kHz signal frequency.

Table 1. Angular response curves of BBS: black line, 150 kHz, data from samples; dashed black line, 150 kHz, data from object-based image classification.

Class ID	BBS (dB) 150 kHz	Seabed Image/Composition
VFS	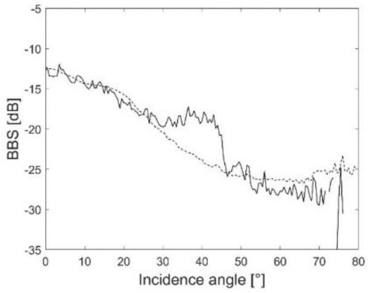	 Bare, flat area of very fine sand with worm burrows
S	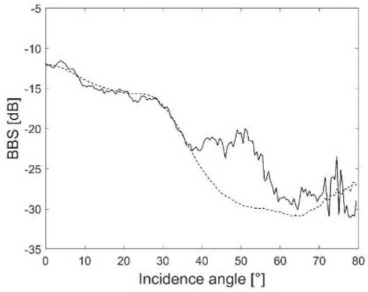	 Sand or slightly gravelly sand with ripple marks
SG-GS	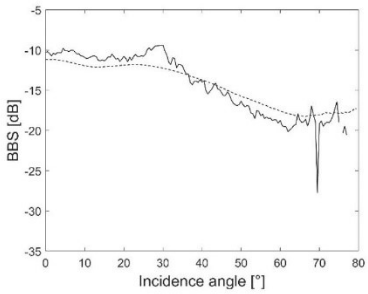	 Sandy gravel or gravelly sand, rare boulders with barnacles and *Mytilus trossulus*
B	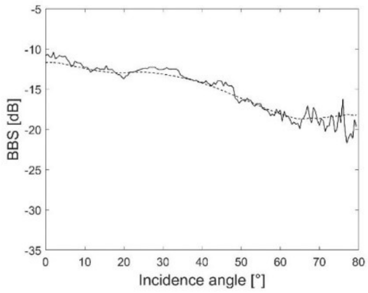	 High concentration of *Mytilus trossulus* on dense boulder substratum

Table 1. *Cont.*

Class ID	BBS (dB) 150 kHz	Seabed Image/Composition
R	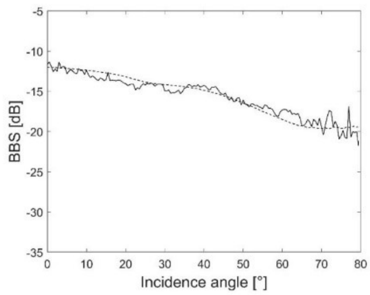	 Large dense patches of red algae with a high concentration of *Mytilus trossulus* on boulder substratum

Figure 9 and Table 1 present the angular response curves of absolute BBS. Close to an angle of 80°, there were large fluctuations in the values, because, in the extreme part of the swath, fewer measuring points were recorded in equiangle mode, many points from the outer beams were rejected in the cleaning process, and the values from the individual registered measuring points varied considerably. Figure 9a,b do not perfectly show the BBS relationships for the given benthic habitats. Figure 9a presents BBS values averaged within the habitat classes, whose boundaries were determined in a semi-automatic classification process; hence, they are not perfectly defined despite having high classification accuracy. Figure 9b presents BBS values averaged within 3 m radius circles around the ground-truth data, which is a theoretical assumption, because there can also be other habitats present in these buffers.

3.2. Backscatter Maps: BBS-Coder Result

Figure 10 shows backscatter value maps prepared in this study for registration using 150 kHz signal frequency. Figure 10A presents backscatter mosaic grids with relative backscatter values without angular (AVG) and bottom slope (BAC) correction. The near 0° incidence angle showed the strongest signals and also the fastest drop-off. Figure 10B was created with the manufacturer's MBES calibration (NORBIT) and bottom slope correction (correction of reverberation area, which is improved by bottom slope and calculated range) but without our AVG correction. Figure 10C was created with the manufacturer's calibration (NORBIT), bottom slope correction, and the BBS-Coder AVG correction developed in this study and described in Section 2.3.2. The near 0° incidence angle represented the strongest signal fluctuations.

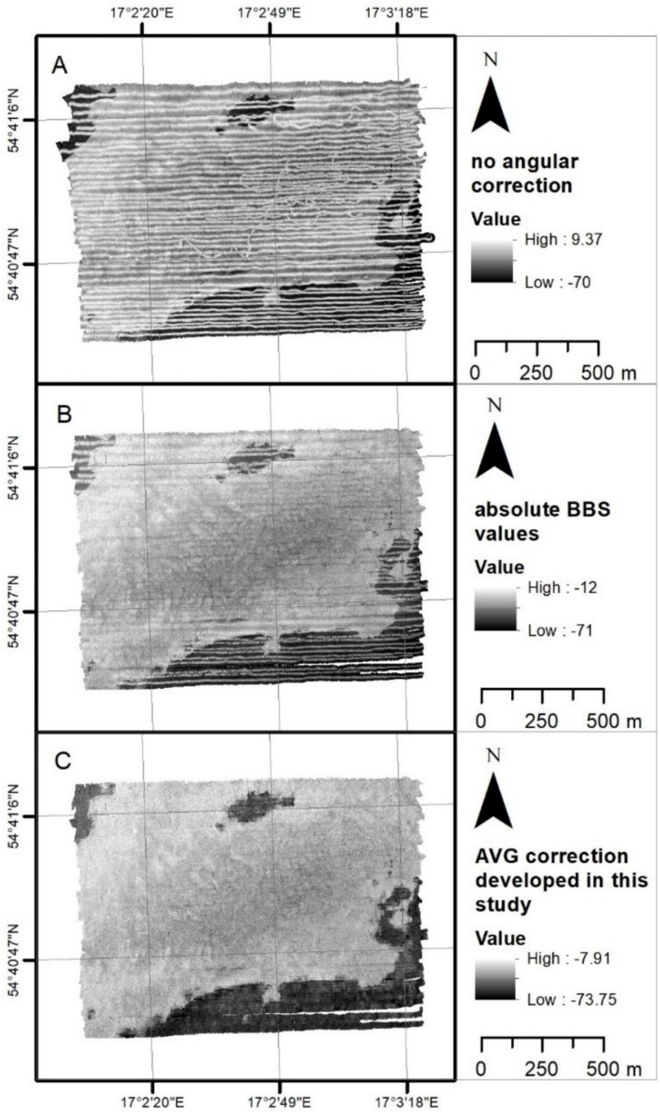

Figure 10. Backscatter mosaic grids of research area for 150 kHz signal frequency: (**A**) with relative backscatter values, without any corrections; (**B**) with absolute BBS values and bottom slope correction developed in this study; (**C**) with AVG correction developed in this study applied to absolute BBS values containing bottom slope correction.

4. Discussion

Calibrating the MBES makes it possible to obtain absolute values of BBS, which is an essential feature for specific geoacoustic settings on the seabed and benthic habitats and very helpful in distinguishing them. Only a few studies with absolute BBS have been reported due to technical difficulties associated with MBES calibration and post-measurement data correction; moreover, MBES studies with resulting ARCs are extremely sparse [13,16].

Any physically correct calibration method improves data quality and provides valuable information. The technology now developed for working with MBES makes it possible to fully calibrate the instrument, and the validity and usefulness of the absolute BBS values make it necessary to always use calibrated echosounders.

Several papers have already been written showing absolute BBS values recorded by MBES for bottom habitats. Eleftherakis et al. [16] performed a calibration of the backscatter strength values recorded by MBES with reference to data recorded in the same place by an acoustically calibrated single-beam echosounder (SBES). They presented the dependence of backscatter strength on the angle of incidence in three research areas with different types of sediment at 200 and 333 kHz. Wendelboe [13] presented average values of seabed backscattering strength obtained in the frequency range from 190 to 400 kHz, for grazing angles from 20° to 90°. This study showed that seabed backscattering strength ranged from −8.5 to −19 dB for 400 kHz and from −13.5 to −23 dB for 200 kHz. Weber and Ward [15] took measurements with a calibrated SBES at 170 and 250 kHz in an area with sand, gravel, and bedrock seafloor. Williams et al. [14] measured backscattering at frequencies of 20–150 kHz with grazing angles of 20–30°, and, in subsequent work [17], they measured backscattering at frequencies of 200–500 kHz with grazing angles of 32° and 42°. They recorded increasing values with increased frequency. Stanic et al. [18] performed acoustic bottom backscattering measurements east of Jacksonville, Florida, and recorded data from sidescan sonar. Measurements were made in a coarse shelly area with frequencies of 20–180 kHz and grazing angles of 5–30°. It was found that backscattering strength values slightly decreased with increasing frequency.

To compare our results on BBS measurements with those recently reported by other researchers, we summarized the basic information on the particular works in Figure 11. In general, the results obtained in this work on the dependence of BBS on the angle of incidence are in line with those achieved by other authors who performed MBES measurements [16,32], as well as the theoretical predictions.

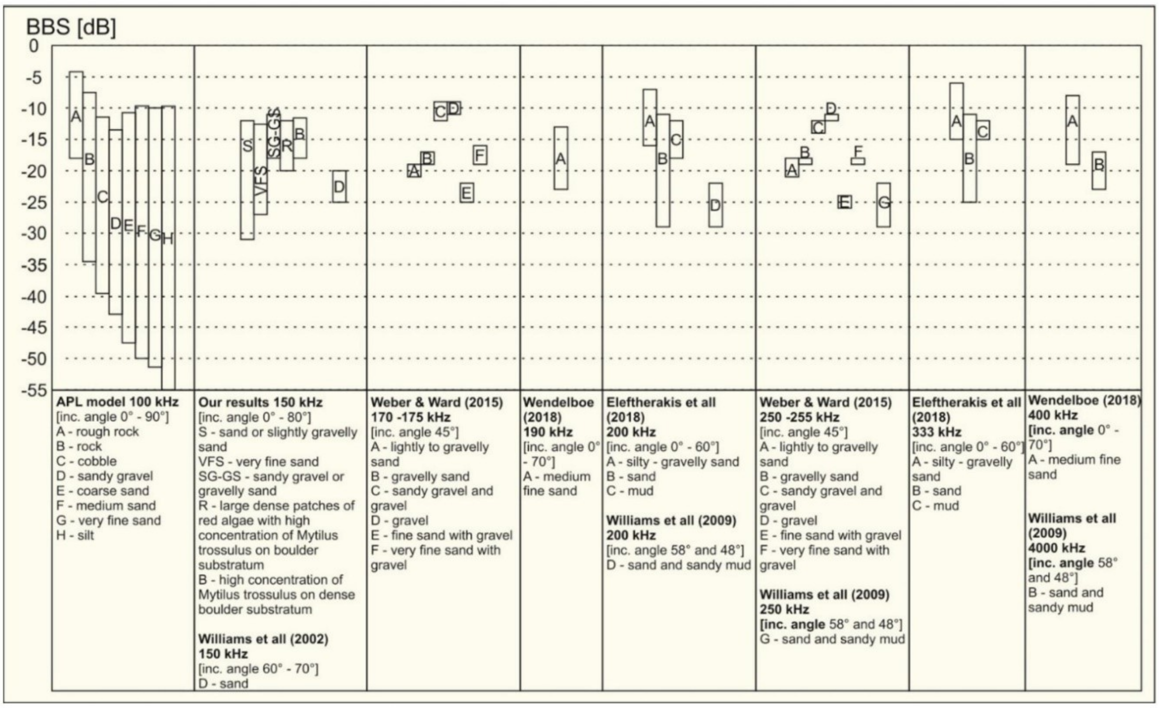

Figure 11. Summary of BBS obtained by different studies, including frequency and incident angles.

It is difficult to compare data recorded by different authors because there are few papers and the benthic habitats studied vary; however, the BBS values we obtained for sand are similar to those obtained at 60–70° incidence angle and 150 kHz by Williams et al. [14] and to those using the APL model at 100 kHz [29]. The values presented for S (−12 to −31 dB) and VFS (−12.5 to −27 dB) are similar to those of Eleftherakis et al. [16] in the Camaret area with sand (−11 to −29 dB at 200 kHz); the values for SG-GS (−10.5 to −18 dB) are similar to data in the Carré Renard area [16] with silty–gravelly sand (−7 to −17 dB at 200 kHz); the values for R (−12 to −20 dB) and B (−11.5 to −18 dB) are similar to data in the Aulne area [16] with mud (−12 to −18 dB at 200 kHz).

The BBS for S and VFS has similar values and angular relationships (Figure 12) to seabed backscattering strength values presented by Wendelboe [13] obtained at a frequency of 190 kHz for medium–fine sand. For the entire angular range, the BBS for SG-GS, R, and B reaches higher values than for S and VFS. Habitats S and VFS have a characteristic shape typical of the ARC curve of fine-grained sediments in the APL model (Figure 12). In contrast, the SG-GS, R, and B habitats have a characteristic shape typical of the ARC curve of acoustically hard sediment such as rock in the APL model at 100 kHz (Figure 12). Habitats SG-GS, R, and B achieve similar BBS values to sandy gravel and cobble in the APL model at 100 kHz. For incidence angles from 25° to 65°, the ARC curve showed a significant decrease in value greater than the APL model at 100 kHz, and this may be related to the higher frequency of the tested signal, 150 kHz.

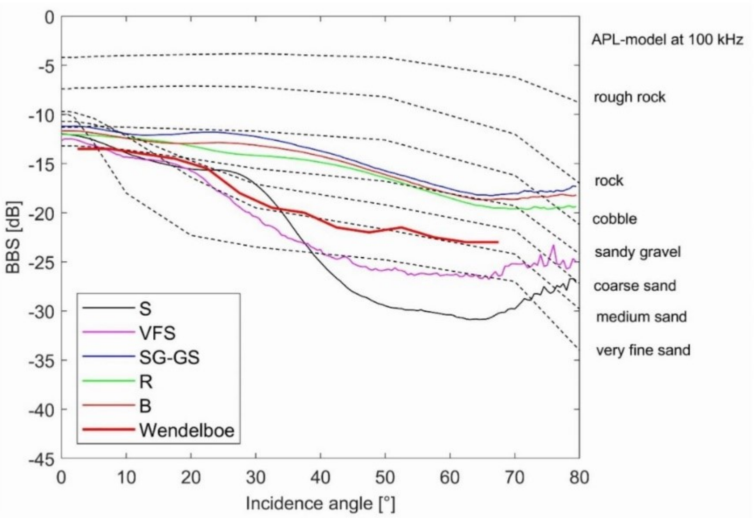

Figure 12. Dependence of BBS at 150 kHz on incidence angle for sand (S), very fine sand (VFS), sandy gravel or gravelly sand (SG-GS), red algae on boulders (R), and boulders (B) and seabed backscattering strength values estimated from Wendelboe [13] obtained at a frequency of 190 kHz for medium fine sand. Dashed lines: BBS for different sediment type with APL model at 100 kHz [29].

In the summary of BBS values obtained by researchers, it is difficult to see a trend of increasing value with increasing frequency. However, such a trend was indicated in some studies that considered different frequencies [14,17]. Williams et al. [14,17] suggested that, at high frequencies, scattering from large fragments of shells is dominated by a different scattering mechanism than surface or volume scattering. Weber and Ward [15] recorded a weak increase in backscattering strength with increased frequency for moderately well-sorted medium sand and a slight decrease in all other locations. In many places, higher backscattering strength values were recorded for 170 kHz than for 250 kHz (as shown in Figures 6 and 7 in [15]). Weber and Ward [8] speculated that the maximum backscattering strength existed at a frequency lower than what they tested (below 170 kHz), and that backscattering strength may be connected with some characteristic length scale via which diffuse scattering reaches a maximum for this type of sediment [15].

Roughness is a matter of the wavelength of the acoustic pulse and the size of bottom irregularity. For one and the same seafloor, in the case of high frequencies, the bottom may appear rough, while, for low frequencies, the bottom acoustically behaves like a smooth seafloor, all determined by the Rayleigh parameter [53].

We suggest that the higher BBS values for higher frequencies are associated with strong scattering of higher-frequency signals on an rough seafloor surface [53].

In the ARC curves presented here, the sand habitat (S) showed that an increase in BBS value around 30° incidence is not in line with the APL model curve. This may be due to the presence of sand ripple marks in the study area, similar to Lurton et al. [54]. Although BBS values were corrected for the slope of the seabed, irregularities less than 1 m can still be significant. Seabed slope was calculated using a bathymetric map with 0.5 m resolution; however, from an acoustic and snippet backscattering perspective, modulation of the backscattering strength through microroughness becomes likely. In addition, local grain size changes were noted in the study area where ripple marks occurred on ridges with fine-grained sand and in valleys with coarse-grained sand, which we believe affected the recorded BBS values.

The differences in Figures 9 and 10 between the angular relationships of BBS values obtained from (a) averaging of habitat classifications and (b) ground-truth samples are more visible for habitat types VFS and S than for SG-GS, B, and R. This may mean that the latter three bottom types are more specific, and that the areas they include are more homogeneous. Habitat types VFS and S are more general and may include areas with different characteristics (different sediment/habitat types could have been assigned to them, both in the course of classification and in the 3 m areas around the cores).

For flatter bottom types (VFS, S) there is a large drop in BBS with increased deviation of the direction of the wave from the vertical, and, for cases with more irregular structure/shape (SG-GS, B, R), this drop is smaller. This is due to the low rate of diffusion scattering on the bottom surface, which usually dominates at large incidence angles.

Fonseca et al. [32] provided information on backscatter strength for 95–98 kHz frequency. According to the division of bands introduced by Fonseca et al. [32], the near range includes incident angles from 0° to 25°, the far range includes incident angles from 25° to 55°, and the outer range includes incident angles from 55° to 85°. In our data, we noted the occurrence of three similar zones from 0° to 25° with a weak slope of the curve, from 25° to 65° with a significant slope, and from 65° to 80° with a weak slope. However, high variability of habitats within the half-swath remains a problem for the method described by Fonseca et al. A possible future workaround could be to use automatic segmentation methods to determine the boundaries of individual habitats.

Unadjusted backscatter values have been successfully used for many purposes, including habitat classification [8,19–21]. For more advanced environmental analyses, such as studies of diurnal and seasonal variability of the seabed itself and seagrass scattering variation over time, it might be necessary to work with absolute BBS, because a few dB can determine the variability, as has been demonstrated [55]. Furthermore, the use of absolute BBS is necessary to compare results from different areas recorded at different times. Although the habitats are apparently similar, there are significant differences in their BBS. Sand in the Mediterranean Sea may have different BBS values than sand in the Baltic Sea because they have different physical properties. Habitats with similar physical properties (e.g., number and size of air bubbles in sediment, density) will have similar values. BBS is an intrinsic property of the seafloor and the prevailing habitat (not the multibeam echosounder); thus, it might be better to look for specific habitat-related features that can facilitate habitat recognition. Habitats and their BBS are very different from each other, and substantial research is necessary to know the scattering values of each habitat.

For automatic classification, e.g., object-based (OBIA) or texture (GLCM) analyses, backscatter maps reduced to a single incident angle are needed. There are few techniques for this correction. The methods used range from simple Lambert correction to complex models such as Geocoder. Due to the strong near-nadir errors in the mosaics prepared with the help of Geocoder, we developed our own correction method. It removes the influence of the incidence angle and brings the backscattering strength to an incidence angle of our choice (in this case, 40°).

Other useful backscatter mosaics with smoothed backscatter outcomes without angular dependency can be created using Geocoder [22]. The near 0° incidence angle represents a stronger signal standard deviation. Median filtering of BSS near the 0° incidence angle might be a good solution. Geocoder assigns quality flags to backscatter samples. Data samples closer to and further from the nadir have low values, while samples in the middle range have higher values and a greater influence on the final backscatter mosaic [22]. When our MBES data were recorded with a large overlap, all values found in the raster grid were averaged to generate the mosaic. The BBS-Coder presented here is less complex than the current Geocoder in FMGT QPS software; it is simple and effective, and it will be freely available on the ECOMAP project website (https://www.bonus-ecomap.eu/, accessed on 1 January 2021). The AVG correction scheme presented in this paper assumes the use of a radiometric and geometric correction tool (in this case, QPS Qimera software).

5. Conclusions

The continuous development of measurement technology provides new opportunities for seabed identification and mapping, as exemplified by the real BBS values presented here gathered with a modern GNSS-guided MBES. The absolute BBS should be used to describe habitats precisely, by a physically defined parameter. In the future, this may affect the way acoustic measurements are conducted by reducing the number of samples required to classify benthic habitats and making it easier to compare the scattering of acoustic signals on the bottom in different seasons.

This paper presented the angular dependence of BBS measurement results for several benthic habitats in the Baltic Sea at 150 kHz. The methods of correction used to measure the absolute value of the angular dependence of BBS included laboratory tank calibration, seabed slope correction, and the AVG correction developed in the work, and examples of the obtained mosaics as a result of the applied corrections (BBS-Coder) were shown. The BBS values obtained were −12 to −31 dB for sand (S), −12.5 to −27 dB for very fine sand (VFS), −10.5 to −18 dB for sandy gravel or gravelly sand (SG-GS), −12 to −20 dB for red algae on boulders (R), and −11.5 to −18 dB boulders (B). The AVG correction method presented is a simple and effective tool for preparing a backscatter mosaic useful for seafloor habitat classification.

For the entire angular range, the BBS values obtained for SG-GS, R, and B were higher than those for S and VFS. Habitats S and VFS had characteristic shapes typical of the ARC curve of fine-grained sediment in the APL model (Figure 12).

Examples of measurements presented by different studies suggest high variability of BBS. This may be related to variation within a single habitat, which, in different basins, may have different physical characteristics that vary with time of day and season. It is necessary to find the limits of BBS for specific habitats in specific basins according to numerous empirical studies.

Visual assessment of backscatter mosaic grids created using our methods shows their usefulness for further application, such as sustainable management of seabed resources, exploration of the sea bottom, benthic habitat mapping, and geological mapping of the seabed. The results presented were obtained using the NORBIT echosounder and software, which will be made available on the website associated with the ECOMAP project.

Corrected BBS values are very useful for the characterization of benthic habitats based on acoustic dependence characteristics. Their differentiation based on acoustic signatures may help to classify seabed properties only by specific acoustic responses. It may help to increase the importance of noninvasive underwater acoustic research, reducing the number of sediment ground-truth samples and expanding the classification of known benthic habitats for newly explored areas. However, it should be underlined that this kind of quantitative characterization of the seafloor substrate requires corrected BBS values [23,27]. Advances in calibrated multibeam echosounders are still in the development phase; however, thanks to recent advances by manufacturers, several MBES models calibrated in a test tank are now available. This provides an opportunity for habitat mapping and monitoring using the absolute response of the seafloor to backscattering, as well as its changes over time. We recommend measuring BBS using an acoustically calibrated echosounder and using such data to classify benthic habitats.

Author Contributions: Conceptualization, K.T., J.T., P.P., J.Z., A.K. and J.S.v.D.; data curation, K.T., J.T., P.P., L.J., A.K. and M.R.; formal analysis, K.T. and J.T.; investigation, K.T., J.T., P.P., L.J., J.Z., A.K., M.R., Z.L. and J.S.v.D.; methodology, K.T., J.T., P.P., J.Z., A.K. and J.S.v.D.; project administration, J.T. and J.S.v.D.; software, K.T., P.P. and J.Z.; supervision, J.T. and J.S.v.D.; validation, K.T., J.T. and P.P.; visualization, K.T., L.J., P.P. and M.R.; writing—original draft, K.T., J.T., P.P., L.J., A.K., M.R. and Z.L.; writing—review and editing, J.T., Z.L. and J.S.v.D. All authors have read and agreed to the published version of the manuscript.

Funding: This research resulted from the BONUS ECOMAP project, supported by BONUS (Art 185), funded jointly by the EU and the Federal Ministry of Education and Research of Germany (BMBF), the National Center for Research and Development of Poland (NCBR; grant number BONUS-BB/ECOMAP/07/2017), and the Innovation Fund Denmark (Innovationsfonden).

Institutional Review Board Statement: Not applicable.

Informed Consent Statement: Not applicable.

Data Availability Statement: https://www.bonus-ecomap.eu/. Available on 1 January 2022.

Acknowledgments: We would like to thank the rv Oceanograf and Zelint crews for their help with the marine surveys.

Conflicts of Interest: The authors declare no conflict of interest.

References

1. Parnum, I.; Siwabessy, P.J.W.; Gavrilov, A.N. Identification of Seafloor Habitats in Coastal Shelf Waters Using a Multibeam Echosounder. In Proceedings of the ACOUSTICS 2004, Gold Coast, Australia, 3–5 November 2004; pp. 181–186.
2. Madricardo, F.; Foglini, F.; Kruss, A.; Bellafiore, D.; Trincardi, F. The high resolution mapping of the Venice Lagoon tidal network. *Gen. Assem. Conf. Abstr.* **2017**, *19*, 19505.
3. Guinan, J.; McKeon, C.; O'keeffe, E.; Monteys, X.; Sacchetti, F.; Coughlan, M.; Aonghusa, C.N. Infomar data supports offshore energy development and marine spatial planning in the irish offshore via the emodnet geology portal. *Q. J. Eng. Geol. Hydrogeol.* **2020**, *54*, 33. [CrossRef]
4. Blondel, P.; Gómez Sichi, O. Textural analyses of multibeam sonar imagery from Stanton Banks, Northern Ireland continental shelf. *Appl. Acoust.* **2009**, *70*, 1288–1297. [CrossRef]
5. Marsh, I.; Brown, C. Neural network classification of multibeam backscatter and bathymetry data from Stanton Bank (Area IV). *Appl. Acoust.* **2009**, *70*, 1269–1276. [CrossRef]
6. Prampolini, M.; Blondel, P.; Foglini, F.; Madricardo, F. Habitat mapping of the Maltese continental shelf using acoustic textures and bathymetric analyses. *Estuar. Coast. Shelf Sci.* **2018**, *207*, 483–498. [CrossRef]
7. Schneider von Deimling, J.; Held, P.; Feldens, P.; Wilken, D. Effects of using inclined parametric echosounding on sub-bottom acoustic imaging and advances in buried object detection. *Geo-Mar. Lett.* **2016**, *36*, 113–119. [CrossRef]
8. Janowski, L.; Trzcinska, K.; Tegowski, J.; Kruss, A.; Rucinska-Zjadacz, M.; Pocwiardowski, P. Nearshore benthic habitat mapping based on multi-frequency, multibeam echosounder data using a combined object-based approach: A case study from the Rowy Site in the Southern Baltic Sea. *Remote Sens.* **2018**, *10*, 1983. [CrossRef]
9. Trzcinska, K.; Janowski, L.; Nowak, J.; Rucinska-Zjadacz, M.; Kruss, A.; Schneider von Deimling, J.; Pocwiardowski, P.; Tegowski, J. Spectral features of dual-frequency multibeam echosounder data for benthic habitat mapping. *Mar. Geol.* **2020**, *427*, 106239. [CrossRef]
10. Lamarche, G.; Lurton, X. Recommendations for improved and coherent acquisition and processing of backscatter data from seafloor-mapping sonars. *Mar. Geophys. Res.* **2018**, *39*, 5–22. [CrossRef]
11. Kunde, T.; Held, P.; Sternberg, H.; Schneider von Deimling, J. Ammunition detection using high frequency multibeam snippet backscatter information. *Mar. Pollut. Bull.* **2018**, *133*, 481–490. [CrossRef] [PubMed]
12. Schimel, A.C.G.; Beaudoin, J.; Parnum, I.M.; Le Bas, T.; Schmidt, V.; Keith, G.; Ierodiaconou, D. Multibeam sonar backscatter data processing. *Mar. Geophys. Res.* **2018**, *39*, 121–137. [CrossRef]

13. Wendelboe, G. Backscattering from a sandy seabed measured by a calibrated multibeam echosounder in the 190–400 kHz frequency range. *Mar. Geophys. Res.* **2018**, *39*, 105–120. [CrossRef]
14. Williams, K.L.; Jackson, D.R.; Thorsos, E.I.; Tang, D.; Briggs, K.B. Acoustic backscattering experiments in a well characterized sand sediment: Data/model comparisons using sediment fluid and Biot models. *IEEE J. Ocean. Eng.* **2002**, *27*, 376–387. [CrossRef]
15. Weber, T.C.; Ward, L.G. Observations of backscatter from sand and gravel seafloors between 170 and 250 kHz. *J. Acoust. Soc. Am.* **2015**, *138*, 2169–2180. [CrossRef] [PubMed]
16. Eleftherakis, D.; Berger, L.; Le Bouffant, N.; Pacault, A.; Augustin, J.M.; Lurton, X. Backscatter calibration of high-frequency multibeam echosounder using a reference single-beam system, on natural seafloor. *Mar. Geophys. Res.* **2018**, *39*, 55–73. [CrossRef]
17. Williams, K.L.; Jackson, D.R.; Tang, D.; Briggs, K.B.; Thorsos, E.I. Acoustic Backscattering From a Sand and a Sand/Mud Environment: Experiments and Data/Model Comparisons. *IEEE J. Ocean. Eng.* **2009**, *34*, 388–398. [CrossRef]
18. Stanic, S.; Briggs, K.B.; Fleischer, P.; Sawyer, W.B.; Ray, R.I. High-frequency acoustic backscattering from a coarse shell ocean bottom. *J. Acoust. Soc. Am.* **1989**, *85*, 125–136. [CrossRef]
19. Gaida, T.C.; Mohammadloo, T.H.; Snellen, M.; Simons, D.G. Mapping the seabed and shallow subsurface with multi-frequency multibeam echosounders. *Remote Sens.* **2020**, *12*, 52. [CrossRef]
20. Buscombe, D.; Grams, P.E.; Kaplinski, M.A. Characterizing riverbed sediment using high-frequency acoustics: Scattering signatures of Colorado River bed sediment in Marble and Grand Canyons. *J. Geophys. Res. Earth Surf.* **2014**, *119*, 2692–2710. [CrossRef]
21. Preston, J. Automated acoustic seabed classification of multibeam images of Stanton Banks. *Appl. Acoust.* **2009**, *70*, 1277–1287. [CrossRef]
22. Fonseca, L.; Calder, B. Geocoder: An Efficient Backscatter Map Constructor. In Proceedings of the U.S. Hydro 2005 Conference, San Diego, CA, USA, 22 September 2005; p. 9.
23. Lurton, X.; Lamarche, G. (Eds.) *Backscatter Measurements by Seafloor-Mapping Sonars. Guidelines and Recommendations*; GeoHab Backscatter Working Group: 2015. Available online: https://geohab.org/wp-content/uploads/2018/09/BWSG-REPORT-MAY2015.pdf (accessed on 24 November 2021).
24. Francois, R.E.; Garrison, G.R. Sound absorption based on ocean measurements. *J. Acoust. Soc. Am.* **1982**, *72*, 1879–1890. [CrossRef]
25. Lurtone, X. *An Introduction to Underwater Acoustics*, 2nd ed.; Springer: Berlin/Heidelberg, Germany, 2010.
26. IHO Standards for Hydrographic Surveys. Monaco. 2008. Available online: https://iho.int/uploads/user/pubs/standards/s-44/S-44_5E.pdf (accessed on 24 November 2021).
27. Lamarche, G.; Lurton, X.; Verdier, A.L.; Augustin, J.M. Quantitative characterisation of seafloor substrate and bedforms using advanced processing of multibeam backscatter—Application to Cook Strait, New Zealand. *Cont. Shelf Res.* **2011**, *31*, 93–109. [CrossRef]
28. Van Walree, P.A.; Ainslie, M.A.; Simons, D.G. Mean grain size mapping with single-beam echo sounders. *J. Acoust. Soc. Am.* **2006**, *120*, 2555–2566. [CrossRef]
29. APL-UW. *High-Frequency Ocean Environmental Acoustics Models Handbook*; Defense Technical Information Center: Seattle, WA, USA, 1994; APL-UW TR 9407.
30. Jackson, D.R.; Richardson, M.D. *High-Frequency Seafloor Acoustics*; Springer: Berlin/Heidelberg, Germany, 2007.
31. Díaz, J.V.M. Analysis of Multibeam Sonar Data for the Characterization of Seafloor Habitats. Master's Thesis, The University of New Brunswick, Fredericton, NB, Canada, 1999.
32. Fonseca, L.; Brown, C.; Calder, B.; Mayer, L.; Rzhanov, Y. Angular range analysis of acoustic themes from Stanton Banks Ireland: A link between visual interpretation and multibeam echosounder angular signatures. *Appl. Acoust.* **2009**, *70*, 1298–1304. [CrossRef]
33. Eleftherakis, D.; Snellen, M.; Amiri-Simkooei, A.; Simons, D.G.; Siemes, K. Observations regarding coarse sediment classification based on multi-beam echo-sounder's backscatter strength and depth residuals in Dutch rivers. *J. Acoust. Soc. Am.* **2014**, *135*, 3305–3315. [CrossRef] [PubMed]
34. Weber, T.C.; Rice, G.; Smith, M. Toward a standard line for use in multibeam echo sounder calibration. *Mar. Geophys. Res.* **2018**, *39*, 75–87. [CrossRef]
35. Roche, M.; Degrendele, K.; Vrignaud, C.; Loyer, S.; Le Bas, T.; Augustin, J.M.; Lurton, X. Control of the repeatability of high frequency multibeam echosounder backscatter by using natural reference areas. *Mar. Geophys. Res.* **2018**, *39*, 89–104. [CrossRef]
36. Ladroit, Y.; Lamarche, G.; Pallentin, A. Seafloor multibeam backscatter calibration experiment: Comparing 45°-tilted 38-kHz split-beam echosounder and 30-kHz multibeam data. *Mar. Geophys. Res.* **2018**, *39*, 41–53. [CrossRef]
37. Mutschler, M.; Maillard, E.; Pocwiardowski, P. Combination of bathymetry and calibrated imagery in multibeam echosounder. In *Underwater Acoustic Measurements: Technologies and Results, Proceedings of the 3rd International Conference & Exhibition on Underwater Acoustic Measurements: Technologies and Results, Nafplion, Greece, 21–26 June 2009*; Papadakis, J.S., Bjørnø, L., Eds.; pp. 883–890. Available online: https://www.uaconferences.org/docs/Past_Proceedings/UAM2009_Proceedings.pdf (accessed on 24 November 2021).
38. Perrot, Y.; Brehmer, P.; Roudaut, G.; Gerstoft, P.; Josse, E.; Perrot, Y.; Brehmer, P.; Roudaut, G.; Josse, E.; Plouzané, F.-; et al. Efficient multibeam sonar calibration and performance evaluation. *Int. J. Innov. Res. Sci. Eng. Technol.* **2014**, *3*, 808–820.
39. Lanzoni, J.C.; Weber, T.C. High-resolution calibration of a multibeam echo sounder. In Proceedings of the OCEANS 2010 MTS/IEEE SEATTLE, Seattle, WA, USA, 20–23 September 2010; pp. 1–7.

40. Wendelboe, G.; Dahl, H.; Maillard, E.; Bjorno, L. Towards a fully calibrated multibeam echosounder. *Proc. Meet. Acoust.* **2012**, *17*, 070025.
41. Foote, K.G.; Chu, D.; Hammar, T.R.; Baldwin, K.C.; Mayer, L.A.; Hufnagle, L.C.; Jech, J.M. Protocols for calibrating multibeam sonar. *J. Acoust. Soc. Am.* **2005**, *117*, 2013–2027. [CrossRef] [PubMed]
42. Urick, R.J. *Principles of Underwater Sounds for Engineers*; McGraw-Hill: New York, NY, USA, 1967.
43. Kloser, R.; Reid, D.G. *NO. 286 Acoustic Seabed Classification of Marine Physical and Biological Landscapes*. Anderson, J.T., Ed.; 2007. Available online: https://www.ices.dk/sites/pub/Publication%20Reports/Forms/DispForm.aspx?ID=35841 (accessed on 24 November 2021).
44. Kendzierska, H. Stilo-Ustka. In *Atlas of Polish Marine Area Bottom Habitats*; Gic-Grusza, G., Kryla-Straszewska, L., Urbanski, J., Warzocha, J., Weslawski, J.M., Eds.; Broker-Innowacji: Gdynia, Poland, 2009; pp. 158–165.
45. ASG Eupos. Available online: http://www.asgeupos.pl/index.php?wpg_type=serv&sub=nawgeo_rtn (accessed on 15 September 2021).
46. Folk, R.L.; Ward, W.C. Brazos River bar [Texas]; A study in the significance of grain size parameters. *J. Sediment. Petrol.* **1957**, *27*, 3–26. [CrossRef]
47. Wentworth, C.K. A Scale of Grade and Class Terms for Clastic Sediments. *J. Geol.* **1922**, *30*, 377–392. [CrossRef]
48. Github. Available online: https://github.com/dlang (accessed on 7 November 2021).
49. Simons, D.G.; Snellen, M. A Bayesian approach to seafloor classification using multi-beam echo-sounder backscatter data. *Appl. Acoust.* **2009**, *70*, 1258–1268. [CrossRef]
50. Malik, M.; Lurton, X.; Mayer, L. A framework to quantify uncertainties of seafloor backscatter from swath mapping echosounders. *Mar. Geophys. Res.* **2018**, *39*, 151–168. [CrossRef]
51. Malik, M. Sources and impacts of bottom slope uncertainty on estimation of seafloor backscatter from swath sonars. *Geosciences* **2019**, *9*, 183. [CrossRef]
52. Fonseca, L.; Mayer, L. Remote estimation of surficial seafloor properties through the application Angular Range Analysis to multibeam sonar data. *Mar. Geophys. Res.* **2007**, *28*, 119–126. [CrossRef]
53. Ogilvy, J. *Theory of Wave Scattering from Random Rough Surfaces*; Adam Higler: Bristol, UK, 1991.
54. Lurton, X.; Eleftherakis, D.; Augustin, J.M. Analysis of seafloor backscatter strength dependence on the survey azimuth using multibeam echosounder data. *Mar. Geophys. Res.* **2018**, *39*, 183–203. [CrossRef]
55. Feldens, P.; Schulze, I.; Papenmeier, S.; Schönke, M.; Schneider von Deimling, J. Improved interpretation of marine sedimentary environments using multi-frequency multibeam backscatter data. *Geosciences* **2018**, *8*, 214. [CrossRef]

Oświadczenia współautorów

Mgr Karolina Trzcińska
Department of Geophysics
Institute of Oceanography, University of Gdańsk
(e-mail: karolina.trzcinska@ug.edu.pl)

Gdańsk, 07 February 2022

Author Contribution Statement

I declare that my contribution to the paper:

Trzcinska, K.; Tegowski, J.; Pocwiardowski, P.; Janowski, L.; Zdroik, J.; Kruss, A.; Rucinska, M.; Lubniewski, Z.; Schneider von Deimling, J. Measurement of Seafloor Acoustic Backscatter Angular Dependence at 150 kHz Using a Multibeam Echosounder. *Remote Sens*. 2021, 13, 4771. https://doi.org/10.3390/rs13234771

included:

- conceptualization,
- data curation,
- formal analysis,
- investigation,
- methodology,
- software,
- validation,
- visualization,
- writing—original draft.

Overall, I estimate that my contribution to this work is **75%**.

I have done the following work:

- planning of works connected with obtaining real BBS,
- participation in data recording,
- data processing including correction of the bottom slope, calculation of the real incidence angles of the acoustic beam on the uneven bottom, calculation of the reverberation area, correction of the recorded intensities by the parameters calculated by me,
- development of the BBS-Coder algorithm,
- visualization and interpretation of results.

Karolina Trzcińska

Karolina Trzcińska

Prof. dr hab. Jarosław Tęgowski
Department of Geophysics
Institute of Oceanography, University of Gdańsk
(e-mail: jaroslaw.tegowski@ug.edu.pl)

Gdańsk, 07 February 2022

Author Contribution Statement

I declare that my contribution to the paper:

Trzcinska, K.; Tegowski, J.; Pocwiardowski, P.; Janowski, L.; Zdroik, J.; Kruss, A.; Rucinska, M.; Lubniewski, Z.; Schneider von Deimling, J. Measurement of Seafloor Acoustic Backscatter Angular Dependence at 150 kHz Using a Multibeam Echosounder. *Remote Sens*. 2021, 13, 4771. https://doi.org/10.3390/rs13234771

included:

- conceptualization,
- data curation,
- formal analysis,
- investigation,
- methodology,
- project administration,
- supervision,
- validation,
- writing—original draft,
- writing—review and editing.

Overall, I estimate that my contribution to this work is **6 %**.

....

Jarosław Tęgowski

Dr Paweł Poćwiardowski
NORBIT-Poland Sp. z o.o.
(e-mail: pawel@norbit.com)

Santa Barbara, 07 February 2022
(city)

Author Contribution Statement

I declare that my contribution to the paper:

Trzcinska, K.; Tegowski, J.; Pocwiardowski, P.; Janowski, L.; Zdroik, J.; Kruss, A.; Rucinska, M.; Lubniewski, Z.; Schneider von Deimling, J. Measurement of Seafloor Acoustic Backscatter Angular Dependence at 150 kHz Using a Multibeam Echosounder. *Remote Sens*. 2021, 13, 4771. https://doi.org/10.3390/rs13234771

included:

- conceptualization,
- data curation,
- investigation,
- methodology,
- software,
- validation,
- visualization,
- writing—original draft.

Overall, I estimate that my contribution to this work is **5%**.

Poćwiardowski
………………………………
Paweł Poćwiardowski

Dr Łukasz Janowski
Maritime Institute,
Gdynia Maritime University,
(e-mail: ljanowski@im.umg.edu.pl)

Gdańsk, 07 February 2022
(city)

Author Contribution Statement

I declare that my contribution to the paper:

Trzcinska, K.; Tegowski, J.; Pocwiardowski, P.; Janowski, L.; Zdroik, J.; Kruss, A.; Rucinska, M.; Lubniewski, Z.; Schneider von Deimling, J. Measurement of Seafloor Acoustic Backscatter Angular Dependence at 150 kHz Using a Multibeam Echosounder. *Remote Sens*. 2021, 13, 4771. https://doi.org/10.3390/rs13234771

included:

- data curation,
- investigation,
- visualization,
- writing—original draft.

Overall, I estimate that my contribution to this work is **3%**.

Łukasz Janowski

Łukasz Janowski

Mgr Jakub Zdroik
Division of Physical Oceanography,
Institute of Oceanography, University of Gdańsk
(e-mail: jakub.zdroik@ug.edu.pl)

Gdańsk, 07 February 2022

Author Contribution Statement

I declare that my contribution to the paper:

Trzcinska, K.; Tegowski, J.; Pocwiardowski, P.; Janowski, L.; Zdroik, J.; Kruss, A.; Rucinska, M.; Lubniewski, Z.; Schneider von Deimling, J. Measurement of Seafloor Acoustic Backscatter Angular Dependence at 150 kHz Using a Multibeam Echosounder. *Remote Sens.* 2021, 13, 4771. https://doi.org/10.3390/rs13234771

included:

- conceptualization,
- investigation,
- methodology,
- software.

Overall, I estimate that my contribution to this work is **3 %**.

Jakub Zdroik

Dr Aleksandra Kruss
NORBIT-Poland Sp. z o.o.
(e-mail: aleksandra.kruss@norbit.com)

Sopot, 07 February 2022
(city)

Author Contribution Statement

I declare that my contribution to the paper:

Trzcinska, K.; Tegowski, J.; Pocwiardowski, P.; Janowski, L.; Zdroik, J.; Kruss, A.; Rucinska, M.; Lubniewski, Z.; Schneider von Deimling, J. Measurement of Seafloor Acoustic Backscatter Angular Dependence at 150 kHz Using a Multibeam Echosounder. *Remote Sens*. 2021, 13, 4771. https://doi.org/10.3390/rs13234771

included:

- conceptualization,
- data curation,
- investigation,
- methodology,
- writing—original draft.

Overall, I estimate that my contribution to this work is **1%**.

Aleksandra Kruss

Aleksandra Kruss

Dr Maria Rucińska
Department of Geophysics
Institute of Oceanography, University of Gdańsk
(e-mail: maria.rucinska@ug.edu.pl)

Gdańsk, 07 February 2022

Author Contribution Statement

I declare that my contribution to the paper:

Trzcinska, K.; Tegowski, J.; Pocwiardowski, P.; Janowski, L.; Zdroik, J.; Kruss, A.; Rucinska, M.; Lubniewski, Z.; Schneider von Deimling, J. Measurement of Seafloor Acoustic Backscatter Angular Dependence at 150 kHz Using a Multibeam Echosounder. *Remote Sens*. 2021, 13, 4771. https://doi.org/10.3390/rs13234771

included:

- data curation,
- investigation,
- visualization,
- writing—original draft.

Overall, I estimate that my contribution to this work is **1%**.

Rucińska
....

Maria Rucińska

dr hab. inż. Zbigniew Łubniewski, prof. PG
Department of Geoinformatics,
Faculty of Electronics, Telecommunications and Informatics,
Gdansk University of Technology,
(e-mail: zbigniew.lubniewski@eti.pg.edu.pl)

Gdańsk, 07 February 2022
(city)

Author Contribution Statement

I declare that my contribution to the paper:

Trzcinska, K.; Tegowski, J.; Pocwiardowski, P.; Janowski, L.; Zdroik, J.; Kruss, A.; Rucinska, M.; Lubniewski, Z.; Schneider von Deimling, J. Measurement of Seafloor Acoustic Backscatter Angular Dependence at 150 kHz Using a Multibeam Echosounder. *Remote Sens*. 2021, 13, 4771. https://doi.org/10.3390/rs13234771

included:

- investigation,
- writing—original draft,
- writing—review and editing.

Overall, I estimate that my contribution to this work is **2 %**.

....
Zbigniew Łubniewski

Dr Jens Schneider von Deimling,
Marine Geophysics and Hydroacoustics
Christian-Albrechts-Universität zu Kiel, Germany
(e-mail: jens.schneider@ifg.uni-kiel.de)

Kiel, 07 February 2022
(city)

Author Contribution Statement

I declare that my contribution to the paper:

Trzcinska, K.; Tegowski, J.; Pocwiardowski, P.; Janowski, L.; Zdroik, J.; Kruss, A.; Rucinska, M.; Lubniewski, Z.; Schneider von Deimling, J. Measurement of Seafloor Acoustic Backscatter Angular Dependence at 150 kHz Using a Multibeam Echosounder. *Remote Sens*. 2021, 13, 4771. https://doi.org/10.3390/rs13234771

included:

- conceptualization,
- investigation,
- methodology,
- project administration,
- supervision,
- writing—review and editing.

Overall, I estimate that my contribution to this work is **4 %**.

....

Jens Schneider von Deimling